Towards Application of Silica-Encapsulated DNA (DNAcol) in Subsurface Environments Understanding the behavior of DNAcol through systematic laboratory-scale studies

Kianfar, B.

DOI
10.4233/uuid:d0e7c5bb-0a47-405a-aff0-9c07a1908f32

Publication date
2025

Document Version
Final published version

Citation (APA)
Kianfar, B. (2025). *Towards Application of Silica-Encapsulated DNA (DNAcol) in Subsurface Environments: Understanding the behavior of DNAcol through systematic laboratory-scale studies*. [Dissertation (TU Delft), Delft University of Technology]. https://doi.org/10.4233/uuid:d0e7c5bb-0a47-405a-aff0-9c07a1908f32

Towards Application of Silica-Encapsulated DNA (DNAcol) in Subsurface Environments

Understanding the behavior of DNAcol through systematic laboratory-scale studies

TOWARDS APPLICATION OF SILICA-ENCAPSULATED DNA (DNACOL) IN SUBSURFACE ENVIRONMENTS

UNDERSTANDING THE BEHAVIOR OF DNACOL THROUGH SYSTEMATIC LABORATORY-SCALE STUDIES

Dissertation

for the purpose of obtaining the degree of doctor
at Delft University of Technology
by the authority of the Rector Magnificus, prof. dr. ir. T.H.J.J. van der Hagen,
chair of the Board for Doctorates
to be defended publicly on
Wednesday 29 January 2025 at 10:00 o'clock

by

Bahareh KIANFAR

Master of Science in Environmental Engineering,
ETH Zürich, Switzerland,
born in Andimeshk, Iran.

This dissertation has been approved by the

promotor: Prof.dr. T. A. Bogaard
promotor: Dr. J. W. A. Foppen

Composition of the doctoral committee:

Rector Magnificus,	chairperson
Prof. dr. T. A. Bogaard	Delft University of Technology, *promotor*
Dr. J. W. A. Foppen	Delft University of Technology, *promotor*
Independent members:	
Prof. dr. L. Aquilanti	Universita Politecnica delle Marche, Italy
Prof. dr. J. F. Schijven	Utrecht University and RIVM, the Netherlands
Prof. dr. ir. M. K. de Kreuk	Delft University of Technology
Dr. M. Teixido Planes	IDEA-CSIC, Spain
Prof. dr. ir. D. van Halem	Delft University of Technology, reserve member
Other member:	
Prof. dr. ir. S. M. Hassanizadeh	Utrecht University, the Netherlands

Keywords: Silica-encapsulated-DNA, Microparticle, Colloidal particle, Transport mechanism, Retention and Attachment mechanism

Printed by: Ipskamp Printing

Cover by: Pegah Pourrajab

ISBN 978-94-6518-001-4

An electronic copy of this dissertation is available at
https://repository.tudelft.nl/.

To my family

CONTENTS

SUMMARY

Protecting water resource quality is a global concern, as both solute and colloidal contaminants from various sources can infiltrate into soil and eventually pollute groundwater. Understanding the fate and transport of colloidal contaminants- such as engineered nano- and micro-particles, as well as biological entities like bacteria and viruses- is crucial for mitigating their associated risks. The transport and deposition of the colloidal contaminants are complex and multiscale processes in porous media.

This dissertation explored the application of DNA-based particles as potential tracer agents. Advances in nanotechnology and molecular biology have enabled the development of synthetic DNA-based particles that synthetic DNA act as "barcodes". These particles are highly detectable and quantifiable at low concentrations using qPCR techniques, making them ideal for mapping contamination pathways, determining aquifer hydraulic connectivity, tracking multiple sources simultaneously, and serving as surrogates for tracking the transport and pathways of colloidal contaminants.

DNA-based particles have recently been used as tracers in hydrological studies. The focus of the dissertation is on DNA-based particles with a core-shell structure made of silica encapsulating double-stranded DNA (referred to as DNAcol). Since DNA-based particles can be classified as colloidal particles, this research aims to better understand the mechanisms governing their transport and fate under varying physicochemical conditions. By examining its responses to different tested conditions, the study seeks to identify the environmental conditions in which this tracer can be most effectively applied.

Chapter 2 of this dissertation investigated the transport and deposition kinetics of DNAcol using saturated sand column experiments under various conditions, including different porewater chemistries, flow rates, and sand grain size distributions, to identify optimal environmental conditions for DNAcol use. The results indicated that DNAcol transport is well-described by first-order kinetics for both attachment and detachment processes. Calculated sticking efficiencies showed that a significant fraction of DNAcol that collided with sand grain surfaces attached to them at high ionic strength, while transient porewater chemistry conditions caused substantial re-entrainment. The results highlighted DNAcol's sensitivity to physical and chemical factors, limiting its effectiveness as a hydrological tracer for studying subsurface flow paths, particularly in fine-grained sands or at low-flow velocities. DNAcol is most suitable for investigating flow paths and travel times in coarse-grained aquifers with relatively high flow rates over short distances (i.e., meter scale).

Chapter 3 examined the transport and release of DNAcol in porous media under varying porewater chemistry conditions, focusing on the effects of natural organic matter (NOM) concentrations and ionic strength ($CaCl_2$). The study aimed to identify the main factors influencing DNAcol deposition and release during steady and transient porewa-

ter chemistry conditions. Under steady porewater chemistry conditions, DNAcol deposition rates significantly increased at 1 and 10 mM ionic strength ($CaCl_2$), resulting in approximately 98-99% removal with the sand columns. In contrast, deposition rates decreased as NOM concentrations increased. The calculated sticking efficiency for DNAcol under 1 and 10 mM $CaCl_2$ in the absence of NOM indicated favorable attachment conditions but decreased to 0.03-0.49 in the presence of 5 and 20 mg-C L^{-1} NOM. During transient porewater chemistry conditions, breakthrough curves showed clear evidence of colloid remobilization, with higher remobilization rates observed when the initial ionic strength was 10 mM compared to 1 mM. These findings highlighted the complex interactions between water quality parameters and the behavior of colloidal matter in porous media, emphasizing the impact of environmental changes on colloidal deposition and release.

Chapter 4 explored the potential application of DNAcol in agricultural fields using organic-rich natural groundwater. Building on the findings from Chapter 3, controlled column experiments were conducted to examine DNAcol transport and retention dynamics. Breakthrough curves from sand columns using two types of groundwater showed moderate DNAcol removal. While, experiments with synthetic groundwater lacking organic matter showed increased DNAcol removal. Additionally, DNAcol's hydrodynamic size changed over a period of two hours, indicating homo-aggregation. In sand columns using synthetic groundwater, DNAcol exhibited 2-3 log removal. DNAcol concentrations in the effluent of undisturbed soil columns were very low. Consistent with findings in Chapter 3, a reduction in porewater ionic strength resulted in DNAcol mobilization, highlighting the influence of transient water quality on its transport behavior.

Chapter 5 described an event-based multi-tracer experiment using DNAcol at the plot scale on a hillslope to assess the contributions of different parts of the hillslope to subsurface runoff and the impact of preferential flow paths. The results indicated that the experiment did not achieve its intended goals. To address these challenges and enhance the effectiveness of future experiments, this chapter proposed several improvements for future experiments: optimizing tracer concentration and sampling duration, developing and validating methods to increase DNA concentration in collected samples, investigating the presence of inhibitory compounds in environmental water samples, and defining strategies to mitigation these issues.

Chapter 6 concluded the dissertation, discussed its limitations, and suggested some potential avenues for future research on DNA-tagged particles.

This dissertation systematically investigated several factors influencing DNAcol transport and removal mechanisms. The findings highlighted variations in DNAcol behavior, particularly under varying natural organic matter concentrations and ionic strengths. The results also underscored the importance of accounting for the remobilization of engineered microparticles and biological contaminants in response to changes in porewater chemistry.

By conducting systematic studies, we can deepen our understanding of colloidal transport dynamics, improving our ability to predict their behavior in subsurface environments. This knowledge is crucial for developing effective risk management strategies to protect groundwater and provides practical insights for mitigating colloidal contamination risks.

SAMENVATTING

Bescherming van de waterkwaliteit is een wereldwijde zorg, aangezien zowel opgeloste als colloïdale verontreinigingen uit verschillende bronnen in de bodem kunnen komen en uiteindelijk het grondwater vervuilen. Het begrijpen van het transport van colloïdale verontreinigingen, zoals gesynthetiseerde nano- en microdeeltjes, evenals biologische verontreinigingen zoals bacteriën en virussen, is cruciaal om de bijbehorende risico's te verminderen. Het transport en de verwijdering van colloïdale verontreinigingen in poreuze media zijn zeer complexe processen.

Dit proefschrift onderzoekt de toepassing van DNA-gebaseerde deeltjes als potentiële tracer. Recente vooruitgang in nanotechnologie en moleculaire biologie heeft de ontwikkeling mogelijk gemaakt van synthetisch DNA-gebaseerde deeltjes waarbij het synthetisch DNA fungeert als een "streepjescode". Deze deeltjes zijn zeer goed te meten met behulp van qPCR-technieken, ook in hele lage concentraties. Hierdoor zijn ze ideaal voor het in kaart brengen van transport van verontreiniging, het bepalen van hydraulische eigenschappen van aquifers, het gelijktijdig traceren van meerdere bronnen en kunnen ze dienen als surrogaat voor het volgen van colloïdale verontreinigingen.

Een aantal verschillende op DNA-gebaseerde deeltjes zijn recentelijk gebruikt als tracers in hydrologische studies. De focus van dit proefschrift ligt op DNA-gebaseerde deeltjes (DNAcol genaamd in dit proefschrift) met een silica kern, dan het DNA en dan weer een beschermende schil van silica. Dit onderzoek streeft ernaar de mechanismen te begrijpen die het transport en gedrag bepalen van de colloïdale DNAcol deeltjes onder verschillende fysisch-chemische omstandigheden. Deze studie heeft tot doel de natuurlijke omstandigheden te identificeren waarin deze tracer effectief kan worden toegepast.

Hoofdstuk 2 van dit proefschrift onderzocht het transport en depositie van DNAcol door middel van experimenten in verzadigde zandkolommen onder verschillende omstandigheden. Hierbij werd gekeken naar waterkwaliteit, stromingssnelheden en korrelgroottes van het zand. De resultaten gaven aan dat het transport en gedrag van DNAcol goed kan worden beschreven door een 1e orde evenwichtsvergelijking voor zowel binding als remobilisatie van DNAcol in het zand. De berekende 'sticking'efficiënties toonden aan dat een aanzienlijk deel van de DNAcol dat in botsing kwam met de zandkorrels zich bij hoge ionsterkte hechtte, terwijl veranderende grondwaterkwaliteit aanzienlijke remobilistaie veroorzaakte. De resultaten benadrukten de gevoeligheid van DNAcol voor fysische en chemische factoren, wat de effectiviteit als hydrologische tracer voor het bestuderen van ondergrondse stroming enigszins beperkt, vooral in fijnkorrelige zanden of bij lage grondwaterstroomsnelheden. DNAcol is het geschiktst voor onderzoek naar stroombanen en reistijden in grofkorrelige watervoerende lagen met relatief hoge stroomsnelheden over kortere afstanden (d.w.z. meterschaal).

Hoofdstuk 3 onderzocht het transport van DNAcol in poreuze media met verschillende grondwaterkwaliteit, en met een focus op de effecten van concentraties van natuurlijke

organische stoffen (NOM) en ionsterkte ($CaCl_2$). Het doel was het effect van NOM te identificeren dat DNAcol binding en remobilisatie beïnvloedt tijdens constante en veranderende grondwaterkwaliteit. Als de chemische samenstelling van het poriewater niet veranderende tijdens een experiment, nam de depositie van het DNAcol aan het zand aanzienlijk toe van 1 naar 10 mM ionsterkte ($CaCl_2$), wat resulteerde in ongeveer 98-99% verwijdering in de zandkolommen. Daarentegen nam de depositie sterk af naarmate de NOM-concentraties toenam. Berekeningen van de 'sticking' efficiëntie voor DNAcol bij 1 en 10 mM $CaCl_2$ zonder NOM gaven aan dat de deeltjes zich erg goed hechtte aan het zand, maar dat deze afnamen naar 0.03-0.49 in aanwezigheid van 5 en 20 mg-C L^{-1} NOM. Als de waterkwaliteit vervolgens veranderd werd, toonden doorbraakcurves duidelijk bewijs van remobilisatie van de DNAcol. Hogere remobilisatiesnelheden werden waargenomen wanneer de initiële ionsterkte 10 mM was in vergelijking met 1 mM. Deze bevindingen benadrukten de complexe interacties tussen waterkwaliteit en het gedrag van colloïdaal materiaal in poreuze media en de impact van veranderende chemische samenstelling van het water bij binden en remobilisatie van colloïdale deeltjes.

Hoofdstuk 4 onderzocht de toepassing van DNAcol in landbouwgebieden met behulp van organisch-rijk natuurlijk grondwater. Voortbouwend op de bevindingen van Hoofdstuk 3 werden kolomexperimenten uitgevoerd om het transport en de retentiedynamiek van DNAcol te bestuderen. Doorbraakcurves van zandkolommen met twee soorten grondwater toonden een matige verwijdering van DNAcol. Experimenten met synthetisch grondwater zonder organisch materiaal lieten daarentegen een verhoogde verwijdering van DNAcol zien. Bovendien veranderde de hydrodynamische grootte van DNAcol binnen twee uur, wat duidde op homo-aggregatie. In zandkolommen met synthetisch grondwater vertoonde DNAcol een 2-3 log verwijdering. De DNAcol-concentraties in het uitstromende water van ongestoorde bodemkolommen waren zeer laag. In overeenstemming met de bevindingen in Hoofdstuk 3 leidde een verlaging van de ionsterkte van het poriewater tot mobilisatie van DNAcol, wat de invloed benadrukte van veranderingen in waterkwaliteit op het transportgedrag.

Hoofdstuk 5 beschrijft een plotschaal multi-tracer experiment op een helling met daarbij ook DNAcol als tracer. Het experiment was opgezet om de bijdragen van verschillende locaties van de helling aan ondergrondse afstroming van water in kaart te brengen en de impact van voorkeursstroombanen te bestuderen. De resultaten gaven aan dat het experiment met DNAcol niet de beoogde doelen bereikte. Om deze uitdagingen aan te pakken en de effectiviteit van toekomstige experimenten te verbeteren, stelt dit hoofdstuk verschillende verbeteringen voor: optimalisatie van tracerconcentratie en bemonsteringsduur, ontwikkeling en validatie van methoden om de DNAcol concentratie in de watermonsters te verhogen, en onderzoek naar de aanwezigheid van stoffen in de watermonsters die DNA analyses hinderen.

Hoofdstuk 6 sluit het proefschrift af en bespreekt de beperkingen van het onderzoek en geeft enkele suggesties voor toekomstig onderzoek naar DNA-gelabelde deeltjes. Dit proefschrift deed systematisch onderzoek naar verschillende factoren die het transport en de verwijderingsmechanismen van DNAcol beïnvloeden in de ondergrond. De bevindingen benadrukten veranderingen in het gedrag van DNAcol, met name onder wisselende concentraties van NOM en ionsterkte in het grondwater. De resultaten benadruk-

ten ook het belang van het rekening houden met de remobilisatie van DNAcol en biologische verontreinigingen als reactie op veranderingen in de grondwaterkwaliteit.

Door systematische en gecontroleerde studies uit te voeren, kunnen we ons begrip van het transport van colloïdale deeltjes vergroten en hun gedrag in ondergrondse omgevingen beter voorspellen. Deze kennis is essentieel voor het ontwikkelen van effectieve strategieën om grondwater te beschermen en biedt praktische inzichten voor het verminderen van risico's op colloïdale verontreiniging.

1

INTRODUCTION

1

1.1. INTRODUCTION

Water is vital for life, and access to safe, clean water is crucial for health and well-being. Groundwater, a critical component of our water resources, supports diverse ecosystems, serves as a source of drinking water, and is indispensable for agriculture and industry in many regions. Ensuring the sustainable management and monitoring of groundwater is vital to protect these invaluable resources for current and future generations. Effective strategies help mitigate water scarcity, prevent over-extraction, and shield against contamination from urban, agricultural, industrial, and waste disposal activities. Tracking the sources and pathways of contamination- such as emerging pollutants, inorganic compounds, chlorinated chemicals, pesticides, nanoparticles, and biological agents like bacteria and viruses- is fundamental to preventing water pollution. Addressing water pollution demands comprehensive approaches due to the complexity and heterogeneity of hydrological systems [1]. To address these challenges, in-situ observations, pumping tests, tracer studies [1–6], and modeling techniques are often combined. These integrated approaches provide deeper insights into the connectivity and behavior of groundwater systems, helping to develop effective solutions to maintain clean and safe water supplies.

1.2. HYDROLOGICAL TRACER

Tracer tools play a vital role in hydrological studies, especially in soil and groundwater systems where direct observations are limited [1]. The applications of tracer studies date to the 1950s [6]. Tracers used in hydrological studies are generally categorized into environmental tracers and artificial tracers. Environmental tracers are naturally occurring substances in the environment. For instance, isotopes are commonly used environmental tracers in hydrology, such as Deuterium (^{2}H) and Oxygen-18 (^{18}O) [4]. The second category consists of artificial tracers, or human-applied tracers, such as fluorescent dyes, and salts. Inorganic anions like Cl^{-}, Br^{-} also fall under this category. Among artificial tracers, dye tracers have proven to be highly effective tools [3], due to their direct observability or indirect detectability [4].

Bacteria, viruses, phages, DNA, and microparticles have been used as drifting particle tracers to explore filtration capacity of aquifer and vadose zone, flow pathways and patterns of groundwater biological and particle contaminants in aquifer, sewage, and irrigation water [3, 7–10]. Microsphere tracers of varying sizes and surface properties and bacteria have been predominantly used in karstic regions [8, 11, 12].

Both categories of tracers have their advantages and disadvantages depending on the specific applications [1]. In hydrological studies, an ideal tracer would possess distinct detectability within the system, ensuring it can be easily identified and measured through the experiment. Additionally, it should exhibit physicochemical stability, remaining resistant to changes in solution chemistry, such as fluctuations in pH, ionic strength, and alkalinity to ensure consistent performance over time. Environmental friendliness is another key criterion [3], as the tracer should not pose any risk to ecosystems or human health. Finally, economic viability, as the tracer must be cost-effective to deploy on a large scale. However, in practice, non-ideal

tracers can be particularly valuable when their specific properties align well with the specific applications or requirements of a study [1], offering tailored solutions in complex environments.

One of the most promising approaches in tracer applications for understanding the spatial-temporal patterns of environmental systems is the injection of multiple tracers through multi-time or multi-point experiments. This technique offers significant potential for gathering extensive information while reducing the amount of fieldwork required [2, 13]. However, it necessitates the use of multiple, distinguishable tracers and often requires advanced analytical and laboratory techniques [14], which limits its application.

To overcome the limitations of the multiple-tracer technique, synthetic DNA tracers have been proposed for hydrological studies. These tracers offer the potential to generate a vast number of easily distinguishable markers that exhibit identical transport behavior, are cost-effective, environmentally safe [15, 16], and have no environmental background, making them detectable even in diluted systems due to a unique sequence of DNA. Theoretically, DNA can be detected at the level of a single molecule [17], enhancing the precision of tracer studies.

Over the past two decades, both free DNA and encapsulated synthetic DNA (DNA-based particle) have been applied in several studies, demonstrating their efficiency and potential for improving hydrological research. Comprehensive reviews by Foppen [18] and Zhang and Huang [19] further highlight the advancement and applications of DNA tracers in hydrological studies.

1.3. FREE DNA TRACER

DNA, or deoxyribonucleic acid, consists of a linear sequence of nucleotides, as described by Watson and Crick [20]. Each nucleotide in DNA consists of a deoxyribose sugar, a phosphate group, and one of four nitrogenous bases: adenine (A), thymine (T), cytosine (C), or guanine (G). Synthetic DNA strands used as tracers are designed in either single-stranded (ssDNA) or double-stranded (dsDNA) forms, with lengths ranging from 50 to 500 nucleotides [18]. To ensure their uniqueness and verify that the designed synthetic DNA sequences do not match any existing genetic material in the environment, BLAST software, a publicly available tool, can be used [17, 21].

Synthetic DNA can be detected and quantified using quantitative polymerase chain reaction (qPCR) [22]. qPCR is a technique used to amplify and quantify a targeted DNA sequence in real-time. This process involves polymerase enzymes exponentially replicating a specific DNA sequence through a series of thermal cycles: denaturation, annealing, and extension. Fluorescent probes or dyes (e.g., SYBR Green) are added to the reaction to monitor the accumulation of DNA during the extension phase. SYBR Green binds to double-stranded DNA and emits fluorescence during extension. qPCR monitors the fluorescence emitted at the end of each cycle. The cycle threshold (Ct) or quantification cycle (Cq) is the point at which the fluorescence exceeds a defined threshold. This value is inversely proportional to the amount of target DNA in the sample; meaning lower Cq values indicate higher initial amounts of target DNA. To

quantify DNA in each sample, a calibration curve is created using serial dilutions of known DNA concentrations. The calibration curve plots the logarithmic values of DNA concentration against the corresponding Cq values.

The first synthetic DNA molecule used as a novel tracing technique was developed by Aleström [23]. Following this innovation, Mahler *et al.* [24] conducted laboratory experiments to bind synthetic DNA strands to powdered silica and montmorillonite clay particles, measuring DNA concentrations over three weeks [24]. Since then, free synthetic DNA, in the form of either ssDNA or dsDNA, has been applied as a tracer in both laboratory and field experiments.

These applications include groundwater studies in fractured rock aquifers [16, 25], well-injected tracer tests [13] and research on karstic [26], fractured, fissured rock groundwater in Italy [27, 28]. They have also been used to track domestic effluent discharges in groundwater [29], and in laboratory-saturated column experiments packed with aquifer media [13], and in sloped lysimeter packed with crushed rock (late Pleistocene basaltic tephra) [30].

In surface water studies, synthetic DNA has also been used in surface water field studies in the Netherlands [15], and stream water studies using multiple synthetic DNA tracers in Luxembourg and the Netherlands [31]. Multi DNA-tracer experiment was also conducted in a small glacier valley in northern Sweden [14].

Results from free DNA tracer tests conducted in various conditions, including column and field experiments, frequently showed earlier arrivals of DNA compared to other solute tracers [13, 29, 30, 32] likely due to size exclusion or anion exclusion [30]. Additionally, some studies have indicated less dispersion [14, 29, 32, 33]. However, a few studies have reported similar peak arrivals compared to other solute tracers [15, 26, 31]. Most studies showed low mass recovery of free DNA tracers [14, 15, 29, 30, 32, 33], while in some cases, DNA tracers have better performance in terms of mass recovery rates, with mass recovery of DNA tracer 87% compared to 33.5% for salt tracers [26]. Pang *et al.* [29] highlighted the potential of DNA tracers for tracking effluent discharge in groundwater studies by injecting just 36 μg of dsDNA into groundwater. The tracer signal was detected over three orders of magnitude above the detection limit at a distance of 37 meters down-gradient in the alluvial gravel aquifer. This finding underscores the potential of DNA tracers in monitoring and detecting effluent discharge in groundwater and soil. Although they suggested further research is needed to fully understand the interaction between DNA and discharges [29].

The primary reason for the high initial mass loss of free DNA tracers is unclear. However, it is likely related to several factors, including water quality, the presence of trivalent or multivalent positively charged ions, sorption or attachment to suspended solids, microbial consumption [15, 29, 31], and degradation due to the presence organic matter or chemicals in the effluent [29].

Another limitation of free DNA tracers is their stability under varying environmental stresses. Factors such as low pH, reactive oxygen species, microbial activity [16], and elevated temperatures can negatively affect the stability of DNA molecules [34]. These challenges highlight the importance of considering environmental settings when using free DNA tracers to ensure reliable results.

1.4. ENCAPSULATED DNA PARTICLES

The fabrication of synthetic DNA tracers has significantly advanced through the incorporation of various coating substances designed to protect the DNA from environmental stresses. According to Foppen [18], six types of DNA-based particles have been fabricated and used in hydrological applications. One approach involves using a self-assembling system where DNA is wrapped in a condensed form by Poly-amidoamine (PAA), a cationic homopolymer, and a PEG-PAA-PEG like (poly(ethylene glycol)) copolymer [35]. Another design incorporates iron oxide as a core, encapsulating DNA within Polylactic Acid (PLA), as fabricated by Sharma, Luo, and Walter [21]. A variation of this method, employed by Dahlke *et al.* [14], using polyvinyl acetate (PVA) (based on Liu *et al.* [36]) and poly-lactic-co-glycolic acid (PLGA) as the shell, as demonstrated in studies by McNew *et al.* [37] and Georgakakos, Richards, and Walter [38]. Silica (SiO_2) core-shell particles represent another innovative approach, where DNA is encapsulated within silica core-shell particles, as initially fabricated by Paunescu *et al.* [34] and later reproduced with modifications by Mikutis *et al.* [39], Zhang [40] and Zhang *et al.* [41]. SiO_2-encapsulated DNA particle has been extensively used by researchers [39, 42–50]. Another core-shell structure design features superparamagnetic iron cores with a silica shell to protect the DNA as developed by Puddu *et al.* [51] and later optimized by Sharma *et al.* [52]. This design has been used by Chakraborty *et al.* [53] and Tang *et al.* [54]. Chitosan-alginate coatings involve binding DNA to chitosan and covering it with alginate [33]. Lastly, another design includes superparamagnetic iron cores encapsulating plasmid DNA (pDNA) within PLA [55].

Some notable features of these DNA-based particles include the inclusion of paramagnetic iron oxide, which facilitates sampling in dilute water environments [21, 51, 55]. Polylactic acid (PLA) serves as a biodegradable material that gradually degrades over several weeks to months [21]. SiO_2-encapsulated DNA remains stable in terms of size and charge in deionized water at 105 °C for approximately two weeks [39]; however, the recovery rate of SiO_2-encapsulated DNA particles in environmental water depends on the surrounding temperature [39].

The application of encapsulated DNA particles has been studied in various laboratory and environmental systems. Research has explored their behavior and utility in porous media columns [21, 33, 39, 40, 42, 56], sand tank [53], aquifers and fractured rock [33, 39, 46, 48], lysimeter [33], tracing septic tank leakage [38], overland flow [21], hillslope [37], laboratory open channels [50, 54, 55], surface flow [21], glacial environment [14], and wastewater treatment plant to track submicron-sized silica particles during the activated sludge process [43].

In surface water, Sharma, Luo, and Walter [21] reported that DNA-based particle tracers exhibited behavior similar to dye tracers, with a slightly faster arrival at the longest distance. Additionally, the mass recovery rate of DNA-based particle tracers was nearly twice that of dye tracers, likely due to the adsorption of dye on the streambed and vegetation [21]. Pang *et al.* [33] also reported detectable DNA-based particles at least 1 km downstream, with peak concentration times comparable to those of the salt tracer. The peak concentrations of DNA-based particles 1-3 logs higher than free DNA, a difference attributed to the greater stability and more

negative charge of DNA-based particles [33].

Under an overland flow condition, DNA particle tracers experienced approximately 85% mass loss [21].

In a laboratory soil column, Sharma, Luo, and Walter [21] demonstrated the proof of concept for DNA-based particle tracers, showing they were detectable and quantifiable in effluent samples, traveling at velocities comparable to water [21]. In another study, Kong *et al.* [48] used silica-encapsulated DNA particles with tomographic inversion to determine field-scale hydraulic conductivity, finding lower dispersion, higher mass recovery, and shorter residence times compared to dye tracers. Mikutis *et al.* [39] applied silica-encapsulated DNA particles to determine hydraulic conductivity in an unconsolidated aquifer. They also conducted laboratory column experiments to compare encapsulated DNA particles of various sizes with solute tracers [39]. Their column experiment results showed that silica-encapsulated DNA particles, with a size of 159 nm, traveled at higher velocities and achieved greater mass recovery than dye tracers but noted recovery rate decreases with increasing particle size [39]. In fractured crystalline rock, Kittilä *et al.* [46] found higher average velocities but lower mass recovery and dispersion for silica-encapsulated DNA particles compared to dye tracers. Pang *et al.* [33] investigated the behavior of both free and encapsulated DNA tracers across diverse environments, including a stream, an alluvial gravel aquifer, a fine coastal aquifer, and a lysimeter with undisturbed silt loamy sand. Encapsulated DNA tracers in an alluvial gravel aquifer exhibited two orders of magnitude lower recovery than free DNA tracers potentially due to higher filtration rates and lower injection concentrations of encapsulated DNA tracers compared to free DNA tracers [33]. The encapsulated DNA tracer performance was poor in a coastal sand aquifer with slow groundwater flow (19 cm day^{-1}) [33]. In the lysimeter experiments, DNA tracers were detectable but showed lower mass recovery and dispersion compared to salt tracers [33]. Georgakakos, Richards, and Walter [38] used encapsulated DNA tracers to track septic tank pollution, confirming their detectability at both local and watershed scales and highlighting evidence of potential preferential flow paths at local scale [38]. Interestingly, Chakraborty, Foppen, and Schijven [42] reported that the attachment rate coefficient of DNA-based particles decreased with increasing concentrations of injected particles. Additionally, a recent study by Chakraborty *et al.* [53] examined the effect of ionic strength on estimated hydraulic parameters using silica-encapsulated magnetic DNA particles in a sand tank. Their findings suggest that these particles are promising tracers for determining hydraulic parameters such as hydraulic conductivity, effective porosity, and longitudinal dispersivity over short distances [53].

Encapsulated DNA particles have demonstrated sharper and slightly earlier breakthrough curves compared to solute tracers in several studies involving columns, fractured rock, aquifers, and a lysimeter attributed to size exclusion, preferential flow paths, and reduced dispersion [33, 39, 46, 48, 57]. In contrast, Chakraborty *et al.* [53] reported that size exclusion and earlier breakthrough of silica-encapsulated magnetic DNA particles were not observed in the sand tank experiment. Mass recovery rates for encapsulated DNA particles varied significantly across experimental and field

conditions. For instance, Mikutis *et al.* [39] reported an 85.9% recovery rate for 159 nm silica-encapsulated DNA particles in the sand column, outperforming dye tracers, but also reported a decline in recovery with increasing particle size. Pang *et al.* [33], also reported lower recovery rates in field studies, primarily due to particle filtration. Reduced performance in fine sands with low-velocity groundwater was also reported Pang *et al.* [33]. Other factors affecting encapsulated DNA particle recovery included size-dependent behavior, with larger particles exhibiting reduced recovery [39], density effects [46], and microbial activity [39], and biofilm formation, especially in samples stored at higher temperatures [39]. Additionally, scattered breakthrough curves for encapsulated DNA particles have been observed in some studies [21], which may result from particles attaching and detaching from sand grains, as suggested by Smith *et al.* [58], incomplete dispersion during the injection pulse by the pump Sharma, Luo, and Walter [21], or variability in qPCR sample analysis Kittilä *et al.* [46].

These studies highlighted the complexity and variability associated with using DNA-based particles in environmental systems. A deeper understanding of the effects of environmental factors is crucial for the effective application of DNA-based particles as colloidal tracers in subsurface environments.

1.5. RESEARCH OBJECTIVES

DNA-based particles are increasingly used in environmental applications as hydrological tracers, but it is essential to recognize them as colloidal particulates, ranging from 1 nm to 1 μm. As previously discussed, one of the main challenges is the variation in mass recovery of DNA-based particles. The transport behavior of colloidal particles can be influenced by mechanisms such as attachment, detachment, interception, and sedimentation within porous media. Additionally, the stability of colloidal particles can be affected by homo- and/or hetero-aggregation under certain conditions.

Given the observed mass loss of DNA-based particles under environmental conditions, this research aims to systematically explore the effects of several environmental factors on the transport, attachment, and release mechanisms of silica-encapsulated DNA colloid (DNAcol). This includes examining its stability in terms of charge and size. The study aims to understand the potential mechanisms controlling DNAcol tracer behavior from a colloidal science perspective, particularly in response to changes in physicochemical conditions. From the standpoint of tracer science, the research seeks to identify the environmental conditions in which these tracers can be most effectively applied.

This research addresses several key objectives:

- Investigating the transport and deposition kinetics of DNAcol under various physicochemical conditions.
- Enhancing our understanding of the effects of natural organic matter and ionic strength on the transport, retention and/or attachment, and release of DNAcol under both steady and transient porewater chemistry conditions.

- Broadening our understanding of how organic-rich natural groundwater and undisturbed sand affect the transport of DNAcol.
- Assessing the impact of changes in ionic strength on the remobilization of attached and/or retained DNAcol under transient porewater chemistry conditions.
- Evaluating and validating the application of DNAcol as a multi-tracer in plot-scale studies on a hillslope.

1.6. RESEARCH OUTLINE

The dissertation begins with an introduction to tracer hydrology and the use of free DNA and DNA-based particles in hydrological studies in Chapter 1.

Chapter 2 presents a series of laboratory tests designed to evaluate the transport of DNAcol under varying porewater chemistries (demineralized water, NaCl, $CaCl_2$), flow rates, and sand grain size distributions. Saturated sand column experiments were conducted to identify optimal environmental conditions for DNAcol usage. Transport parameters of DNAcol were determined using the HYDRUS-1D model, followed by an analysis of colloid-grain surface interactions.

Chapter 3 systematically explores the effects of natural organic matter and ionic strength ($CaCl_2$) on the transport, retention and/or attachment, and release of DNAcol in saturated sand columns. The transport and release of DNAcol were examined under steady and transient porewater chemistry conditions.

Chapter 4 extends the investigation from Chapter 3 by further exploring the role of natural organic matter, comparing DNAcol transport and mass recoveries in sand columns using organic-rich natural groundwater versus synthetic groundwater without organic content. The study also examines how undisturbed soil affects DNAcol transport and release under both steady and transient conditions.

Chapter 5 explores the application of DNAcol as a multi-tracer in an event-based experiment conducted at a plot-scale hillslope in Germany, alongside a deuterium tracer experiment designed by Rinderer *et al.* [59]. This research aims to validate the tractability of DNAcol in the vadose zone and identify specific hillslope areas contributing to subsurface runoff.

Chapter 6 concludes the dissertation, discusses the challenges and limitations encountered in the research, and suggests potential insights for future studies on the application of DNAcol as a surrogate for colloidal contaminants in subsurface environments.

2

TRANSPORT CHARACTERISTICS OF DNA-TAGGED SILICA COLLOIDS AS A COLLOIDAL TRACER IN SATURATED SAND COLUMNS; ROLE OF SOLUTION CHEMISTRY, FLOW VELOCITY, AND SAND GRAIN SIZE

This chapter is based on:
Kianfar, B., Tian, J., Rozemeijer, J., van der Zaan, B., Bogaard, T. A., Foppen, J. W. (2022). Transport characteristics of DNA-tagged silica colloids as a colloidal tracer in saturated sand columns; role of solution chemistry, flow velocity, and sand grain size. Journal of Contaminant Hydrology, 246, 103954. [44]

In recent years, DNA-tagged silica colloids have been used as an environmental tracer. A major advantage of this technique is that the DNA-coding provides an unlimited number of unique tracers without a background concentration. However, little is known about the effects of physicochemical subsurface properties on the transport behaviour of DNA-tagged silica tracers. We are the first to explore the deposition kinetics of this new DNA-tagged silica tracer for different pore water chemistries, flow rates, and sand grain size distributions in a series of saturated sand column experiments in order to predict environmental conditions for which the DNA-tagged silica tracer can best be employed. Our results indicated that the transport of DNA-tagged silica tracer can be well described by first order kinetic attachment and detachment. Because of massive re-entrainment under transient chemistry conditions, we inferred that attachment was primarily in the secondary energy minimum. Based on calculated sticking efficiencies of the DNA-tagged silica tracer to the sand grains, we concluded that a large fraction of the DNA-tagged silica tracer colliding with the sand grain surface did also stick to that surface, when the ionic strength of the system was higher. The experimental results revealed the sensitivity of DNA-tagged silica tracer to both physical and chemical factors. This reduces its applicability as a conservative hydrological tracer for studying subsurface flow paths. Based on our experiments, the DNA-tagged silica tracer is best applicable for studying flow routes and travel times in coarse grained aquifers, with a relatively high flow rate. DNA-tagged silica tracers may also be applied for simulating the transport of engineered or biological colloidal pollution, such as microplastics and pathogens.

2.1. INTRODUCTION

Tracers are widely used in hydrological studies, such as tracking contamination in the subsurface. In recent years, DNA-tagged silica colloids (abbreviated to DNAcol) have been used as an environmental tracer in various applications, e.g., in fractured reservoir characterization [40], in a coarse-grained aquifer [39], in fractured crystalline rock [46], and at smaller scale for tomographic reservoir imaging [48]. The use of silica colloids tagged with DNA is not limited to water and oil applications: examples include pesticide spraying [49], and waste water sludge [43]. More recently, DNAcol were also used as a surrogate model to study the microbial transmission in healthcare [60], and in the setting up of a "DNA-of-things" as the storage material [61]. The main advantages of tagging silica colloids with DNA are that it gives the colloids a unique DNA sequence and enables analysis at low concentrations using standard microbial techniques (e.g. quantitative polymerase chain reaction (qPCR)). These properties provide us with a virtually unlimited amount of unique tracer particles which make DNAcol a promising tool for hydrological and colloidal contaminant transport research.

Transport of colloids through saturated porous media is often described at the continuum scale (i.e., macroscopic scale) with the classic advection–dispersion partial differential equation (e.g. [62–65]), using a first-order kinetic retention parameter. This parameter can be correlated to colloid filtration theory using a mechanistical

model, including the use of a correlation equation (e.g. [66–71]), to estimate the trajectory of a colloid near a collector. More recently, the importance of colloid size dependent dispersion [72], gravity effects of colloids [73], mechanical equilibrium and maximum retention function [74, 75], fraction of the collector surface area (S_f) contributing to colloid attachment, and importance of applied hydrodynamic and adhesive torques [76, 77], concentration dependent colloid transport [76], and nanoscale heterogeneity [77–79] were explored and highlighted.

When silica colloids travel in columns of saturated quartz sand, their transport can be characterized by first order kinetic attachment to the sand [80–87], which is more or less depending on ionic strength [81, 83, 88], pH [88], pore water flow velocity ([81] their exp. 5 and 9), composition of the collector surface [80, 85, 89–91] or presence of humics [92, 93]. Furthermore, size exclusion effects might play a role (e.g. Fig. 10a of [94], [39]). Finally, silica colloids can enhance contaminant transport [95–98]. In the subsurface, therefore, all of the aforementioned physicochemical factors can influence aggregation, deposition, and remobilization of colloidal matter. To better predict the behavior of DNAcol as a tracer or surrogate we conducted a series of saturated sand column experiments.

The objective of this study was two-fold. First, to systematically explore the use of DNAcol in columns of quartz sand in order to compare deposition kinetics with existing literature. Second, we wanted to identify removal of DNAcol under various saturated porous media conditions in order to start predicting their value in environmental applications. Thereto, we carried out column experiments with DNAcol in which we varied solution chemistry, flow rate and grain size. In addition, we used HYDRUS-1D to quantify transport parameters and assist in analyzing colloid-grain surface interaction processes.

2.2. MATERIALS AND METHODS

2.2.1. THE DNA-TAGGED SILICA PARTICLE

The DNAcol was composed of a silica outer shell (SiO_2), a layer of DNA molecules, and a silica core [34]. A 1 ml 10 mg ml^{-1} DNAcol suspension, equal to ~4×10^{11} particles ml^{-1} [34], was kindly fabricated and provided by the Functional Materials Laboratory Group at ETH Zurich. Average diameter of DNA-tagged silica particles was ~270 nm, and density of 2.2 g cm^{-1} [49]. The double-stranded DNA sequence, which was sandwiched between silica core and protective cover layer, was 80 nucleotides long (details in the Appendix A.1). Prior to use, DNAcol was washed in a diluted commercial bleach solution (10 μl bleach to 10 ml water) to ensure no free DNA in suspension. Then, 10000× diluted DNAcol batches (5 μl to 50 ml; DNAcol concentration = 0.001 mg ml^{-1} or ~ 4×10^{7} particles ml^{-1}) were prepared in Milli-Q water, NaCl (33 mM, pH=5.5), and $CaCl_2$ (41 mM, pH=5.8). The effect of solution chemistries on the stability of DNAcol was measured via the zeta potential (ζ) using a NanoSizer (Nano Series, Malvern Instrument Ltd., UK). The ζ was determined from electrophoretic mobility using Smoluchowski's formula (at 25 °C temperature, and the dielectric constant of water medium 78.54). Thereto, three DNAcol batches were prepared in Milli-Q water (resistivity 18 MΩ cm), NaCl (IS=33 mM, pH=5.5),

and $CaCl_2$ (IS=41 mM, pH=5.8) in a 10 ppm concentration (0.01 mg ml^{-1}). After vortexing, ζ was -42.5±5.3 mV in Milli-Q water, -33.9±6.1 mV in NaCl, and -20.7±3.3 mV in $CaCl_2$ solution, respectively. We used these values for DLVO calculations (see Appendix A.4, Fig A.4-A.5).

2.2.2. POROUS MEDIUM

We used two different sand types. One was quartz sand (J.T. Baker, Inc., Phillipsburg, New Jersey) sieved to a fraction of 1000-1400 μm grain size range (coarse sand), and the other was so-called silver sand (M31, Sibelco, Belgium) sieved to a fraction of 500-630 μm grain size range (fine sand). To remove impurities, the sands were soaked in 65% concentrated 4N HNO_3 solution for 2 h at 100 °C. After cooling, the acid was decanted and the sand was rinsed repeatedly with deionized water until the pH stabilized around 7 and the electrical conductivity of the rinse water became less than 1-2 μS cm^{-1}. Then the acid-washed sand was oven dried for 24 h at 105 °C. The clean and dry sand was stored in a capped container for further use. The zeta potential of both fine and coarse sand was determined with a crushed fraction. Thereto, both fine and coarse sand were ground manually using a mortar and pestle. Then, ~0.5 g of crushed sand was added to 10 ml of each Milli-Q water, NaCl, and $CaCl_2$ solution. Each suspension was vortexed three times and allowed to settle for 2 min. The supernatant was used for measuring the zeta potential. The ζ-potential for fine sand was -34.4±5.4 mV (in Milli-Q water), -39.4±5.4 mV (in NaCl), and -15.3±4.3 mV (in $CaCl_2$) while for coarse sand it was -33.1±4.7 mV (in Milli-Q water), -41.2±7.1 mV (in NaCl), and -11.3±4.5 mV (in $CaCl_2$). The mean and standard deviation values are calculated from the average of mean and standard deviation of triplicate measurements.

2.2.3. COLUMN EXPERIMENTS

Soil column experiments were conducted with adjustable-height chromatography columns, made of borosilicate glass (Omnifit, Cambridge, UK). The column, with an inner diameter of 2.5 cm, was wet-packed with one of the two sands to a height of 6.5 cm. Before packing the column, CO_2 gas was flushed into the dry sand to increase wettability of the sand upon wet-packing. During wet-packing, the column was vibrated with a plastic bar to facilitate uniform packing. After connecting the pump, demineralized water was injected in an upward direction at a constant flow rate. Typically, two columns were prepared; one with fine sand, and one with coarse sand. These columns were run in parallel at similar pump speed (see Table 2.1 for an overview). First, 2-2.5 pore volumes of NaCl solution was injected in order to determine dispersivity and porosity of the sand. Thereto, at specific time intervals, as a proxy for NaCl-concentration, the Electrical Conductivity (EC) of the effluent was measured. Then, the influent solution was switched back to Demineralized water (DM water) to flush out remaining NaCl solution. Next, a 2-2.5 Pore Volumes (PV) of a 10^{-3} mg ml^{-1} (~ 4×10^{7} particles ml^{-1}) DNAcol suspension in DM water under continuous mixing was injected in the column, followed by at least 3 PV flushing with DNAcol-free solution. The column was flushed overnight with NaCl, and then

a 2-2.5 PV of a 10^{-3} mg ml^{-1} (~ 4×10^{7} particles ml^{-1}) DNAcol suspension in NaCl under continuous mixing was injected in the column, followed by at least 3 PV flushing with DNAcol-free solution. The column was flushed overnight with $CaCl_2$, and then a 2-2.5 PV of a 10^{-3} mg ml^{-1} (~ 4×10^{7} particles ml^{-1}) DNAcol suspension in $CaCl_2$ under continuous mixing was injected in the column, followed by at least 3 PV flushing with DNAcol-free solution. So, per column, a total of 4 experiments were carried out. The tubing pore volume was negligible.

Table 2.1.: Overview of experimental conditions for column experiments with DNAcol.

Solution chemistry[1]	Sand[2]	Flow[3]	Data shown in Fig 2.1	Remarks
DM water	Coarse	High	1E	
	Fine	High	1F	
	Coarse	Low	1G	
	Fine	Low	1H	
NaCl	Coarse	High	1I	
	Fine	High	1J	
	Coarse	Low	1K	Extra Milli-Q water flush
	Fine	Low	1L	Extra Milli-Q water flush
$CaCl_2$	Coarse	High	1M	
	Fine	High	1N	
	Coarse	Low	1O	Extra Milli-Q water flush
	Fine	Low	1P	Extra Milli-Q water flush

[1] DM: demineralised water; [NaCl]= 33 mM (pH=5.5); [$CaCl_2$]= 41 mM (pH=5.8).
[2] Coarse sand: 1000-1400 μm; fine sand: 500-630 μm.
[3] High flow: pump rate 0.8±0.02 ml min^{-1}; low flow: pump rate 0.16±0.01 ml min^{-1}.

For a number of experiments ('Extra Milli-Q water flush' in see Table 2.1) at the end of the experiment we applied a 3 PV flush of demineralized water in order to mimic transient chemistry conditions and to possibly re-entrain previously attached DNAcol. Most experiments were carried out in duplicate. For each experiment ~0.8 ml column effluent was collected in a 20-ml centrifuge tube using a fraction collector (OMNICOLL, LAMBDA Laboratory Systems, Switzerland). Of this, 100 μl was pipetted into a 1.5 ml Eppendorf vial and stored at 4 °C in the fridge for DNA release and qPCR analysis later.

2.2.4. DNA RELEASE AND QPCR ANALYSIS

The concentration of DNA in a sample was determined using the qPCR technique. In order to dissolve the silica shell and release the encapsulated DNA, 20 μl of collected sample was mixed with 1 μl of buffer oxide etch (BOE; a mixture of NH_4FHF (Merck, Germany) and NH_4F (Sigma-Aldrich), diluted 10 times in Milli-Q water; see for details Paunescu *et al.* [34]). After this, 100 μl Tris-HCl buffer at pH

8.3 was added to adjust pH to near-neutral value, and of this 5 μl was added to each qPCR tube (8-tube strip) (BIOplastics, the Netherlands), together with 1 μl of each forward and reverse primer (DNA oligomers (Biolegio, Nijmegen, Netherlands)): 5′-GAT TAGCTT GAC CCG CTC TG-3′ and 5′-AGT TGG GGT TTG CAG TTG TC-3′), 10 μl Kapa SYBR Green Fast qPCR Mastermix (Kapa biosystems, Sigma-Aldrich), and 3 μl DEPC treated water (Sigma-Aldrich). The pre-qPCR samples tubes were closed with optical 8-cap strip (BIOplastics, the Netherlands). Sample preparation of first set of experiments was done by manual pipetting; later, qPCR sample preparation was carried out using a pipetting robot (QIAgility instrument; Qiagen, Hilden, Germany). DNA concentrations were determined using a Mini-Opticon (Bio-Rad, Hercules, CA, USA) programmed to run 400 sec at 95 °C and then 42 cycles of [14 sec at 95 °C, 27 sec at 58 °C, 25 sec at 72 °C]. Results in terms of threshold cycles (Ct) were analyzed using the Bio-Rad CFX Manager 3.1 software and applying the regression function in the Cq determination mode (as opposed to the manually adjustable baseline subtraction). DNAcol concentrations were then read from a calibration curve from duplicated samples, which was prepared for each solution chemistry (Appendix A.2; Fig. A.1-A.3.

2.2.5. MODELING TRANSPORT OF DNACOL

Transport of silica colloids in saturated porous media can be described by the advection-dispersion equation with first order attachment and detachment (e.g. [81, 83, 84, 92]):

$$\frac{\partial C}{\partial t} + \frac{\rho_b}{\theta}\frac{\partial S}{\partial t} = \lambda_L v \frac{\partial^2 C}{\partial x^2} - v\frac{\partial C}{\partial x} \tag{2.1}$$

$$\rho_b \frac{\partial S}{\partial t} = k_{att}\theta C - k_{det}\rho_b S \tag{2.2}$$

where C is the concentration of silica colloid in the aqueous phase [ML^{-3}], S is the concentration of silica colloid in the solid phase [MM^{-1}], ρ_b is the dry bulk density [ML^{-3}], θ is volumetric water content [M^3M^{-3}], t is time [T], λ_L is the dispersivity [L], v is the pore water velocity [MT^{-1}], x is the traveled distance [L], and k_{att} and k_{det} are attachment and detachment rate coefficients [T^{-1}], respectively. A large number of advection-dispersion models have been developed to describe solute and colloid transport in porous media analytically and/or numerically, either with one- or two-site kinetic attachment or adsorption [99–104]. In this work, we used HYDRUS-1D [105] to determine values of dispersivity, porosity, and attachment and detachment rate coefficients. The first two parameters (i.e., dispersivity (λ_L), porosity (ϵ)) were determined by fitting the NaCl tracer data, while for the latter two parameters (first-order attachment (k_{att}), and detachment rate coefficients (k_{det})) the DNAcol breakthrough data were used by invoking porosity and dispersivity values obtained from the NaCl tracer experiment, whereby the code was set to log-resident concentrations. In doing so, we excluded colloid size dependent dispersivity and mechanical equilibrium (see Introduction section). The former assumption underestimated colloid dispersivity. Also, gravity effects were excluded,

since the DNAcol was small resulting in negligible restricted settling velocity as a function of column orientation and flow direction [73]. The model presented here (Eqs. 2.1 and 2.2) is implemented in the HYDRUS-1D software package [106]. Briefly, a Galerkin-type linear finite element method was used for spatial discretization, while finite difference methods were used to approximate temporal derivatives, and a Crank–Nicholson finite difference scheme was used for solution of the advection–dispersion equation. Parameter optimization was carried out by first defining an objective function [107], which was then minimized using the Levenberg-Marquardt non-linear minimization method, which is a weighted least-squares approach based on Marquardt's maximum neighborhood method [108]. We used HYDRUS-1D because it is open source, widely-used and well documented, and it includes various colloid transport models, including the one we used.

The dimensionless sticking efficiency, α, was then determined from (e.g. [70, 82, 109–111]):

$$\alpha = k_{att-HUDRUS}\frac{2d_g}{3(1-\epsilon)v\eta_0} \tag{2.3}$$

where $k_{att-HYDRUS}$ is the attachment rate coefficient obtained from HYDRUS modeling, η_0 is the single collector efficiency [-], ϵ is porosity of sand column [-], and d_g the collector or sand grain diameter [L]. The sticking efficiency is defined as the fraction of DNAcol sticking to the sand grain surface over the total DNAcol colliding with the sand grain surface. When α=0, then no DNAcol would stick to the surface and when α=1 then all DNAcol colliding would also stick. The collision efficiency was determined using the Tufenkji and Elimelech (TE) correlation equation [70]. Thereto, 2.2 g cm^{-3} was assumed for the DNAcol [49], while the Hamaker constant was assumed to be 0.7×10^{-20} J for the combination of silica-water-silica [112].

2.2.6. EVALUATING HYPOTHETICAL DNACOL REMOVAL UPON TRAVELED DISTANCE

When the flow field is in steady state, and when transport of DNAcol is considered to be one-dimensional and in steady state without detachment, then the mass balance for DNAcol in the fluid phase reduces to:

With boundary conditions

$$\lambda_L v\frac{\partial^2 C}{\partial x^2} - v\frac{\partial C}{\partial x} - k_{att}C = 0 \tag{2.4}$$

$$C(0) = C_0 and \frac{\partial C}{\partial x}(\infty) = 0 \tag{2.5}$$

equation 2.4 can be solved analytically [113]:

$$C = C_0 \exp\left\{\frac{\left(v - v\left(\frac{4k_{att}\lambda_L v}{v^2}\right)^{\frac{1}{2}}\right)x}{2\lambda_L v}\right\} \tag{2.6}$$

whereby

$$k_{att} = \frac{3(1-\epsilon)}{2d_g} v\eta_0\alpha \tag{2.7}$$

For sticking efficiency values obtained from our experiments, a series of hypothetical collector grain sizes, and a representative Darcy groundwater flow velocity, we used Eqs. 2.6 and 2.7 to predict DNAcol removal as a function of transport distance and to evaluate the usefulness of DNAcol in aquifer experiments at three different distances.

2.3. RESULTS

2.3.1. COLUMN BREAKTHROUGH CURVES (BTCS)

In case of NaCl, from 0-0.5 PV, the relative concentration $(C/C_0)_{NaCl}$, whereby C is the effluent EC-value as a proxy for NaCl concentration and C_0 the influent EC-value, was around 1×10^{-3} (see Fig. 2.1A-D). The values were not lower, since the EC of the sand column effluent prior to NaCl injection was around 1-2 μS cm^{-1}, and the EC of the NaCl tracer injected through the column was around 4×10^{3} μS cm^{-1}. At PV=1, $(C/C_0)_{NaCl}$ in all cases reached 0.5 and then continued to rise to 1. At PV 2-2.5 when $(C/C_0)_{NaCl}$ was ~1, we stopped injection of NaCl tracer. We considered this to be of sufficient contrast to determine dispersivity and porosity with HYDRUS-1D. The shape of the NaCl tracer breakthrough curve also confirmed the setup of the column in all cases was adequate, without leakage, and the front displacement inside the column was perpendicular to flow. In our experimental conditions, since Peclet numbers were high (>> 1; an indication of advection-dominant transport), the dispersivity value of DNAcol was taken from the NaCl tracer experiments.

Upon injection of DNAcol in DM water, $(C/C_0)_{DNAcol}$ started to rise slightly difference than the initial rise of the NaCl tracer (Fig. 2.1E-H). At 1.5-2.0 PV $(C/C_0)_{DNAcol}$ reached ~1 (Fig. 2.1E-H). During elution, $(C/C_0)_{DNAcol}$ rapidly decreased at PV 3-4, and at PV 4-6, the tail of the breakthrough curve in most cases flattened (Fig. 2.1E-H).

In case of DNAcol in NaCl more specifically the coarse sand - high flow case (Fig. 2.1I), the moment of rise, rising limb, plateau phase, and declining limb of $(C/C_0)_{DNAcol}$ were comparable to $(C/C_0)_{DNAcol}$ in DM water. In other words, attachment was negligible in this case. However, for the fine sand and/or low flow rates conditions, maximum $(C/C_0)_{DNAcol}$ during the plateau phase decreased from ~0.06 in Fig. 2.1J to ~0.02 in case of Fig. 2.1K and L. During elution (after PV 3.5), $(C/C_0)_{DNAcol}$ in NaCl declined sharply, and, after PV 4, became constant at ~ 1×10^{-3} (Fig. 2.1K-L). In case of Figs. 2.1K and L, an extra Milli-Q water flush was passed through the columns, giving rise to a peak $(C/C_0)_{DNAcol}$ at ~ PV 7 of ~200 times the maximum $(C/C_0)_{DNAcol}$ during the plateau phase in Fig. 2.1L.

In case of DNAcol in $CaCl_2$ (Fig. 2.1M-P), maximum $(C/C_0)_{DNAcol}$ during the plateau phase was 0.5 (Fig. 2.1M), and this value decreased to 0.015 for Fig. 2.1N and O, and to ~0.004 for Fig. 2.1P, respectively. After ~ PV 4, during elution, $(C/C_0)_{DNAcol}$ of Fig. 2.1M remained rather high at ~ 1×10^{-3}, while for the other

BTCs (Fig. 2.1N-P), $(C/C_0)_{DNAcol}$ during tailing was lower at ~ 1×10^{-4} to 1×10^{-3}. Like in the NaCl case, an extra Milli-Q water flush, which was passed through the columns (Figs. 2.1O and P), gave rise to a peak $(C/C_0)_{DNAcol}$ at ~ PV 7 of ~200 times the maximum $(C/C_0)_{DNAcol}$ during the plateau phase (Fig. 2.1P).

Finally, in some BTCs (e.g. Figs. 2.1I and J), from 0-0.5 PV the $(C/C_0)_{DNAcol}$ varied between 1×10^{-4} and 1×10^{-3}. This was because we used SYBR Green to detect DNA. SYBR-Green is a non-specific dye, which also shows amplification of non-target DNA. In fact, when $(C/C_0)_{DNAcol}$ was ~ 1×10^{-4} the detection limit of the qPCR analysis was reached. See Appendix A.2 for details regarding the standard curves, negative control, or no-template control (NTC), the lowest limit of detection level. The cutoff value was assigned to Ct=30.

2.3.2. MODELLING WITH HYDRUS AND DETERMINING STICKING EFFICIENCIES

All DNAcol BTCs could be well fitted with an attachment rate (k_{att}) and a detachment rate coefficient (k_{det}): except for the experiment in $CaCl_2$ fine sand-low flow yielding very low breakthrough, the R^2 values of the models ranged between 25 and 92% (Table 2.2). Fitted curves overestimated $(C/C_0)_{DNAcol}$ between PV 2 and 3, which gave rise to somewhat lowered R^2-values. Attachment of DNAcol in DM water was lowest with k_{att} ranging from 2.68×10^{-4} to 9.37×10^{-3}, while in $CaCl_2$ k_{att} of DNAcol was highest and ranged from 5.78×10^{-3} to 1.97×10^{-1}. For detachment, we observed the opposite: in DM water, k_{det} ranged from 2.32×10^{-3} to 1.07×10^{-1} and was relatively high, while in $CaCl_2$ k_{det} ranged from 8.56×10^{-6} to 5.25×10^{-2}, which was, relatively speaking, the lowest set of detachment rate coefficients. We identified three reasons for the 25-92% efficiency variations. Firstly, the high sensitivity of the qPCR technique, which is essentially an enzyme-based technique to determine concentrations, we used in detecting target DNA in each sample. A variation/error of Cq values was inevitable, because errors may propagate from pipetting or intrinsic variances of enzymatic efficiency due to minor temperature differences in the qPCR apparatus [31]. Secondly, the use of the one-site kinetic model (Eqs 2.1 and 2.2) may have oversimplified the true DNAcol transport processes in the columns. Thirdly, we observed that the model could not capture the earlier breakthrough curve of DNAcol data in several cases. This limitation was associated with assigning the dispersivity value of NaCl tracer to the DNAcol. As mentioned in the Methods Section, such assumption can lead to underestimation of the colloid dispersivity.

From k_{att} values determined with HYDRUS, we calculated the sticking efficiency values of the DNAcol per experiment by making use of Eq. 2.3 (Table 2.2). In DM water, sticking efficiencies ranged from 0.008-0.27 and in both NaCl and $CaCl_2$, sticking efficiencies ranged from ~0.02 to 1.56. Based on these values we concluded that sticking efficiencies in DM water were relatively lowest, while in NaCl and $CaCl_2$ they were highest. Also, there was no significant difference between the use of either NaCl or $CaCl_2$ solution chemistry when applying DNAcol. Sticking efficiencies higher than 1 are physically impossible, since the fraction sticking to the sand grain surface cannot exceed the total fraction DNAcol colliding with the sand grain surface. We attributed this to the irregular shapes of the collector silica grains; the correlation

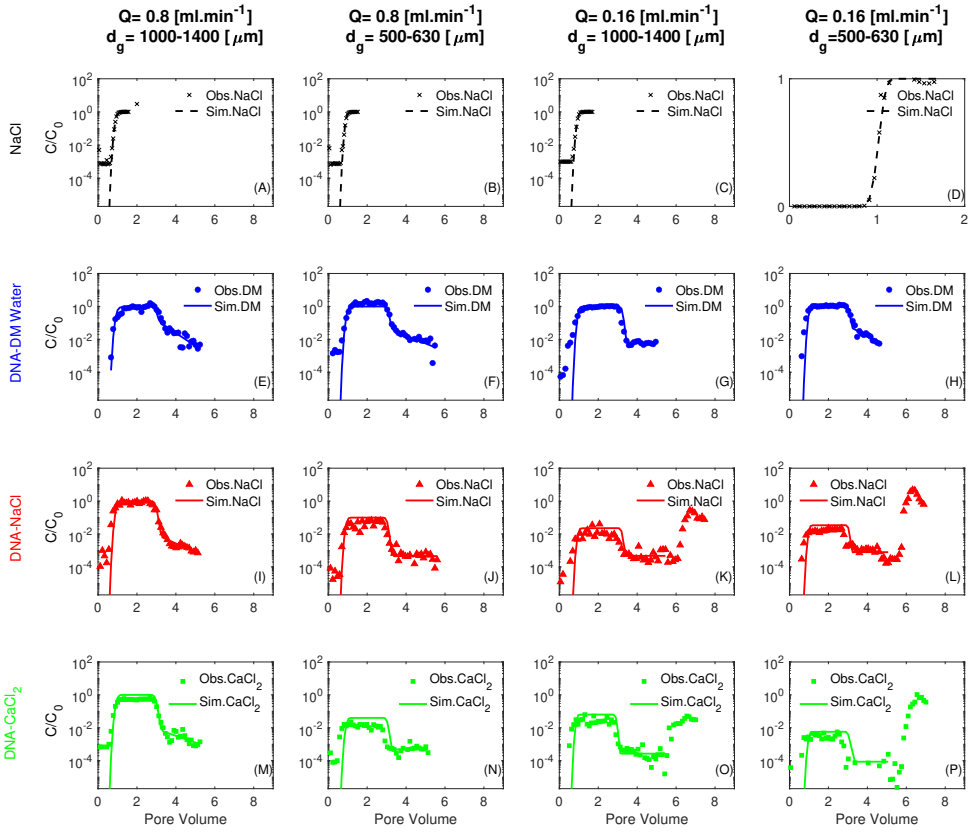

Figure 2.1.: Experimental data of NaCl tracer, DNAcol (symbols) and fitted breakthrough curves with HYDRUS (lines). Different panels illustrate relative concentrations as a function of pore volume within the sand columns at two different pump rates (0.8 ml min^{-1} and 0.16 ml min^{-1}), two types of sand (d_g=1000-1400 μm (coarse sand) and 500-630 μm (fine sand)), and three solution chemistries (DM water, NaCl, $CaCl_2$). First row: NaCl tracer; second row: DNAcol breakthrough curves in DM water; third row: DNAcol breakthrough curves in NaCl; final row: DNAcol breakthrough curves in $CaCl_2$; first column: coarse sand-fast flow, second column: fine sand-fast flow, third column: coarse sand-low flow, final column: fine sand-low flow. Note, panel (D) is in a linear scale.

equation we used in order to determine single collector efficiency was essentially developed for spherical collectors and not irregularly shaped collector grains, which likely gave rise to inaccuracies in determining sticking efficiencies. The calculated sticking efficiencies demonstrated that, in our experiments, a large fraction and in some experiments all DNAcol, colliding with the sand grain surface did also stick to the surface.

Table 2.2.: HYDRUS model parameters, statistics determined from curve fitting, and calculated sticking efficiencies.

Solution	Q	[ml min^{-1}]	0.8	0.8	0.16	0.16
	d_g	μm	1000-1400	500-630	1000-1400	500-630
NaCl	λ_L	[cm]	2.8×10^{-2}	2.2×10^{-2}	1.6×10^{-2}	1.2×10^{-2}
	ϵ	[-]	0.45	0.43	0.4	0.44
DNA-DM	k_{att}	[min^{-1}]	9.37×10^{-03}	3.14×10^{-03}	2.68×10^{-04}	7.49×10^{-04}
	k_{det}	[min^{-1}]	1.07×10^{-01}	6.60×10^{-02}	2.32×10^{-03}	1.78×10^{-02}
	R^2	[%]	92	44	60	66
	α	[-]	2.72×10^{-01}	2.49×10^{-02}	8.45×10^{-03}	9.51×10^{-03}
DNA-NaCl	k_{att}	[min^{-1}]	5.88×10^{-04}	1.43×10^{-01}	4.91×10^{-02}	3.84×10^{-02}
	k_{det}	[min^{-1}]	6.89×10^{-02}	5.54×10^{-05}	3.08×10^{-05}	3.83×10^{-05}
	R^2	[%]	51	56	53	40
	α	[-]	1.71×10^{-02}	$1.13\times10^{+00}$	$1.55\times10^{+00}$	4.87×10^{-01}
DNA-$CaCl_2$	k_{att}	[min^{-1}]	5.78×10^{-03}	1.97×10^{-01}	3.55×10^{-02}	5.89×10^{-02}
	k_{det}	[min^{-1}]	5.25×10^{-02}	1.05×10^{-04}	8.56×10^{-06}	1.65×10^{-05}
	R^2	[%]	47	40	41	25
	α	[-]	1.68×10^{-01}	$1.56\times10^{+00}$	$1.12\times10^{+00}$	7.48×10^{-01}

2.4. DISCUSSION

In this work, we aimed at investigating the sensitivity of DNA-tagged silica particles to solution chemistry, and studied mechanisms controlling transport and retention. Based on the HYDRUS-1D modeling of the observed breakthrough curves we concluded, that the transport of DNAcol in columns of saturated quartz sand could be well described by a first order kinetic attachment and detachment rate coefficient. However, for several cases, we observed discrepancies between experimental data and the fitted model. Likely, more elaborate models including two kinetic sites, gravity effects, colloid-size dependent dispersivity, and/or nanoscale heterogeneity need to be invoked in order to further reduce these discrepancies, which we, however, considered to be outside the scope of this work.

In their 14.5 cm sand columns, Saiers, Hornberger, and Harvey [84] arrived at a similar description of the silica colloid removal process, although their silica concentrations were much higher, the silica particles smaller (91 nm), and the zeta potential more negative (-65 mV). Furthermore, the ionic strength of the solutions

they used was much lower (10^{-3} M NaCl and pH 8.5), while Darcian velocities (~5.7 cm hr^{-1}) were comparable to ours (2 and 10 cm hr^{-1}). The removal of silica in their case, however, was less than 10% (Fig. 1: [84]), while in our case removal could be as high as 2-2.5 log-units or more than 90%. Johnson, Sun, and Elimelech [85]; their Fig. 2 used 10 cm columns of quartz sand (prolate spheroidal shaped, 0.32 nominal grain diameter), 300 nm silica colloids in dilute (10^{-3} M) KCl and, at comparable Darcian velocity or approach velocity as ours, arrived at similar first order kinetic removal of silica colloids, whereby their silica colloid removal rates (less than 5%) were in the same range as Saiers, Hornberger, and Harvey [84]. We think this difference is due to a combination of higher ionic strength used (3.3×10^{-2} M NaCl and 4.1×10^{-2} M $CaCl_2$) in our work, larger DNAcol diameter, and a less negative zeta-potential of the DNAcol. Ionic strength matters, as is clear from the work of Zeng, Shadman, and Sierra-Alvarez [83], Liu *et al.* [80], and Wang *et al.* [82]. These authors used a first order kinetic removal mechanism, and observed a decrease in maximum relative concentration as a function of ionic strength of the solution. On the other hand, under high salinity conditions (8-10% w/v NaCl + $CaCl_2$ brines) Kim *et al.* [81] observed aggregation of silica colloids, which could be transported through a 30 cm column of 0.35 mm Ottawa sand. The high Darcian flow (71 m day^{-1}) Kim *et al.* [81] used, could well have contributed to the lack of first order kinetic attachment.

In addition to first order kinetic attachment, we used a first order kinetic rate constant to describe detachment of previously attached particles, while maintaining identical ionic strength conditions. In all cases, detachment during the tail of the breakthrough curve (from PV 4-6) did not lead to high $(C/C_0)_{DNAcol}$ values, and was a few orders of magnitude lower than maximum $(C/C_0)_{DNAcol}$ from PV 2-3. Detachment rate constants were generally higher for the DM water cases plus the fast flow-coarse sand experiments, while in most experiments using NaCl and $CaCl_2$ solutions, detachment rate constants were low (in the order of 10^{-4}-10^{-5}). Despite the use of a first order kinetic detachment rate constant, in literature, without exception, silica colloid breakthrough curves are shown using a linear vertical axis [80–87], emphasizing the effect of flow velocity on the normalized peak value concentration, and the type of plateau (e.g., steady-state, increasing or decreasing over time) but which does not make clear how (un)important the detachment process is.

For the low flow NaCl and $CaCl_2$ cases (Figs. 2.1K, L, O, and P), at the end of the experiment, when we applied a flush of Milli-Q water, we observed massive reentrainment of previously attached particles. Zeng, Shadman, and Sierra-Alvarez [83] also observed massive reentrainment of silica colloids due to DM water flushing at the end of their experiments, which was up to 800 times maximum C/C_0. They attributed this to strong electrostatic repulsion between sand collector and silica colloids as the surfaces of both materials possessed a high concentration of negative charge under the experimental conditions used [83]. Also, Liu *et al.* [80], at the end of the column experiment after a flush of demineralised water, observed reentrainment of silica colloids up to 0.9 times maximum C/C_0. Their two-site dynamic model fitting results showed that reversible retention was related to first-order straining.

Since the average diameter of the DNAcol in our case was 270 nm and the median of the finest grain size we used was ~565 μm, the ratio of the two was 4.8×10^{-4}, which was well below 0.003, defined by Bradford, Torkzaban, and Walker [114] to be the lowest ratio for spherical grains at which straining would occur. In other words, in our case, we think straining was relatively unimportant, and the observed reentrainment was due to electrostatic interaction variations as a result of the transient chemistry conditions we applied. In order to make our case, we calculated the DLVO profiles and added them to the Appendix A.4. Since all zeta potential values were more negative than -20 mV, we assumed aggregation did not take place in our column experiments. From the DLVO profiles, a primary energy minimum and secondary energy minimum appeared for both NaCl and $CaCl_2$. However, in case of NaCl the energy barrier was higher (~600 k_BT) than for $CaCl_2$ (~100 k_BT), possibly giving rise to more attachment in the primary energy minimum for the latter case. Furthermore, the massive reentrainment of the attached DNAcol, when we applied the flushing step of Milli-Q water to the soil columns after NaCl and $CaCl_2$ experiments, was well explained by the DLVO profile in Milli-Q water.

From calculating the sticking efficiencies, we concluded that a large fraction, if not all, DNAcol colliding with the sand grain surface did also stick to that sand grain surface. From the reentrainment of DNAcol under transient chemistry conditions, we also conclude that in terms of DLVO theory, a large fraction of retained DNAcol resided in the secondary energy minimum. Hereby we assumed a negative charge for both silica sand and DNAcol, giving rise to a primary energy minimum due to attractive Van der Waals forces at close distance of the sand grain (nm range), an energy barrier further away, followed by a secondary energy minimum as a result of the net electrostatic forces between DNAcol and sand grain. In literature, we have not come across sticking efficiency values for silica colloid – silica collector grains under conditions of similarly charged surfaces. From transport of bacteria and viruses in aquifers, we know that sticking efficiencies must be in the order of 10^{-4} for viruses and 10^{-3} for bacteria in order to be able to travel through an aquifer (e.g. [115]), as sticking efficiencies in the order of 0.1-1 lead to the immediate removal of the biocolloid at short distance from where it enters the aquifer. Assuming a sticking efficiency of 0.59, which is the average of all our experiments, and a Darcy flow velocity of 300 m y^{-1}, and a porosity of 0.35, we determined the relative DNAcol concentration as a function of transport distance (Fig. 2.2) upon traveling through aquifers composed of 1-5 mm size silica grains. If the vial of 1 ml 10 mg ml^{-1} DNAcol suspension we used in this study, equal to $\sim4\times10^{11}$ particles ml^{-1}, would have been completely diluted in 1 l aquifer water, which would have been injected into the aquifer without further dilution, and if we assume a lowest limit of detection of 5 individual DNAcol in a 4 μl sample in a qPCR well (or 1.25×10^5 DNAcol per l), then a removal of $4\times10^{11}/1.25\times10^5 = 3.2\times10^6$ can be allowed for detection. This assumes no further dilution will take place due to diverging or converging flow lines in the aquifer (e.g. due to injection or abstraction). Also, this assumes the aquifer is fully composed of negative surface charge, which is, due to the presence of minerals like calcite or iron (III) oxyhydroxide coatings around aquifer grains, not very realistic. In such cases, removal of DNAcol will likely be higher [85, 89, 91].

Finally, this assumes no detachment is taking place, which is not true: in reality detachment takes place, but with such slow detachment rate that it has negligible effect.

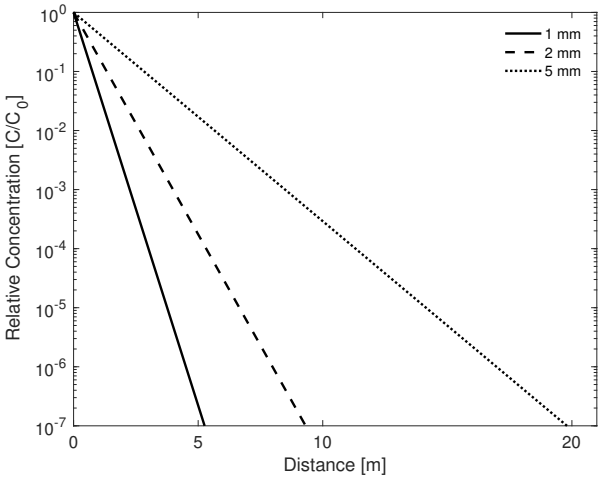

Figure 2.2.: Hypothetical case of DNAcol for various collector grain sizes (Darcy velocity = 300 m y^{-1}; sticking efficiency = 0.59; other parameter values: see a print-out of the calculation in the Appendix A.3.

For an aquifer composed of 1 mm silica grains, the maximum traveled distance would be ~5 m and for a 5 mm silica grain aquifer, maximum travel distance would be ~20 m. Larger transport distances are of course possible by increasing DNAcol injection mass or by up-concentrating sample volumes. This example serves to illustrate the potential of DNAcol: for fine grained aquifers (e.g. silts, clays, or mixtures) DNAcol will have limited applicability under natural groundwater chemistry, since the particle will not travel very far. Straining of DNAcol in such conditions will of course further limit DNAcol transport. Also, due to this DNAcol mass loss (attachment, straining, etc.), it will be impossible to determine the entire DNAcol mass and to prepare a mass balance. Also, since chemical conditions in the aquifer will be transient in nature by default, previously attached DNAcol can likely be reentrained. For aquifers predominantly composed of silica, DNAcol can be used in high concentrations in case of short distance, high flow, coarse aquifer grain conditions to map contaminant sources, understand flowpaths and determine travel times. There is a fair chance the aquifer grains will be covered by a layer of humic substances and/or a biofilm. In those cases, reaching the secondary minimum might be sterically hindered, which reduces DNAcol attachment and increases transport distance. On the other hand, Zhang *et al.* [93] observed clustering of Si nanoparticles and humic acid due to calcium bridging, which increased retention, due to the presence of Ca^{2+}, so those same humic substances can also increase attachment and reduce transport distance. Finally, the DNAcol can be pre-conditioned, whereby

the formation of an eco-corona at the outer surface of each individual DNA silica colloid is allowed to take place (e.g. [116–118]), in order to reduce removal and to enhance DNAcol transport. For those conditions, the fate of each unique DNAcol should be studied, and more research work is required.

2.5. CONCLUSIONS

We are the first to explore the deposition kinetics of this new DNA-tagged silica tracer for different pore water chemistries, flow rates, and sand grain size distributions in a series of saturated sand column experiments in order to predict environmental conditions for which the DNA-tagged silica tracer can best be employed.

Based on the HYDRUS modeling of the observed breakthrough curves, we concluded that the transport of the DNAcol in columns of saturated quartz sand could be well described by a first order kinetic attachment and detachment rate coefficient. Attachment was primarily in the secondary energy minimum, so the DNAcol could be reentrained under transient flow conditions. Based on calculated average sticking efficiencies, we concluded that a large fraction, if not all, the DNAcol colliding with the sand grain surface did also stick to that sand grain surface. Therefore, the potential of current DNAcol as a tracer for fine grained aquifers (e.g. fine sand, silts and natural groundwater) will be limited, since the particle will not travel very far. For such cases, DNAcol with different physico-chemical characteristics need to be developed. For sandy aquifers, the DNAcol can be used potentially in high concentrations in case of short distance (i.e. meter scale), high flow velocities, coarse aquifer grain conditions and distinct preferential flow paths to map contaminant sources, understand flowpaths and determine travel times. Overall, the DNAcol exhibited some limitations for the application as a generic hydrological tracer in subsurface flow, especially in the presence of fine grains or low flow velocity. Despite such limitations, DNAcol showed potential to be used as colloidal tracer to study fate and transport of biological and engineered colloidal particles (like pathogens or microplastics).

3

Natural Organic Matter and Ionic Strength ($CaCl_2$) Affect Transport, Retention and Remobilization of Silica Encapsulated DNA Colloids (DNAcol) in Saturated Sand Columns

This chapter is based on:
Kianfar, B., Hassanizadeh, S. M., Abdelrady, A., Bogaard, T., Foppen, J. W. (2023). Natural organic matter and ionic strength (CaCl2) affect transport, retention and remobilization of silica encapsulated DNA colloids (DNAcol) in saturated sand columns. Colloids and Surfaces A: Physicochemical and Engineering Aspects, 678, 132476. [45]

In the terrestrial environment, interactions between natural organic matter (NOM) and colloids can lead to the formation of an environmental corona around colloids, influencing their transport behaviour and, ultimately, their ecotoxicity. We used a synthetically designed colloid tagged with DNA (DNAcol) as a surrogate for natural colloids and investigated its transport in saturated sand columns. We varied the concentrations of NOM and ionic strength ($CaCl_2$), to better understand the transport and release of DNAcol in porous media under both steady and transient porewater chemistry conditions. In addition, we aimed to understand the main factors that control deposition and release of DNAcol under tested conditions. To induce transient chemistry, we replaced the injection solution containing NOM and/or $CaCl_2$ with Milli-Q water. The results showed that the deposition rate of DNAcol was inversely proportional to the concentration of NOM. The deposition rate increased significantly even under low ionic strength ($CaCl_2$) conditions of tested conditions. Notably, the influence of NOM on the transport of DNAcol was most pronounced at the lowest range of $[Ca^{2+}]$/DOC ratios, and the attachment of DNAcol to the sand grains was negligible. Moreover, the results showed while the DLVO theory captured the general trend of experimental results, it significantly underestimated the deposition of DNAcol in the presence of $CaCl_2$. Under transient porewater chemistry conditions, colloid remobilization was observed upon flushing the column with Milli-Q water, leading to a secondary peak in the breakthrough curves. We observed that under transient porewater chemistry conditions, when the ionic strength of the solution was 10 mM, the magnitude of the remobilization peak was more significant compared to conditions with 1mM ionic strength. Our work emphasized the complex interplay between water quality on the one hand and deposition and release of colloidal matter in saturated porous media on the other hand.

Graphical Abstract

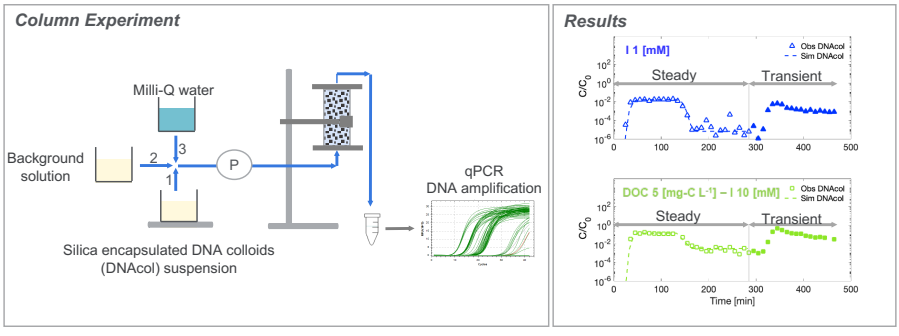

3.1. INTRODUCTION

Predicting the fate and transport of engineered and biological colloidal matter in the environment has been proven to be essential in a variety of applications, including human health, and ecological risk management [119–121]. However, predicting the fate and transport of nanoparticles remains challenging, in particular in the natural environment [122].

The understanding of the transport and fate of colloidal matter in heterogeneous subsurface environments faces a primary challenge because the transport of colloidal matter is highly sensitive to chemical conditions of the subsurface environment. These conditions encompass factors such as pH [123], ionic strength [124–127], ion composition [128–130], and the presence of natural organic matter (NOM; e.g., [131–134]). Such chemical factors can impact deposition, as well as hetero- and homo-aggregation of colloidal matter, which is potentially leading to uncertainties in risk management.

NOM such as humic and fulvic substance, proteins, and extracellular polymeric substances can adsorb onto the surface of colloids, acting as surfactant- or polymer-coating material, and forming a soft-corona or environmental corona [116, 133, 135–137]. Adsorption of those macromolecules onto the surface of colloids can impact their stability [134, 138–140], transport [93, 124, 131, 133, 134, 138, 139, 141–148], and, ultimately, their eco-toxicity [148, 149]. Several studies have mentioned that the effect of NOM on the transport of the colloids is sensitive to various environmental factors, such as pH [131, 133, 144, 150, 151], ionic strength [131, 152], and ion composition [144]. Furthermore, atomic force microscopy showed that the thickness and mass of the adsorbed layer on the surface of particle (silver) and collector (mica) was dependent on ionic strength (as presence of Ca^{2+}) of the system, and the effects were different for particle and collector [137].

Another critical environmental implication of colloidal matter is related to its remobilization as a consequence of alterations in porewater chemistry or subsurface flow conditions. Previous research in this field has indicated that colloid release can occur due to variations in ionic strength and flow conditions [44, 77, 127, 131, 153–162]. In addition, the primary mechanisms and factors governing the deposition and transport of colloidal matter under steady and transient conditions may differ [77].

Specifically, changes in the ionic strength of porewater can impact the surface charge of both colloids and collectors, subsequently affecting the magnitude of the electrical double-layer energy and, consequently, the adhesive force. Furthermore, changes in ionic strength can influence the “zone of colloid-collector interaction”, a fraction of surface area where repulsive forces can be reduced or eliminated [163–165]. This suggests that under unfavourable conditions in the presence of a strong repulsive energy barrier, predicted by mean-field DLVO theory, the interaction can become locally favourable, depending on the extent of the heterodomain area occupying the zone of colloid-collector interaction [79, 165]. While a significant number of studies have focused on understanding the specific effects of physico-chemical environmental factors on the transport behaviour of colloidal matter under steady conditions, there has been less emphasis on systematically

examining the mechanisms responsible for the release of colloidal particles under transient porewater chemistry conditions. In this study, we used DNAcol, which consisted of silica-encapsulated-DNA particles [34], as a surrogate for colloidal particles. The primary advantage of DNAcol lies in its ability to extend the lower detection limit to the ppb level, due to the embedded DNA molecules on it [43]. Consequently, it might allow us to use it as a substitute for colloidal particles, addressing the challenge associated with colloidal detecting limits. Recently, more research focused on the applications of silica encapsulated-DNA in the subsurface [39–41, 46, 48]. In this study, we used DNAcol with the primary objective of enhancing our understanding of the individual and combined impacts of NOM and ionic strength ($CaCl_2$) on the transport, retention/attachment, and release of DNAcol under both steady and transient porewater chemistry conditions. This involved determining the attachment rate of DNAcol and evaluating its sticking efficiency. Additionally, our goal was to gain deeper insights into the impact of two tested factors, NOM and ionic strength ($CaCl_2$), on attachment/retention and release of DNAcol for steady and transient porewater chemistry conditions.

3.2. Materials and Methods

3.2.1. DNAcol

DNAcol was composed of a silica core, a layer of double-stranded DNA molecules, and a silica shell that protected DNA. DNAcol was fabricated and provided by the Functional Materials Laboratory at ETH Zurich. Details of DNAcol fabrication and quantification were described in Paunescu *et al.* [34]. In brief, DNAcol had a SiO_2 core and SiO_2 shell. The silica core was dispersed in isopropanol N-trimethoxysilylpropyl-N,N,N-trimethylammonium chloride (TMAPS) to alter its surface charge to a positive state [34]. Subsequently, a negatively charged double-stranded DNA (dsDNA) was added to adsorb DNA onto the functionalized silica surface [34]. Then, TMAPS was applied, and, to complete the process, a silica layer was added onto the dsDNAs-silica particle using tetraethoxysilane (TEOS) [34]. After the fabrication process, using ball milling, the agglomerated particles were broken down into individual particles. The mass density and refractive index of DNAcol were assigned to be 2.2 g cm^{-3} and 1.458, respectively [49]. Prior to using DNAcol, in order to ensure that there was no free DNA, the suspension was washed by adding 0.1 μL bleach to 1 mL of stock particle suspension. Then, the suspension was centrifuged at 60000 g for 6 min, the supernatant was removed, and the particle pellet was washed and re-suspended in Milli-Q water three times.

3.2.2. Stock Solution and Organic Matter Characterization

NOM used in this study was provided by Vitens, a Dutch drinking water company, and was extracted from groundwater [166]. The NOM molecular weight distribution (M_w) of the stock was similar to Caltran *et al.* [166]. The NOM concentration of the prepared stock solution was determined using the combusting technique with a Total Organic Carbon Analyzer (TOC, VCPN, Shimadzu, Japan), and the concentration of

organic matter we finally reported as dissolved non-purgeable organic carbon in mg DOC L^{-1} (mg-C L^{-1}). DNAcol was suspended in nine different solutions. The electrolyte stock solutions were prepared from Milli-Q water (resistivity 18 MΩ.cm, TOC < 3 ppb, Millipore, Switzerland), $CaCl_2.2H_2O$ was added to reach average ionic strengths (I) of 0 (no addition), 1 mM and 10 mM. The concentration of NOM was adjusted to achieve a DOC concentration of 0 (no addition), 5 and 20 mg-C L^{-1} (Table 3.1). All solutions were stored at 4 °C.

About 30 min before each column experiment DNAcol suspensions were prepared by spiking DNAcol into a 70 mL aliquot of stock solution, and then vortexed (3 × 10 s). Final concentration was ~1 mg L^{-1}.

3.2.3. CHARACTERIZATION OF DNACOL

The effect of solution chemistry on the stability of DNAcol was assessed with zeta potential (ζ-potential) and hydrodynamic diameter (d_h), using a ZetaSizer nano (Nano Series, Malvern Instrument Ltd., Worcestershire, UK) for freshly prepared DNAcol concentrations of 10 mg L^{-1}.

HYDRODYNAMIC DIAMETER (d_h)

Hydrodynamic diameter of DNAcol was measured using a Zetasizer (Zetasizer Nano S, Malvern Instr., UK) by dynamic light scattering at a backscatter light angle of 173°, a laser beam with wavelength of 633 nm, and temperature of 25 °C, using a square polystyrene cuvette (DTS0012). The d_h of DNAcol in every suspension was measured periodically 5 times over a 120 min approximate time frame. All measurements were carried out in a triplicate sequential auto-run for a duration of 60 s. The d_h was reported as a Z-average (Z-Ave) diameter with a corresponding polydispersity index (PDI), determined from the intensity autocorrelation function available in the Zetasizer software.

ZETA-POTENTIAL (ζ-POTENTIAL)

The zeta potential (ζ-potential) of DNAcol was determined with the same Zetasizer indirectly from electrophoretic mobility measurements at 25 °C, which were converted to zeta potential using the Smoluchowski equation. The dielectric constant of water medium is 78.54. The ζ-potential was measured using a U-shaped capillary cell that had gold electrodes (DTS1660). Prior to conducting the measurement, each U-shaped capillary cell was washed with ethanol, then rinsed with Milli-Q water several times, and next washed with the desired solution [167]. The ζ-potential of each DNAcol sample was measured in triplicate sequential auto-runs.

3.2.4. POROUS MEDIUM

We used quartz sand as the porous medium, sieved to a 630-800 μm size. The sand was soaked in 10% (v:v) concentrated HNO_3 for approximately 24 hours to remove the impurities (metal oxides) of the sand surface (adapted from Tian *et al.* [168]). Then, the sand was repeatedly washed with Milli-Q water until the pH stabilized

around neutral, and the electrical conductivity of the rinse water became ~2 μS cm^{-1}. Finally, the sand was oven dried at 105 °C for ~24 h.

3.2.5. Sand Column Experiments

A cylindrical acrylic column with an inner diameter of 2.7 cm and a height of 8 cm was filled with acid-washed sand. The columns were uniformly wet-packed using Milli-Q water, and the sand was added incrementally, while tapping the column. Two layers of mesh, one stainless-steel perforated layer and a small piece of nylon mesh, were placed at both ends of each column to ensure flow and tracer were distributed evenly throughout the column and to prevent clogging of tubing connected to the pump. The porosity of each sand column was determined in two ways: based on sand bulk density, assuming a sand grain density of 2.65 g cm^{-3}, and from curve fitting using HYDRUS-1D (see Section 3.2.9).

After packing the column, it was positioned vertically, and the inlet tubing of the column was connected to the pump. The flow was established in an upward direction. The column was flushed with Milli-Q water for more than 15 pore volumes, prior to conducting a tracer test with NaCl. For this NaCl tracer experiment, approximately 2.2 pore volumes (105 min) of NaCl was injected, followed by flushing with Milli-Q water. Then, the column was flushed with the desired solution for around 15 pore volumes to ensure the column was pre-equilibrated for the DNAcol experiment. The DNAcol experiments consisted of three phases: i) DNAcol injection phase (concentration of 1 mg L^{-1}) for 105 min (~2.2 pore volumes), ii) elution phase by injection of background (particle-free) solution for 180 min (~3.9 pore volumes), iii) transient porewater chemistry phase, by flushing the column with Milli-Q water for 180 min (~3.9 pore volumes). During the first two stages, DNAcol retention/attachment and detachment rate coefficients were determined. During the third stage (flushing with Milli-Q water) focus was on release of attached DNAcol. All column experiments were performed in duplicate, each time using cleaned and acid-washed sand. During the injection phase, the suspension was stirred continuously using a magnetic stirrer to ensure homogenous mixing. Over the time frame of DNAcol injection, 5 to 6 samples from the influent suspension were taken to determine DNA concentration and check stability of column influent (C_0).

Measured flow rates were 0.40 mL min^{-1} (±0.02 ml min^{-1}), corresponding to a Darcy velocity of 0.07 cm min^{-1}, and were determined before and after each experiment by gravitationally measuring columns effluent. Column effluent was collected continuously with a sampling period of 5 min using a fraction collector (OMNICOLL, LAMBDA Laboratory Systems, Switzerland). For the NaCl tracer experiment, the Electrical Conductivity (EC) of the column effluent was measured as an indicator of salt concentration using a conductivity meter (GMH 3430 Greisinger, Germany). For DNAcol, collected samples were stored at 4 °C, and every other sample was analysed using quantitative polymerase chain reaction (qPCR).

3.2.6. qPCR ANALYSIS

Of each column effluent sample, a 20 μL subsample was taken and used for qPCR. The qPCR protocol was adapted from Paunescu *et al.* [34] and Mikutis *et al.* [39]; and Kianfar *et al.* [44]. Details regarding qPCR protocol, master mix, and calibration curve are presented in the Appendix (section B.1). In brief, the calibration curve was based on the known concentration of DNA in dilution series. In this study, the calibration curve was performed for each solution chemistry and primer batch specifically. Each calibration curve consisted of an 8-fold serial dilution ranging from 100 mg L^{-1} (D_2) to 0.00001 mg L^{-1} (D_9) (Appendix, Fig. B.1). In addition to column effluent samples, to each qPCR run triplicate negative control samples (no template control (NTC)) containing ultra-pure water (DEPC-treated water), triplicate blank samples of column influent and effluent, and triplicate positive control samples in Milli-Q water, and in a desired background solution were added (Appendix, Fig. B.2). The two types of positive controls contained a concentration of 10 mg L^{-1} (corresponding to D_3 in the calibration curve) of DNAcol in Milli-Q water as a reference positive control, and the other one in the solution used. We did that to ensure there was no inhibition of qPCR signal, to check reproducibility of qPCR signal, to investigate and to compare the stability of DNAcol in various solution chemistries, and -in case of Milli-Q water to check long-term interexperimental stability of DNAcol (Appendix, Fig. B.2).

3.2.7. RELATIVE MASS RECOVERY

The relative mass recovery (M) of DNAcol under steady and transient porewater chemistry conditions was determined from:

$$M = \frac{\sum q \Delta t_i \frac{(C_i + C_{i+1})}{2}}{q t_{inj} C_0} \times 100 \tag{3.1}$$

Where q [cm^3 min] is the flow rate, Δt [min] is the time interval between analyzed column effluent samples, C_i [g cm^{-3}] is the measured sample concentration, t_{inj} [min] is the duration of injection phase of DNAcol (105 min), C_0 [g cm^{-3}] is the DNAcol injection concentration. For steady porewater chemistry conditions, the time interval was from the beginning of the experiment till 285 min, and then for transient porewater chemistry conditions it ended at 465 min.

The mass recovery of DNAcol remobilized during transient porewater chemistry conditions was calculated relative to the mass of retained DNAcol at the end of the steady porewater chemistry conditions. This we tentatively defined as $M_{transient}/M_{retained}$, whereby $M_{retained}$ was calculated as:

$$M_{retained} = M_{injection} - M_{steady} - M_{porewater} \tag{3.2}$$

$$M_{porewater} = (A.L.\theta).C_{porewater} \tag{3.3}$$

Where $M_{porewater}$ was defined as the mass in fluid phase at the end of the steady porewater chemistry conditions (i.e., end of flushing column with background solution), A [cm^2] is column surface, L [cm] is column length, θ [-] is porosity of

the sand column, and ($A.L.\theta$) is equal to the pore volume of each sand column, $C_{porewater}$ represents the average DNAcol concentration in three column samples: the last sample collected during steady porewater chemistry conditions, which was taken at the end of the elution phase, along with the analysed samples preceding and following it.

3.2.8. Sticking Efficiency (α)

Based on colloid filtration theory [66], the deposition of colloidal particles in saturated porous media is governed by collector contact efficiency (η) and sticking efficiency (α). The single-collector contact efficiency (η_0) is associated with the frequency of colloids colliding with the grain surface and governed by diffusion, interception, and gravitational sedimentation [66, 169]. The sticking efficiency (α) is the probability that the particles colliding within saturated porous media will attach to the grain surface (as a collector). Typically, sticking efficiency (α) was obtained experimentally from breakthrough curve data (e.g. [70, 82, 110, 111, 169]):

$$\alpha = \frac{k_{att}}{\eta_0} \frac{2d_g}{3(1-\theta)v_p} \tag{3.4}$$

where k_{att} [cm^{-1}] is attachment or deposition rate coefficient, d_g [cm] is grain diameter, v_p [cm min^{-1}] is average pore water velocity, η_0 [-] is the single-collector contact efficiency. For determining η_0, we used the correlation equation proposed by Tufenkji and Elimelech (TE) [70] (Appendix, section B.4).

3.2.9. Modelling Transport of DNAcol

We used the advection-dispersion-adsorption (see e.g. [170, 171]) to model the macroscale transport of DNAcol:

$$\frac{\partial C}{\partial t} = \lambda_L v_p \frac{\partial^2 C}{\partial x^2} - v_p \frac{\partial C}{\partial x} - \frac{\rho_b}{\theta} \frac{\partial S}{\partial t} \tag{3.5}$$

$$\rho_b \frac{\partial S}{\partial t} = k_{att}\theta C - k_{det}\rho_b S \tag{3.6}$$

Where S [g g^{-1}] is the DNAcol on the solid phase, ρ_b [g cm^{-3}] is the dry bulk density, λ_L [cm] is the longitudinal dispersivity (λ_L= D/v, D: Dispersion coefficient), x [cm] is the travelled distance, and k_{att} and k_{det} [min^{-1}] are attachment and detachment rate coefficients, respectively.

The attachment rate coefficient (k_{att}) can be determined via inverse optimization of the advection-dispersion equation. In this study, we used HYDRUS-1D software [106] to estimate transport parameters. In this approach, first, porosity (θ) and dispersivity (λ_L) were determined from the normalized NaCl tracer experimental data (C/C_0) of each sand column. Then, with values of these two parameters fixed, attachment and detachment rate coefficients (k_{att} and k_{det}) were estimated. In HYDRUS, we employed the linear mode to determine attachment and detachment rate coefficients. We constrained the fitting during inverse modelling to a single

set of parameters for attachment (k_{att}) and detachment (k_{det}). This approach implied that the model treated the attachment and retention as a lump in k_{att}, and detachment and reentrainment as k_{det}. Attachment refers to immobilization of colloids onto the surface of the collector through primary energy minimum, whereas retention refers to the temporary retention of colloids [72].

As mentioned above, we assigned to DNAcol particles the same dispersivity value as obtained for NaCl tracer in order to prevent over-parameterization of the HYDRUS model during the inverse modelling of DNAcol transport results. However, this approach could lead to the underestimation of particle dispersivity [72], since the value also depends on particle size [72]. Additionally, prior research showed that the rate of colloidal deposition can be greater when the flow direction is upward compared to downward [73]. We did not consider the effect of particle settling due to the upward flow direction, given the small size of DNAcol even though its specific density of around 2.2 g cm^{-3}. Therefore, we expected a negligible effect on settling and deposition based on the flow direction.

3.2.10. DLVO INTERACTION ENERGY PROFILE

Derjaguin-Landau-Verwey-Overbeek (DLVO) was used to qualitatively explain the column breakthrough results [172, 173]. Total interaction energy as a function of separation distance was defined based on the sum of electrical double-layer (EDL) and van der Waals (vdW) energies (details in Appendix, section B.5).

3.3. RESULTS

3.3.1. CHARACTERIZATION OF DNACOL

The ζ-potential of DNAcol were negative for all tested conditions (Table 3.1). Average values varied from ~–50 mV to –17 mV, in the presence of DOC 20 mg-C L^{-1} to ionic strength of 10 mM. The measured ζ-potential of DNAcol in water was determined to be –33 mV. However, in the presence of DOC at concentrations of 5 and 20 mg-C L^{-1}, the ζ-potential became more negative, with average values of approximately –42 mV and –50 mV, respectively. Conversely, an opposing trend was observed when $CaCl_2$ was added, and it became –18 to –19 mV. This trend suggested that the presence of $CaCl_2$, lead to a decrease in the absolute value of the ζ-potential. This could be attributed to shielding of the surface charge of the DNAcol, and compression of the double layer [123, 133].

Conversely, in the presence of DOC at concentrations of 5 and 20 mg-C L^{-1}, the ζ-potential became more negative. This shift was possibly due to the adsorption of negatively charged organic matter onto the DNAcol surface. In order to assess colloidal stability of the DNAcol suspension, the ζ-potential was measured after 120 min. Changes in ζ-potential values over time were negligible. Average hydrodynamic diameter, d_h, of DNAcol in Milli-Q water was 311 nm, with a polydispersity index (PDI) of 0.24 (Table 3.1). The average d_h diameter of DNAcol for the tested conditions varied from 296 to 311 nm.

Table 3.1.: The average ζ-potential, and d_h with the corresponding polydispersity index (PDI) of DNAcol in various background solutions.

(I)	(DOC)	Abbreviation	ζ-Potential	d_h	PDI
[mM]	[mg-C L^{-1}]		[mV]	[nm]	[-]
Milli-Q water	-	Milli-Q water	-33.6±6.1	311±8.5	0.24
Milli-Q water	-	Milli-Q water	-34.4±5.3		
1	-	I1	-17.1±5.7	303±14	0.26
1	-	I1	-20.9±6.0		
10	-	I10	-16.8±8.4	302±4	0.26
10	-	I10	-19.7±7.6		
Milli-Q water	5	DOC5	-47.0±11.1		
Milli-Q water	5	DOC5	-40.5±7.6		
1	5	DOC5-I1	-22.7±4.6		
1	5	DOC5-I1	-23.3±5.2		
10	5	DOC5-I10	-21.9±7.8		
10	5	DOC5-I10	-20.1±8.6		
Milli-Q water	20	DOC20	-49.7±13.4	302±9	0.24
Milli-Q water	20	DOC20	-50.8±7.4		
1	20	DOC20-I1	-25.0±6.1	297±6	0.24
1	20	DOC20-I1	-26.2±6.3		
10	20	DOC20-I10	-22.3±8.0	301±9	0.25
10	20	DOC20-I10	-21.3±8.4		

3.3.2. COLUMN BREAKTHROUGH CURVES

STEADY POREWATER CHEMISTRY CONDITIONS

Breakthrough curves of NaCl reached C_{max}/C_0 values of 1 with a characteristic S-shaped rising limb (Appendix, Fig. B.5) from which dispersivity and porosity of the sand column could be determined. Also, the start of the NaCl rising limb and DNAcol breakthrough curves coincided from which we concluded that pore size exclusion effects in our columns did not play an important role (Appendix, Fig. B.5).

Under steady porewater chemistry conditions, the breakthrough of DNAcol in Milli-Q water reached a plateau concentration ($C_{plateau}/C_0$) of 0.78-0.85, where $C_{plateau}$ represented the average concentration between 65-105 min. The mass recovery of DNAcol in this experiment was approximately 81% (Table 3.2). By adding $CaCl_2$ with ionic strength of 1 mM the plateau phase of the breakthrough curves substantially decreased to 0.02 ($C_{plateau}/C_0$), and only ~2% of injected particles mass was recovered from the sand column (Fig. 3.1B, Table 3.2). This outcome pointed towards a high attachment or retention of DNAcol within the sand column. The tailing of the breakthrough curves in this experiment, (Fig. 3.1B), exhibited a sharp decline, indicative of negligible detachment and/or reentrainment. In the case of 10 mM $CaCl_2$ solution, a similar low plateau phase was observed, accompanied by a rapid decrease in the declining limb. The relative mass recovery of DNAcol in

this case was only about 1% (Fig. 3.1C; Table 3.2).

In the presence of 5 mg-C L^{-1} DOC, the plateau concentration ($C_{plateau}/C_0$) ranged approximately from 0.83 to 0.89, suggesting a low attachment rate of DNAcol. In this case, the tailing of the breakthrough curve gradually decreased. The extended declining limb of the breakthrough curve indicated significant re-entrainment. Under this condition, the relative mass recovery of DNAcol was ~85% (Fig. 3.1D; Table 3.2). Upon increasing of porewater's ionic strength to 1 mM $CaCl_2$, while the concentration of organic matter was kept at 5 mg-C L^{-1} DOC, the plateau phase decreased to 0.45-0.52. This reduction highlighted a higher attachment or retention rate of DNAcol within the sand column. Similarly, to the previous case (Fig. 3.1D), the declining limb exhibited a gradual decrease, indicating re-entrainment. However, the mass recovery of DNAcol was only 49% (Fig. 3.1E; Table 3.2). Upon further increasing the ionic strength to 10 mM $CaCl_2$ while maintaining the concentration of 5 mg-C L^{-1} DOC, the mass recovery of DNAcol decreased even further to ~12% (Fig. 3.1F; Table 3.2).

In two experiments conducted with 20 mg-C L^{-1} DOC, both in the absence and presence of 1 mM $CaCl_2$ ionic strength (Fig. 3.1G-H), the breakthrough curves reached their highest plateau values, approximately 0.9. Similar to the previous conditions with a lower DOC concentration, both cases exhibited breakthrough curves with extended tails, followed by a gradual decline (Fig. 3.1G-H). The DNAcol mass recovery exceeded 90% in these experiments (Table 3.2). However, when 20 mg-C L^{-1} DOC was present along with an elevated ionic strength of 10 mM $CaCl_2$, the plateau of the breakthrough curve significantly decreased to a range of 0.14-0.28 (Fig. 3.1I). This pattern demonstrated an increased attachment or retention rate due to the higher ionic strength. Correspondingly, the mass recovery decreased to a range of 14-25% (Table 3.2).

In the experiment conducted at an ionic strength of 1 mM $CaCl_2$ with 20 mg-C L^{-1} DOC, we observed that the mass recovery of DNAcol exceeded 100%, which was likely associated with sensitivity of qPCR in detection of DNA. To evaluate variation between subsamples, for some of the experiments, each collected sample was analysed twice, with two different qPCR runs. The variations between these sub-samples was depicted as shaded areas in Appendix, Fig. B.6.

TRANSIENT POREWATER CHEMISTRY CONDITIONS

After the elution phase of DNAcol (i.e., injection of free-particles solution phase), the columns were flushed with Milli-Q water to induce remobilization of colloids. This we called transient porewater chemistry conditions. In all cases, (Figs. 3.1B-I; filled symbols), we observed a second peak upon flushing the column with Milli-Q water. It was evident from the breakthrough curves (Figs. 3.1B-I), the magnitude of the peak differed for the experiments.

Initially, we noticed that $M_{transient}/M_{injection}$ was always lower than 22% (Table 3.2). These results indicated that the fraction of remobilized DNAcol was relatively small. Additionally, in experiments conducted with the ionic strength ≤1 mM $CaCl_2$ the second peak (i.e., transient peak) was low. In contrast, for experiments with ionic strength 10 mM $CaCl_2$ the transient peak appeared rather sharp and more noticeable.

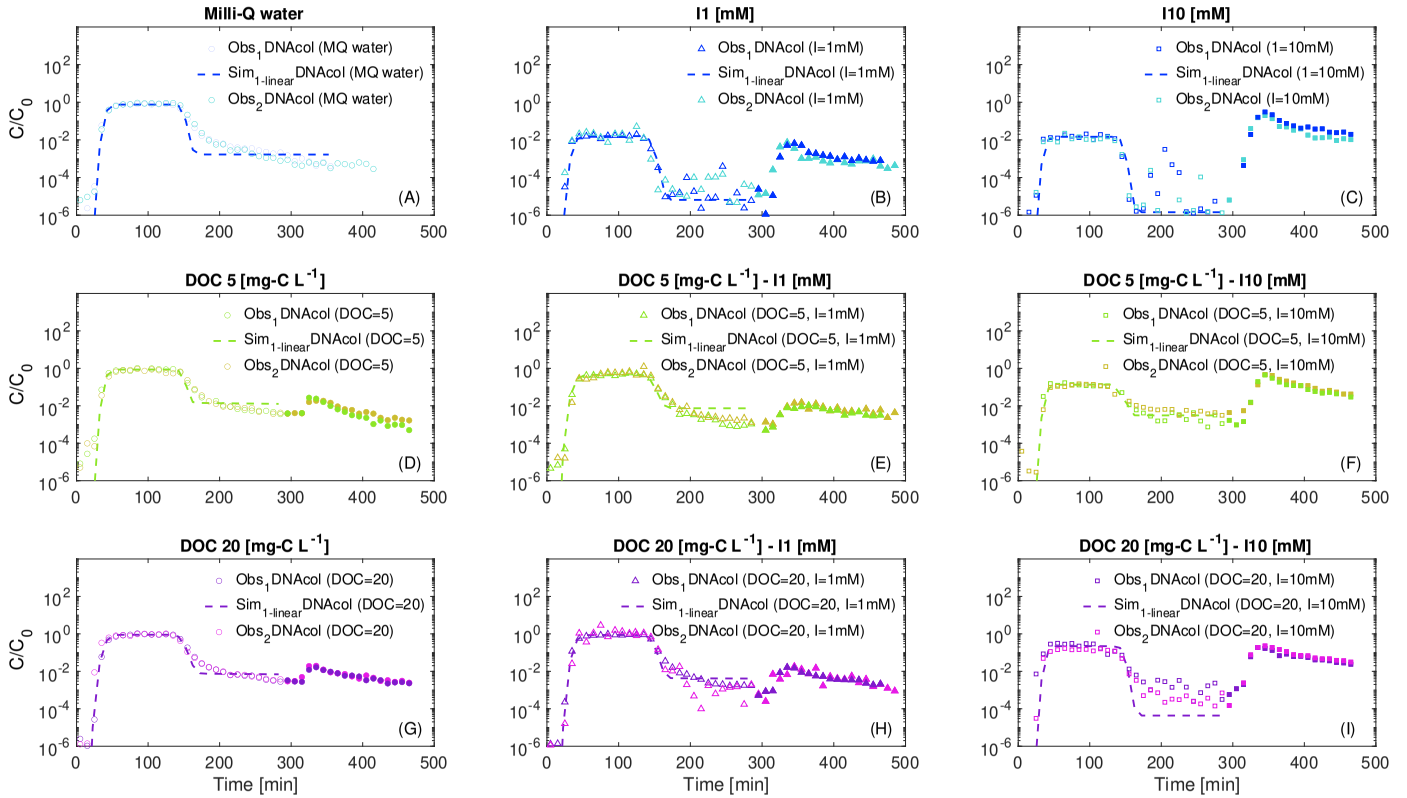

Figure 3.1.: DNAcol breakthrough curves (symbols) and HYDRUS model fits (dashed lines). Background solutions: (A) Milli-Q water, (B) 1 mM $CaCl_2$, (C) 10 mM $CaCl_2$, (D) DOC 5 mg-C L^{-1}, (E) DOC 5 mg-C L^{-1} with 1 mM $CaCl_2$, (F) DOC 5 mg-C L^{-1} with 10 mM $CaCl_2$, (G) DOC 20 mg-C L^{-1}, (H) DOC 20 mg-C L^{-1} with 1 mM $CaCl_2$, (I) DOC 20 mg-C L^{-1} with 10 mM $CaCl_2$. Open symbols represent DNAcol concentration during steady porewater chemistry conditions, and filled symbols represent transient porewater chemistry conditions.

Table 3.2.: Summary of relative mass recovery of DNAcol under steady porewater chemistry conditions ($M_{steady}/M_{injection}$), transient porewater chemistry conditions ($M_{transient}/M_{injection}$), and total mass recovery (M_{total}). C_{max}/C_0 is the maximum relative concentration.

Column Experiment	Solution	C_{max}/C_0 [-]	$M_{steady}/M_{injection}$ [%]	$M_{transient}/M_{injection}$ [%]	M_{total} [%]
A1	Milli-Q water	0.8	76.96	-	76.96
A2	Milli-Q water	0.9	85.20	-	85.20
B1	I1	0.02	1.62	0.29	1.91
B2	I1	0.05	2.07	0.24	2.30
C1	I10	0.02	1.59	11.31	12.90
C2	I10	0.04	1.28	7.54	8.82
D1	DOC	1.0	91.29	1.06	92.35
D2	DOC5	0.9	77.98	1.15	79.13
E1	DOC5-I1	0.6	46.85	0.81	47.67
E2	DOC5-I1	0.7	50.66	0.99	51.65
F1	DOC5-I10	0.2	13.31	17.21	30.52
F2	DOC5-I10	0.1	11.64	21.31	32.95
G1	DOC20	1.0	91.20	0.97	92.17
G2	DOC20	1.0	93.50	1.12	94.62
H1	DOC20-I1	1.0	88.66	0.88	89.55
H2	DOC20-I1	2.9	123.33	0.97	124.30
I1	DOC20-I10	0.3	24.63	10.18	34.82
I2	DOC20-I10	0.2	14.38	13.29	27.68

In detail, during transient porewater chemistry conditions, in the cases of ≤1 mM $CaCl_2$ the relative mass recovery ($M_{transient}/M_{injection}$) of DNAcol was around 1%, and for the three cases with an ionic strength of 10 mM $CaCl_2$ the relative mass recovery ($M_{transient}/M_{injection}$) of DNAcol ranged between ~7-21% (Table 3.2; Fig. 3.2A). When comparing the breakthrough curves DNAcol for ionic strength 1 and 10 mM $CaCl_2$ conditions, under steady porewater chemistry conditions, the obtained mass recovery was 1% and 2%, respectively. However, under transient porewater chemistry conditions, the relative mass recovery averaged around 0.26% and 9% for ionic strength 1 mM and 10 mM conditions, respectively (Table 3.2). The difference in the magnitude of relative mass recovery indicated distinct attachment and release patterns. Additionally, in the experiment with ionic strength of 10 mM $CaCl_2$, the relative mass recovery during transient porewater chemistry conditions was ~7 times higher than relative mass recovery during steady porewater chemistry conditions. In the experiment of 10 mM $CaCl_2$ with 5 mg-C L^{-1} DOC the relative mass recovery ($M_{transient}/M_{injection}$) was ~19%, which then reduced to ~12% in presence of 20 mg-C L^{-1} DOC (Table 3.2).

Fig. 3.2B shows also the mass recovery of DNAcol remobilized during transient porewater chemistry conditions relative to the mass of retained DNAcol at the end of the steady porewater chemistry conditions. Fig. 3.2B shows $M_{transient}/M_{retained}$ values were lowest for ionic strength of 1 mM $CaCl_2$. However, care should be taken

in interpreting the experiments in case of experiments 5, 20 mg-C L^{-1} DOC, and 20 mg-C L^{-1} DOC with ionic strength 1 mM as there was not much DNAcol mass retained in the column before flushing the column with Milli-Q water (Table 3.2: steady porewater chemistry conditions mass recovery ~85-106%). Note that, in a few cases of those experiments, the relative concentration of the samples was (C/C_0 slightly above 1.

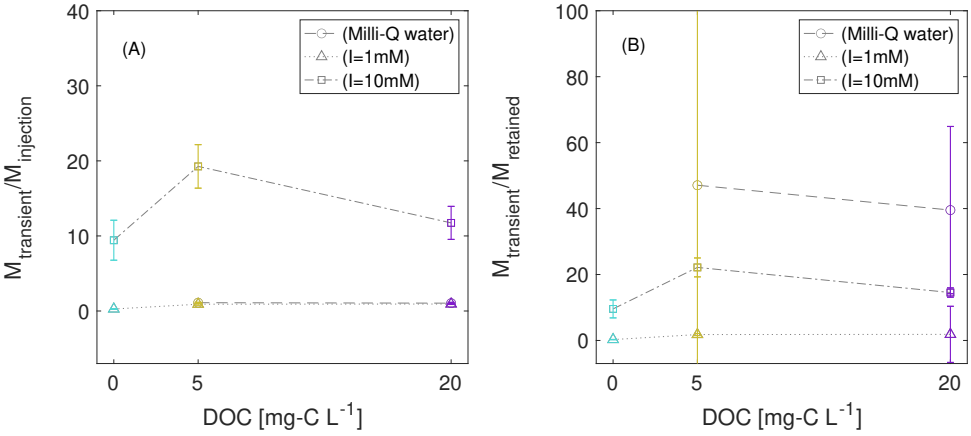

Figure 3.2.: (A) Ratios determined from mass recoveries during transient porewater chemistry conditions to mass injection as a function of DOC concentration ($M_{transient}/M_{injection}$), and (B) Ratios determined from mass recoveries during transient porewater chemistry conditions to mass retained in the column ($M_{transient}/M_{retained}$).

HYDRUS-1D Curve Fitting and Sticking Efficiencies

HYDRUS-1D was used to fit a model through the breakthrough data and determine attachment and detachment rate coefficients (Fig. 3.1, dashed lines; Table3.3). The overall values of the goodness of fits (R^2) ranged from 0.77-0.99. In general, attachment rate coefficients decreased as a function of DOC and increased as a function of ionic strength ($CaCl_2$) (Table 3.3). Furthermore, detachment rate coefficients decreased upon increase of ionic strength ($CaCl_2$), while an increase in DOC in most cases led to a higher detachment rate coefficient (Table 3.3). The calculated sticking efficiency (α) for Milli-Q water and porewater containing DOC was ~10^{-2} (Table 3.3). However, for porewater containing 1 or 10 mM of $CaCl_2$, it increased to 1, which indicated more favourable attachment conditions. In case both $CaCl_2$ and DOC were present, the order of magnitude of α was ~10^{-1}-10^{-2} (Table 3.3).

Interaction Energy Profiles

Upon increase of ionic strength as function of $CaCl_2$ concentration, the height of the energy barrier decreased and the depth of the secondary minimum increased (see

Table 3.3.: Estimated attachment-detachment rate coefficients from HYDRUS and sticking efficiency values (α). For the single-collector contact efficiency (η_0) of the sand-column system, the value was 0.04. Sticking efficiencies were calculated using d_p= 280 [nm], d_g= 0.715 [mm], Hamaker constant: H= 0.7×10^{-20} [J], ρ_p=2200 [kg m^{-3}].

Solution	HYDRUS		α
	k_{att}[min^{-1}]	k_{det}[min^{-1}]	Eq 3.4
Milli-Q water	6.65×10^{-3}	0.08×10^{-3}	0.07
I1	100.39×10^{-3}	0.002×10^{-3}	1.07
I10	103.39×10^{-3}	0.0002×10^{-3}	1.05
DOC5	3.52×10^{-3}	1.13×10^{-3}	0.04
DOC5-I1	19.58×10^{-3}	0.2×10^{-3}	0.20
DOC5-I10	48.72×10^{-3}	0.11×10^{-3}	0.49
DOC20	2.59×10^{-3}	0.76×10^{-3}	0.03
DOC20-I1	3.32×10^{-3}	0.35×10^{-3}	0.03
DOC20-I10	36.42×10^{-3}	0.003×10^{-3}	0.37

Appendix, Fig. B.3, Fig. B.4). This explained the higher attachment/retention rates at higher ionic strength. For example, for the case of DOC 5 mg-C L^{-1}, the height of the potential energy barrier was 465k_BT, while for the case of DOC 5 mg-C L^{-1} with ionic strength 10 mM, the height of the energy barrier decreased to 51k_BT, due to the diffuse double layer compressed. In addition, upon increase in ionic strength, the depth of the secondary minimum became pronounced. For the experiment of DOC 5 mg-C L^{-1} with ionic strength 10 mM, the depth of the secondary minimum was –0.358k_BT.

Upon increase in DOC concentration, DNAcol became more negative, leading to higher electrostatic repulsion between DNAcol. However, the DLVO profile could not capture the low attachment rate of DNAcol in the presence of DOC 20 mg-C L^{-1} with ionic strength 1 mM. In all cases, the deep primary energy well remained, mainly because ζ-potentials of DNAcol varied only slightly, while the mass recovery increased substantially. This observation highlighted the importance of steric repulsion in reducing the deposition rate of the DNAcol. In our study, we did not consider the effect of short-range repulsive forces and steric repulsion. The omission of steric repulsion was due to our inability to accurately define the thickness of the adsorbed NOM layer, the distance between the chains on the surface and adsorbed mass, which is crucial in the context of steric repulsion.

3.4. DISCUSSION

We started by examining the experiment with DNAcol suspended in Milli-Q water, without the adding of NOM and $CaCl_2$. In this experiment, we observed that the breakthrough curves reached the plateau phase with a ($C_{plateau}/C_0$) value of ~0.8,

Fig. 3.1A. The relative mass recovery of less than 100% could be attributed to the trapping of some of the particles in the dead-end pores [174], surface roughness, and the presence of patchwise macroscale and nanoscale heterogeneity on the surface of the grain, which could act as attachment sites [111].

In the experiments involving only Ca^{2+} at ionic strengths of 1 and 10 mM, Fig. 3.1B and C, the plateau phase of the breakthrough curves drastically decreased, with a 2 log removal. The tails of both breakthrough curves also exhibited a sharp decline, and negligible tailing. From the literature, we understood that the presence of Ca^{2+} could lead to an increase in attachment. This increase could be attributed to double layer compression, charge screening [133], or Ca-bridging between the silica surface of the sand and DNAcol, or a combination of factors. The calcium bridging between the silica surfaces and anionic surfactant is well known in the literature (e.g. [175]). We initially anticipated a higher attachment rate for the experiment with ionic strength of 10 mM in comparison to the 1 mM experiment. However, the increase in attachment rate was minimal. The sticking efficiencies belonging to these two experiments were approximately around 1, indicating favourable or nearly favourable attachment conditions [64]. Based on these results, we expected that the majority of DNAcol colliding with the sand grain surface could also attach to it. However, despite this expectation, the DLVO profile indicated the presence of a potential barrier. Recent studies have reported the limitation of the mean-field DLVO theory in predicting attachment when potential energy barriers are present [78, 164, 165, 176–178]. For DLVO calculations, we assumed a smooth particle surface with uniform size and charge. This approximation may lead to overestimating unfavourable conditions. Additionally, we assumed the ζ-potential of the sand grains were similar to DNAcol. Beyond these assumptions, a limitation of the DLVO likely was related to the presence of heterogeneity, like charge and roughness on the surfaces [64, 111, 179–182]. The presence of macro and nano scale heterogeneity could play a role in mitigating the repulsive energy barrier. In this direction, recently, mechanistic approaches were presented that aim to explain both attachment and detachment from primary energy minima, even under unfavourable conditions [165, 179].

Upon examining the experiments involving only NOM (Exps. D and G), we expected a higher level of electrostatic repulsion and the presence of steric hindrance, leading to a lower rate of DNAcol attachment. Additionally, NOM was anticipated to have a “masking-effect” [146], reducing surface heterogeneity and enhancing transport of colloidal matter [146, 183, 184]. The adsorption of NOM onto both sand grains and suspended colloidal particles (DNAcol) surfaces led to an increase in electrostatic repulsion force due to the increase in the ζ-potential values [137, 185, 186]. This increase in the negative charge was observed within just 5 min upon adding DNAcol to the solutions. In these two experiments, based on the breakthrough curves results, it became clear that the plateau values of the breakthrough curves reached higher levels, indicating lower DNAcol attachment or retention. The estimated k_{att}, and k_{det} values further confirmed this trend, with k_{att} being lower and k_{det} being higher compared to the experiments of DNAcol in Milli-Q water. The mass recovery of the experiments conducted with Milli-Q water

was approximately 81% (Exp. A), and the mass recoveries increased to 85% and then to around 92% for the experiments involving 5 and 20 mg-C L^{-1} DOC, respectively (Exps. D and G). This indicated that steric hindrance played a role to a certain extent, which was extensively described in the literature [131, 133, 137, 138, 144, 147, 187].

As mentioned earlier, ionic strength had a major effect on transport of DNAcol, leading to a significant increase in the attachment rate. However, DOC had an opposite effect on attachment rate. When both Ca^{2+} and DOC were present in the solution (Exps. E, F, H, and I), then we think the [Ca^{2+}]/DOC ratio started playing a role. In these combined experiments, Ca^{2+} could not only bind to the two silica surfaces present in the system but also to DOC (e.g. [188]). For the lowest [Ca^{2+}]/DOC ratio, where the ionic strength was 1 mM and DOC was 20 mg-C L^{-1} (Exp. H), we observed that the plateau ($C_{plateau}/C_0$) of the breakthrough curves approached values close 0.8-1. Remarkably, in this experiment, the mass recovery increased massively compared to conditions with the same ionic strength but without NOM (no DOC). The associated sticking efficiency for this experiment was 0.03. These results showed that the presence of 20 mg-C L^{-1} of DOC effectively outcompete DNAcol attachment, which was an interesting finding in the framework of the DNAcol application for tracer transport studies or when considering the ecotoxicity of colloids. For the second lowest [Ca^{2+}]/DOC ratio (ionic strength of 1 mM with DOC of 5 mg-C L^{-1}), the k_{att} value was one order of magnitude larger than in the previous case, that contained a higher DOC concentration. In this experiment, the plateau of the breakthrough curves reached approximately 0.48, indicating a higher rate of attachment within the sand column. Finally, for the ionic strength of 10 mM experiments with DOC of 5 and 20 mg-C L^{-1}, the k_{att} values increased further when compared to the conditions with ionic strength of 1 mM. In these two experiments, the mass recoveries increased from 1% (no DOC; Exp. C) to approximately 12-20%, (Exps. F, and I), respectively. The most plausible explanation for this observation could be attributed to inter-molecular cation bridging or complexation facilitated by the presence of Ca^{2+} ion, between the negatively charged surfaces of NOM and the sand grains [138]. Furthermore, as ionic strength increases the zone of colloid-collector interaction shrinks [164], potentially leading to a higher attachment rate [165]. We expected the thickness of the adsorbed organic matter layer on DNAcol would be affected by increasing ionic strength. That meant that repulsion between the nearest adsorbed macromolecules was reduced to some extent due to a decrease in negative charge [152]. Consequently, this could result in a denser and more compacted configuration of the adsorbed organic layer [152, 189]. We initially attempted to indirectly determine the thickness of the adsorbed NOM layer on DNAcol, by comparing the hydrodynamic diameters of DNAcol in the absence and presence of organic matter. However, this approach was impractical due to hydrodynamic diameter being a rather coarse measurement of true particle diameter, coupled with the broad size distribution of the hydrodynamic diameter of DNAcol exceeding the expected thickness of the adsorbed layer.

Under transient porewater chemistry conditions, we observed the release of DNAcol upon flushing with Milli-Q water. Such remobilization phenomenon was

reported by other researchers in relation to various types of colloidal matter (e.g. [44, 127, 131, 144, 157, 159, 160, 190]). The remobilization can provide evidence to enhance our understanding to what extent the colloidal matter was attached reversibly or irreversibly within the sand column. Under transient porewater chemistry conditions, comparing the two experiments with ionic strength of 1 mM and 10 mM revealed distinct differences in the release of DNAcol upon flushing the column with Milli-Q water. While the deposition rates of DNAcol in ionic strength of 1 and 10 mM under steady porewater chemistry conditions were quite similar, the remobilization rate of retained or attached particles significantly differed under transient porewater chemistry conditions. Specifically, the release of DNAcol deposited at an ionic strength of 10 mM was significantly higher compared to those at 1 mM (see Fig. 3.1 and Fig. B.6 in Appendix).

As the study of Nocito-Gobel and Tobiason [191] indicated, the rate of particle release resulting from reducing in ionic strength might be influenced by various factors, such as the magnitude of the ionic strength change, the final ionic strength value, as well as the type and the quantity of previously deposited particles. This study also observed the highest rate of release for particles deposited in the 10 mM experiment [191]. Obviously, for the two experiments with 1 mM and 10 mM ionic strength, we could assume that the final value of the change in ionic strength was similar, as the columns were flushed around 3 PVs with Milli-Q water. Furthermore, the mass recovery values calculated under steady porewater chemistry conditions were 2% and 1% for ionic strength of 1 mM and 10 mM, respectively. Therefore, we could reasonably assume that the amount of the previously deposited particles in both cases were rather similar. Here, the results highlighted the critical role of the magnitude of change in ionic strength in release rate, during transient porewater chemistry conditions. For example, Franchi and O'Melia [131] highlighted that during transient conditions, when the column was rinsed with lower ionic strength, a sharp peak appeared, and the peak magnitude increasing with the change in ionic strength during injection phase. Other studies have indicated that significant remobilization of colloidal particles can occur when the reduction in ionic strength reaches a critical concentration [157, 192]. Our results also showed higher DNAcol release rate upon flushing the column with Milli-Q water for experiments conducted at higher ionic strength (Exps. C, F, and I) than experiments conducted at the lower ionic strength.

Even though the experimental conditions were theoretically performed under unfavourable conditions, it remained unclear what could be the main reason behind the remobilization of DNAcol upon change in pore water chemistry. It is important to emphasize that although the column experiment results improved our understanding of DNAcol transport behaviour, and the rate of removal, more work is necessary to accurately describe the underlying mechanisms involved in the attachment, retention, and remobilization. The one explanation for the higher rate of particles remobilization at 10 mM $CaCl_2$ during the transient porewater chemistry conditions according to DLVO could be linked to the depth and positioning of the secondary minimum [124]. Commonly, the release of particles is associated with a secondary energy minimum in DLVO theory [131, 193]. The DLVO profile indicated

under 10 mM ionic strength conditions, the secondary minimum was deeper and situated closer to the surface of the sand grains. However, upon a closer examination of the DLVO profile, it became apparent that the secondary minimum was quite shallow in cases of 10 mM ionic strength.

The other possible mechanism contributing to the release of DNAcol upon flushing with Milli-Q water, could be detachment of particles from the primary energy. As previously mentioned, the presence of nanoscale heterogeneity on the surface can diminish or even eliminate the repulsive barrier, under unfavourable conditions, thereby leading to attachment in the primary energy well [165]. This nanoscale heterogeneity in surface charge could also account for particle detachment under unfavourable conditions with respect to ionic strength reduction [179, 194]. Moreover, the presence of nanoscale heterogeneity, such as surface physical asperities, might have contributed to the retention of particles [195]. It is important to note that in our experiments conducted with 1 mM and 10 mM ionic strength, only a small fraction of the attached or retained DNAcol were released upon reducing the ionic strength. This observation suggested that in these two cases, the majority of the DNAcol (approximately 98-90%) was strongly bound to the sand grains and remained unreleased. It could be tempting to conclude that Ca-bridging between the sand and DNAcol yielded binding strengths, that could not be broken by the decrease in solution ionic strength.

3.5. CONCLUSIONS

The experimental results indicated that ionic strength and organic matter had opposite effects on the overall transport and attachment rate of DNAcol. As a result, the transport behaviour of DNAcol exhibited substantial variability across the range of tested conditions. Consequently, if we aim for the application of DNAcol as a tracer for mass balance, its applicability may fail due to its high sensitivity to environmental conditions.

So, in summary the results of this study demonstrated that:

- The concentration of DOC in the aqueous system can play a crucial role in the transport and fate of DNAcol.
- The calculations of sticking efficiency indicated that in the presence of organic matter the probability of DNAcol attachment decreased significantly.
- Attachment of DNAcol was regulated by the $[Ca^{2+}]$/DOC ratio, whereby attachment was low at low ratios and increased when $[Ca^{2+}]$/DOC ratio increased. There was a range of $[Ca^{2+}]$/DOC ratios, whereby the attachment of DNAcol to the sand grains was negligible.
- The remobilization of DNAcol was more significant under transient porewater chemistry conditions with 10 mM ionic strength compared to 1 mM $CaCl_2$. These findings emphasize the importance of evaluating the impact of transient porewater chemistry conditions on the potential risk of colloidal transport.

4

Towards Application of DNAcol in Agricultural Lands Role of Natural Organic Matter

4.1. Introduction

Agricultural land is exposed to a wide range of agrochemicals and colloidal particles from diverse sources. For instance, agricultural soils have recently been recognized as significant repositories for nano- and micro-plastics. Major sources of such non-point source plastics include sewage sludge amendment [196, 197], residues from plastic mulching [198, 199], "coated fertilizers" [200], agricultural litter, and atmospheric deposition [201].

Non-point source pollution in agricultural land has the potential to spread and contaminate the vadose zone and groundwater. Soil chemistry is highly heterogeneous, with factors such as pH, ionic strength of the water, and surface characteristics of the soil texture. These factors can greatly influence the transport, sedimentation, attachment, and remobilization of colloidal particles [133]. Agricultural soil, in particular, is known to be rich in organic matter, which can impact the stability [45, 124, 133, 138, 139], and transport of colloidal particles [45, 124, 138, 183].

Moreover, in lowland agricultural regions like the Netherlands, understanding the dynamics of flow and contamination transport patterns is more challenging due to the highly dynamic nature of lowland catchments, which involve interactions between surface water and groundwater, along with a dense drainage network that may facilitate rapid flow [202, 203]. Therefore, monitoring and modeling the spatial-temporal variations of flow, nutrients, and contaminants is crucial for the effective management of surface and subsurface water resources.

An effective method for studying the transport and fate of non-point source contamination in the subsurface environments is the use of multi-point tracer techniques. Encapsulated synthetic DNA particles show promise as potential candidates for tracking non-point source colloidal contaminants. According to a review by Foppen [18], six types of encapsulated DNA particles have been fabricated to date [21, 33–35, 51, 52], and used as tracers in different environmental and laboratory conditions [14, 21, 30, 33, 35, 37, 39, 41–46, 48–50]. These encapsulated DNA particles offer advantages, including a low detection limit due to the presence of DNA, and the ability to synthesize large numbers of distinguishable tracers by tagging each with a unique DNA sequence. This versatility allows for the simultaneous tracing of multiple pathways by tagging different DNA sequences onto tracers that have similar transport properties [21].

However, the main drawback of encapsulated DNA particle is its variation in mass recovery [14, 41, 44–46, 57], and its transport is governed by filtration, which can significantly vary based on the physicochemical environmental conditions [18, 45]. This mass variability may pose limitations in its application as a conservative tracer [45]. Nevertheless, its colloidal property provides the potential to serve as a surrogate for tracing biological colloids (e.g., bacteria) and nano- and micro-particles (e.g., nano-plastics). To fully exploit this potential, however, comprehensive research is needed.

In Chapter 3, we systematically investigated the effect of organic matter and $CaCl_2$ on the transport of silica-encapsulated DNA (DNAcol). The organic matter used as a proxy for natural organic matter was extracted from groundwater in the

Netherlands and provided by Vitens, a drinking water company in the Netherlands. Our research showed significant variation in the transport of DNAcol in the presence of natural organic matter [45], and potential formation of an "eco-corona" or "environmental-corona". Building on these findings, this chapter focuses on the application of DNAcol in agricultural fields and aims to further explore the effect of organic-rich natural groundwater on the transport of DNAcol.

To achieve this, we conducted a series of controlled laboratory experiments. We first examined the transport of DNAcol within sand columns using natural groundwater as the background solution. Next, we prepared synthetic groundwater to mimic the major ion compositions of natural groundwater while excluding natural organic matter. This approach allowed us to specifically assess the transport of colloidal particles in groundwater conditions in the absence of natural organic matter. Furthermore, we investigated the transport of DNAcol within undisturbed soil, using natural groundwater rich in organic matter as the porewater. Additionally, we explored the effect of transient porewater chemistry conditions on the transport of attached and/or retained DNAcol within the sand columns by flushing them with Milli-Q water.

4.2. MATERIALS AND METHODS

4.2.1. GROUNDWATER CHARACTERIZATION

Two groundwater samples were extracted from agricultural fields: one from Huppel 52.00131 N, 6.76112 E, in the eastern part of the Netherlands, and the other one is from Tulip field, Noordwijkerhout, 52.260324 N, 4.473579 E, located in the flower farms region of the western part of the Netherlands. These samples were collected in March 2021 and stored at 4 °C. Before using the extracted groundwater as background solutions for the experiments, both groundwater samples underwent two rounds of vacuum filtration with a pore size of 0.450 μm (cellulose membrane filter, Whatman, Germany) to remove particulate matter.

The major ion composition of both groundwater sources was analyzed using Ion Chromatography (Metrohm) (Table 4.1). In both groundwater, Ca^{2+} was the dominant cation. The Huppel groundwater exhibited a higher concentration of NO_3^-, whereas the Tulip groundwater had elevated levels of SO_4^{2-}.

4.2.2. NATURAL ORGANIC MATTER CHARACTERIZATION

The concentration of dissolved organic matter in the groundwater was determined using a Total Organic Carbon Analyzer (TOC, VCPN, Shimadzu, Japan) and reported as non-purgeable organic carbon (NPOC) in mg L^{-1} (mg-C L^{-1}). Prior to the measurements, the groundwater samples were filtered twice through a 0.450 μm pore size (cellulose membrane filter, Whatman, German).

The composition and origin of natural organic matter in the groundwater were characterized using the Absorbance Excitation-Emission Matrix (FEEM) using A-Team (Aqualog, Horiba Scientific) spectroscopy. All measurements were conducted using a quartz cuvette with a 1 cm path length. Before conducting the sample

Table 4.1.: The major cation and anion composition of natural groundwater (GW) determined by ion chromatography.

Major	Huppel GW	Tulip GW	Huppel GW	Tulip GW
	[mg L^{-1}]	[mg L^{-1}]	[μEq L^{-1}]	[μEq L^{-1}]
Na^+	16.7	20.9	726.3	909.4
Ca^{2+}	117	117	5833.0	5822.7
Mg^{2+}	15.9	9.65	1311.2	794.2
K^+	15.1	38.4	387.1	983.1
Cl^-	29.0	28.1	817.8	793.5
NO_3^-	152	3.80	2457.3	61.3
SO_4^{2-}	58.9	89.4	1226.0	1861.4
PO_4^-	0.06	6.18	1.8	195.3
C^{Z+}			8257.5	8509.4
A^{Z-}			4502.8	2911.5

measurements, the Raman fluorophore of water was examined, showing a peak at 348 nm to verify the instrument's stability. Milli-Q water was used as the blank sample to calibrate the measurement intensity. Fluorescence intensity measurement was taken within an excitation wavelength (EX) spectrum ranging from 230-600 nm (incremental interval=2 nm), and emission wavelength (EM) range between 250-800 nm (incremental interval=3 nm).

4.2.3. Synthetic Groundwater Solution

Two synthetic hard water solutions were prepared based on the major ion compositions of two natural groundwater sources. The salts chosen for creating these solutions followed the hard water recipe protocol developed by Smith, Davison, and Hamilton-Taylor [204], with certain adjustments made to accommodate the specific conditions of our study. PHREEQC [205] was used to determine the masses of salts required to dissolve (Table 4.2).

In accordance with Smith, Davison, and Hamilton-Taylor [204], and to overcome incongruent solubility challenges and ensure the complete dissolution of salts, four electrolyte stock solutions (H1-H4) were prepared in Milli-Q water (Table 4.2). Then, the final synthetic groundwater for each type of groundwater was prepared by mixing the appropriate ratio of H1-H4 stock solutions. The major cations and anions of final synthetic groundwaters were then measured using ion chromatography and are given in Appendix, Table C.1. A comparison between the measured compositions of natural and synthetic groundwater showed some variations but was considered to be within acceptable limits (Table C.1).

Table 4.2.: Chemical composition of four stock solutions used to prepare Huppel and Tulip synthetic groundwater (Syn.)

Stock	H1		H2		H3			H4
Solution	$CaCl_2.6H_2O$	$Ca(NO_3)_2.4H_2O$	$CaCO_3$	CO_2	$KHCO_3$	KH_2PO_4	$NaHCO_3$	$MgSO_4.7H_2O$
Huppel Syn. [mg L^{-1}]	740	3070	160		800	410	1180	600
Tulip Syn. [mg L^{-1}]	880	-	300		800	410	840	600

4.2.4. DNACOL

The silica-encapsulated-DNA colloid (DNAcol) has a core-shell structure with silica composing the shell and core, encapsulating double-stranded DNA molecules. The synthesis took place at ETH Zurich, and the fabrication method was detailed by Paunescu *et al.* [34] and Mikutis *et al.* [39]. The DNA quantification protocol workflow was adapted from Paunescu *et al.* [34] and Mikutis *et al.* [39] and outlined in Chapter 3. For the dispersion of DNAcol in various solutions, DNAcol was spiked into specific background solutions, and three distinct DNAcol variants, labeled S1-S2 and S4 were used in different experiments. The batches of DNAcol suspension were vortexed three times to achieve a homogeneous dispersion.

4.2.5. STABILITY OF DNACOL- HYDRODYNAMIC RADIUS (d_h), AND ZETA-POTENTIAL (ζ-POTENTIAL)

The particle size distribution and electrophoretic mobility of S4 suspended in both natural and synthetic groundwater were determined using a ZetaSizer Nano ZS (Nano Series, Malvern Instrument Ltd., Worcestershire, UK), as described in Chapter 2.

Before the measurement, the DNAcol suspension was prepared at a concentration of 10 mg L^{-1} and vortexed three times to ensure thorough homogenization. To assess the stability of S4 both d_h and ζ-potential were measured after preparation of fresh suspension (within 5 min) and after 120 min using a U-shaped capillary cell with gold electrodes (DTS1070).

4.2.6. SAND COLUMN EXPERIMENTS

The transport behavior of DNAcol was assessed under three different sand column conditions. In the first two series of the experiment, acid-washed sand was used, and in the last series, the column was filled with undisturbed soil. The columns had a cylindrical acrylic structure with an inner diameter of 2.7 cm and a height of 10 cm.

For the acid-washed sand columns, filter sand with a grain size between 425 to 630 μm was used as the sand media. The sand, before use, was acid-washed (protocol described in Chapter 3). The column was uniformly wet-packed, after packing the columns, the inlet tubing was connected to the pump, and the flow was

in an upward direction. Following the column packing, the sand column was initially preconditioned by injecting Milli-Q water for more than 10 pore volumes (PV). The tracer experiment procedure closely followed our earlier study in Chapter 3.

For the undisturbed soil columns, the procedure involved excavating a hole and then vertically pushing a cylinder into the soil at a depth of 70 cm. The dimensions of the columns that were used for undisturbed sand were similar to those used for the acid-washed sand column. For this experiment, local groundwater was used as the background solution. The undisturbed soil columns were then kept in a cold room at a temperature of 4 °C until they were used.

Sand Column Experiments with Natural Groundwater

The transport behavior of DNAcol(S4) was investigated within the sand column using the two natural groundwaters: Tulip and Huppel. In this series of experiments, three sequential tests were conducted per column: i) NaCl tracer as a solute tracer, ii) DNAcol suspended in Milli-Q water (MQ), and iii) DNAcol suspended in natural groundwater. The injection phase of DNAcol lasted for 150 minutes, followed by the elution phase with a background solution for 210 minutes. These two phases are referred to as steady porewater chemistry conditions. Then, after the elution phase, the column was further flushed with Milli-Q water for 180 to 210 minutes to mimic transient porewater chemistry conditions for the experiments. It is important to note that prior to conducting the DNAcol suspended in natural groundwater, the column was preconditioned with a background solution. The experimental procedure is summarized in Table 4.3.

The DNAcol suspension was prepared by spiking DNAcol(S4) to achieve a 1 mg L^{-1} concentration in the background solution. During the injection phase of DNAcol, the injection suspension was continuously stirred using a magnetic stirrer to maintain the uniformity of the concentration. To determine the concentration of the column influent (C_0) for DNAcol experiments, 5-6 samples were collected over the injection time-frame. The effluent of the column was continuously collected with a sampling time frame of 5 minutes. The flow rates were measured before and after each tracer experiment to ensure a constant flow rate through the tests. The average Darcy velocity was 0.07 cm min^{-1}.

Sand Column Experiments with Synthetic Groundwater

In the second series of the experiment, the transport behavior of DNAcol(S4) was investigated using two synthetic groundwaters as the background solution. The procedure for this series of experiments was similar to what we described above for natural groundwater, except that for each sand column, two sequential experiments were conducted: i) NaCl tracer as a solute tracer, ii) DNAcol suspended in synthetic groundwater. This means the transport of DNAcol in Milli-Q water was excluded (Table 4.3).

UNDISTURBED SAND COLUMN EXPERIMENTS WITH NATURAL GROUNDWATER

For the undisturbed soil column, after connecting the inlet and outlet tubing, the column was flushed with several pore volumes of filtered Tulip groundwater at a constant flow rate using a pump with the flow in an upward direction, to ensure that the column was fully saturated. In this series of experiments, the transport behavior of two distinct DNAcol, tagged with two different DNA sequences (S1 and S2), was examined. Three sequential tests were conducted per column: i) DNAcol(S1) suspended in natural groundwater, ii) DNAcol(S2) suspended in natural groundwater, and iii) NaCl tracer as a solute tracer. The two experiments with S1 and S2 were conducted for two different concentrations and two flow velocities (Table 4.3). The first experiment with S1 was conducted at a lower concentration of 0.01 mg L^{-1} and a lower Darcy velocity of 0.04 cm min^{-1} compared to previous experiments in acid-washed sand. The injection phase of S1 for this experiment lasted for 240 min, followed by a 240 min elution phase with groundwater free of DNAcol. At the end of the elution phase, groundwater was continuously flushed within the column to further flush the DNAcol retained within the sand column.

A few days after flushing the column, the second DNAcol(S2) experiment with a higher concentration was performed. For the second experiment, S2 was injected into the column with a concentration of 0.1 mg L^{-1} for 120 min. The column influent was then switched back to groundwater without DNAcol for 120 min as the elution phase. After the elution phase, Milli-Q water was flushed through the column to reduce the salt concentration of the soil column, followed by NaCl tracer. The Darcy velocity was 0.07 cm min^{-1}, and the sampling duration was 5 minutes.

For the NaCl tracer, the concentration of the collected samples was determined based on electrical conductivity (EC). The concentration of the DNAcol tracer was analyzed using the quantitative polymerase chain reaction (qPCR) technique, as described in Chapter 3.

Table 4.3.: Summary of DNAcol experiments conducted in various columns.

Column Experiment	Solution	Injected DNAcol (concentration)	Injection time	Elution time	Transient time	Sand
		[mg L^{-1}]	[min]	[min]	[min]	
Exp. 1	Milli-Q water (1)	1 (S4)*	150	210	-	acid-washed
	Huppel GW(1)	1 (S4)	150	210	180	acid washed
	Huppel GW(2)	1 (S4)	150	210	210	acid washed
Exp. 2	Milli-Q water (1)	1 (S4)	150	210	-	acid washed
	Tulip GW(1)	1 (S4)	150	210	180	acid washed
	Tulip GW(2)	1 (S4)	150	210	210	acid washed
	Tulip GW(3)**	1 (S4)	150	210	210	acid washed
Exp. 3	Huppel Syn.	1 (S4)	150	210	210	acid washed
Exp. 4	Tulip Syn.	1 (S4)	150	210	210	acid washed
Exp. 5	Tulip GW(2)	0.01 (S1)	240	240		Undisturbed
	Tulip GW(1)	0.1 (S2)	120	120	150	Undisturbed

* S4: DNAcol(S4), S1: DNAcol(S1), and S2: DNAcol(S2)

** In this sand column, only the transport of DNAcol in groundwater was investigated.

The details of the primer and dilution series are detailed in Appendix C.2. Table C.2 presents the sequence and GC content of the forward and reverse primer. Calibration curves for S1-S2 and S4 were performed both in Milli-Q water and in various background solutions used in this work (Appendix Fig. C.1-C.2). Fig. C.1-C.2 show the dilution series consisted of 8-fold from 100 mg L^{-1} to 0.00001 mg L^{-1}, corresponding to D_2 to D_9 in the dilution series. In each run of qPCR, alongside the samples, several quality checks were performed to ensure there was no contamination and no signal inhibition. For this purpose, the qPCR run contained a No Template Control (NTC) and a positive control to ensure the absence of contamination and to control the quality of the reaction, respectively. Additionally, for DNAcol(S4) qPCR runs, influent and effluent blank samples were included to ensure there was no false positive signal (Fig. C.3). Furthermore, the stability of DNAcol(S4) in terms of Cq value was occasionally assessed over time (Fig. C.3).

4.2.7. Sticking Efficiency (α)

Based on colloid filtration theory (CFT) [66, 110, 111] the sticking efficiency (α) was calculated based experimental breakthrough curves data using the following equation [62, 70, 111, 169]:

$$\alpha = -\frac{2d_g}{3(1-\epsilon)L\eta_0}\ln\frac{C}{C_0} \tag{4.1}$$

Where, d_g [cm] is average grain diameter, ϵ [-] is porosity of the sand column, L [cm] is column length, η_0 [-] is the single-collector contact efficiency, C_0 [mg L^{-1}] is the influent concentration, C [mg L^{-1}] is the effluent concentration of particles, when the breakthrough curve reached steady condition. In this study, the values of C/C_0 were derived from the average of the normalized breakthrough curves between 65-115 min (~1.2-2.1 PV) for the experiments conducted with acid-washed sand column, and for the undisturbed soil column experiments, the average values were obtained from the breakthrough curves between 85-145 min (~1.2-2.1 PV). The dimensionless single-collector contact efficiency (η_0) was calculated based on the correlation equation developed by Tufenkji and Elimelech [70]. The attachment rate coefficient (k_{att}) of DNAcol was calculated based on the following equation:

$$k_{att} = \frac{3(1-\epsilon)}{2d_g}v_p\eta_0\alpha \tag{4.2}$$

Where, v_p [cm min^{-1}] is porewater flow velocity. In principle, colloid transport is commonly described by the advection-dispersion equation, which incorporates attachment-detachment processes in porous media [171], as described in Chapters 2 and 3. Transport parameters for solute and DNAcol were estimated based on experimental breakthrough curves data using HYDRUS-1D model, which was fitted to the experimental breakthrough curves. The columns' porosity and dispersivity were estimated from NaCl tracer data, while the attachment rate coefficient (k_{att}), and detachment rate coefficient (k_{det}) were estimated from DNAcol breakthrough curves. The values of the attachment rate coefficient (k_{att}) were estimated based on

both experimental data using Eq. 4.2 and alternatively using the HYDRUS-1D model. The mass recovery during steady porewater chemistry conditions ($M_{steady}/M_{inj.}$) was calculated based on the area underneath the first peak, while during transient porewater chemistry conditions, the relative mass recovery ($M_{Transient}/M_{inj.}$) was calculated based on the area underneath the second peak, Eq. 3.1. Specifically, for transient porewater chemistry conditions, the recovered mass was reported as the ratio of DNAcol mass recovered during the transient condition to the total injection mass of DNAcol, not retained within the column.

4.3. RESULTS

4.3.1. STABILITY OF DNACOL- ZETA-POTENTIAL (ζ-POTENTIAL) AND HYDRODYNAMIC DIAMETER (d_h)

The measured ζ-potential values, after 5 minutes of spiking with DNAcol(S4) in both natural groundwaters, averaged around –21 mV (Table 4.4). Similarly, for synthetic groundwater, the ζ-potential was very close to those in natural groundwater conditions, averaging around –22 mV (Table 4.4). After 120 minutes, the ζ-potential of DNAcol in natural groundwater remained almost constant, averaging around ~–22 mV. However, the negative charge of DNAcol(S4) in synthetic groundwater changed to ~–16 and –17 mV (Table 4.4). The change in ζ-potential of DNAcol(S4) in synthetic groundwater is most likely related to the compression of the double layer and charge screening due to the presence of salts.

The hydrodynamic diameter (d_h) of DNAcol(S4) was reported as Z-average particle size. The Z-average particle size distribution of DNAcol(S4) in Huppel groundwater varied from 367 to 335 nm over the 120-minute measurement period. For Tulip groundwater, the Z-average size of DNAcol remained constant at around 375 nm (Table 4.4). For DNAcol(S4) suspended in synthetic groundwater of Huppel and Tulip, the Z-average particle size distribution was 467 nm and 385 nm, respectively, after 5 minutes. However, over the 120-minute measurement period, the d_h of DNAcol(S4) suspended in Huppel and Tulip synthetic groundwater increased to 922 nm, and 2183 nm, respectively (Table 4.4). This indicated that in the absence of organic matter, in synthetic groundwater DNAcol(S4) aggregated.

4.3.2. CHARACTERIZATION OF ORGANIC MATTER OF GROUNDWATER

The concentration of dissolved organic matter, as determined by a DOC analyzer, was approximately 21 mg-C L^{-1} for Tulip groundwater and around 26 mg-C L^{-1} for Huppel groundwater. These concentrations were slightly higher than the maximum concentration used in Chapter 3, which was around ~20 mg-C L^{-1}.

The fluorescence analysis revealed two major peaks for both groundwater types. The first peak, observed around EX/EM=250/450 nm, is indicative of fulvic or humic acid-like compounds [206]. The secondary peak, occurring around EX/EM=340/430 nm, was also humic acid-like [206].

Table 4.4.: The hydrodynamic diameter (d_h) along with its polydispersity (PDI), and ζ-potential of DNAcol(S4) suspended in both Huppel and Tulip natural groundwater and synthetic groundwater, along with their corresponding electrical conductivity (EC) values.

Solution	d_h [nm]		Polydispersity [-]		ζ-potential [mV]		EC [mS cm^{-1}]
	5 min	120 min	5 min	120 min	5 min	120 min	
Huppel GW	366.5	335.3	0.4	0.3	-21	-21.6	0.86
Tulip GW	375.2	374.5	0.4	0.5	-21.6	-23.2	0.83
Huppel Syn.	466.8	922.1	0.5	0.6	-22.2	-15.7	0.85
Tulip Syn.	385.1	2183	0.4	0.7	-22.4		0.84
Tulip Syn.	418.9	1193	0.5	0.8	-23.3	-17.3	

4.3.3. Column Breakthrough Curves Under Steady and Transient Porewater Chemistry Conditions

Sand Column Experiments with Natural Groundwater

Before assessing the transport of DNAcol, a NaCl tracer was conducted to estimate the porosity and dispersivity of each sand column using inverse modeling with HYDRUS-1D. Subsequently, the transport of DNAcol in Milli-Q water was assessed within the two sand columns as a benchmark Fig. 4.1A and 4.1C. The breakthrough curves of normalized DNAcol in Milli-Q reached a maximum relative concentration (C_{max}/C_0) of around 0.6-0.7 (Fig. 4.1A and 4.1C). The tailing of the breakthrough curve gradually decreased, indicating a slow release of some of the retained particles [207].

Next, the transport of DNAcol in two different natural groundwaters was tested. For Huppel groundwater (Fig. 4.1B), duplicate experiments showed that C_{max}/C_0 ranged between 0.38-0.68 (Table 4.5), and the relative mass recovery was around 36-46% ($M_{steady}/M_{inj.}$). In the case of Tulip groundwater (Fig. 4.1D), the breakthrough curves were similar to those in Huppel groundwater, with C_{max}/C_0 ranging approximately from 0.30-0.53. The relative mass recoveries ($M_{steady}/M_{inj.}$) of DNAcol were approximately 22-23%, and 36% among triplicate experiments (Table 4.5). The tailing of the breakthrough curve of DNAcol within both types of groundwater gradually decreased, similar to the Milli-Q experiments. In the last two experiments, after the elution stages of DNAcol with particle-free groundwater solutions, Milli-Q water was injected into the sand column to mimic transient porewater chemistry conditions. During this stage, a second peak appeared in the breakthrough curves. For Huppel groundwater, the relative mass recovery of the second peak was approximately 8-12% ($M_{transient}/M_{inj.}$), and for Tulip groundwater, it varied between 8-30-58% ($M_{transient}/M_{inj.}$).

It should be noted that the samples from the replicated experiment were analyzed after 21 days due to issues with laboratory equipment breakdowns. Although the breakthrough curves of the replicate experiment followed a similar trend (Fig. 4.1B

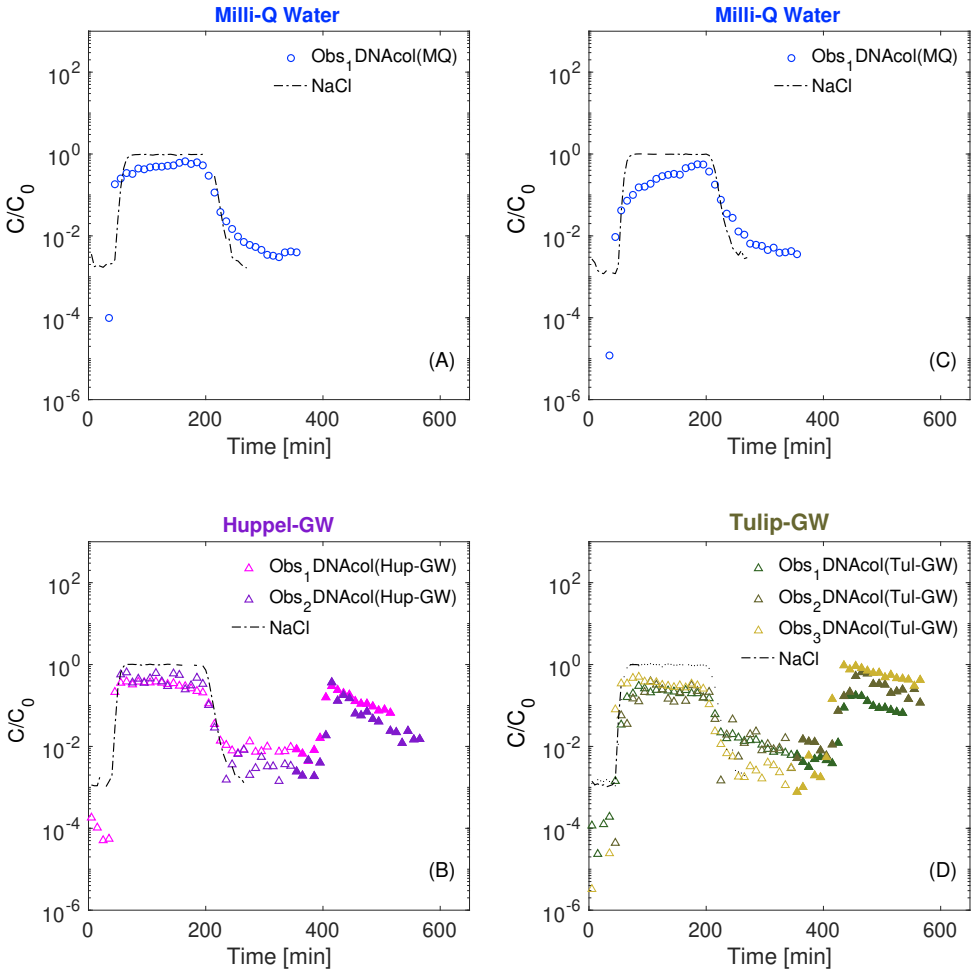

Figure 4.1.: Experimental breakthrough curves of DNAcol (symbols), and NaCl (black dashed lines). The background solutions for DNAcol experiments are: (A) Milli-Q water, (B) Huppel groundwater, (C) Milli-Q water, (D) Tulip groundwater. Open symbols represent steady porewater chemistry conditions, and filled symbols represent transient porewater chemistry conditions.

and 4.1D), a closer examination of the data revealed notable variations, particularly in the Cq values (cycle quantification values, indicating when the fluorescence signal crosses the background noise) of both influent and effluent of the column. While the breakthrough curves were presented as normalized values (C/C_0), making the differences between replicates less noticeable, the overall trend of the breakthrough curves and mass recovery did not deviate significantly. For further clarification

regarding the variation between the replicated experimental data, the values of injected particles (C_0), determined by qPCR, were presented as quantification cycle (Cq) values in Fig. C.3.

In addition to experimental data, the sticking efficiency (α) and attachment rate coefficient (k_{att}) of DNAcol was determined experimentally using Eq. 4.1 and 4.2 and compared with the attachment rate coefficient (k_{att}) estimated from HYDRUS-1D (Table 4.5). For DNAcol in Milli-Q water, k_{att} values ranged between 0.014 and 0.033 (Table 4.5). In the case of DNAcol in Huppel and Tulip groundwater, the average values were 0.015 and 0.022, respectively. The obtained sticking efficiency (α) for DNAcol in Milli-Q water varied between 0.12 to 0.21 (Table 4.5). For DNAcol in Huppel and Tulip groundwater, the sticking efficiency (α) values were on average 0.11 and 0.16, respectively.

Table 4.5.: Summary of flow rate in the DNAcol experiments and estimated transport parameters, along with corresponding sticking efficiencies of DNAcol. Sticking efficiencies were calculated using d_p= 280 [nm], d_g= 0.527 [mm], H= 0.7×10^{-20} [J], ρ_p=2200 [kg m^{-3}].

Solution	Flow rate	Porosity	C_{max}/C_0	k_{att} Eq4.2	α Eq4.1	k_{att} HYDRUS	k_{det} HYDRUS	α	$M_{steady}/M_{inj.}$	$M_{tran.}/M_{inj.}$
	[ml min^{-1}]	[−]	[−]	[min^{-1}]	[−]	[min^{-1}]	[min^{-1}]	[−]	[%]	[%]
MQ water (1)	0.38	0.42	0.71	0.014	0.12	0.012	3.27×10^{-4}	0.09	54	-
Huppel GW (1)	0.39	0.42	0.38	0.016	0.14	0.020	3.13×10^{-6}	0.16	36	12
Huppel GW (2)	0.41	0.36	0.68	0.015	0.09	0.016	4.26×10^{-5}	0.10	46	8
MQ water (1)	0.36	0.37	0.57	0.033	0.21	0.025	1.55×10^{-3}	0.17	33	-
Tulip GW (1)	0.36	0.37	0.30	0.025	0.16	0.030	3.19×10^{-4}	0.20	23	8
Tulip GW (2)	0.35	0.41	0.48	0.024	0.20	0.028	3.47×10^{-5}	0.20	22	30
Tulip GW (3)	0.41	0.38	0.53	0.017	0.12	0.020	2.69×10^{-5}	0.14	36	58
Huppel Syn.	0.40	0.38	0.02	0.078	0.52	0.089	4.69×10^{-6}	0.59	1	46
Tulip Syn.	0.40	0.38	0.03	0.086	0.58	0.088	4.69×10^{-6}	0.58	0.6	70
Tulip GW (S2) (1) undisturbed	0.04	0.48	0.91	0.065	0.328					

SAND COLUMN EXPERIMENTS WITH SYNTHETIC GROUNDWATER

Fig. 4.2A presents the breakthrough curve of DNAcol in Huppel synthetic groundwater. For this condition, the breakthrough curve of DNAcol exhibited C_{max}/C_0 values approached ~0.02 (Fig. 4.2A and Table 4.5). Such a low plateau indicated significant attachment or retention of DNAcol within the column. The tailing of the breakthrough curve declined abruptly, suggesting negligible release of DNAcol from the sand column. Due to the high attachment and/or retention rate, the relative mass recovery of the DNAcol was low, with only 1% of the injected DNAcol being recovered. In Fig. 4.2B, the breakthrough curve of DNAcol suspended in Tulip synthetic groundwater depicts the concentration of collected column samples normalized over the first 3 sub-samples of column influent (C_0). This normalization was conducted due to observed instability in DNAcol concentration during the sampling period, as indicated by variation in the Cq values (further details provided in Appendix Fig. C.3-C.4). When considering only the first 3 sub-samples of column influent, the value of C_{max}/C_0 was 0.03, and the relative mass recovery

($M_{steady}/M_{inj.}$) of DNAcol was 0.6%.

Fig. 4.2A-B also depicts second peaks that appeared under transient porewater chemistry conditions when the columns were flushed with Milli-Q water after the elution phase of DNAcol. The second sharp peak of DNAcol indicated substantial remobilization of DNAcol upon the injection of Milli-Q water, in contrast to the negligible mass recovery of DNAcol during the steady porewater chemistry conditions. During transient porewater chemistry conditions, approximately ($M_{transient}/M_{inj.}$) 46% of the injected DNAcol in Huppel synthetic groundwater was recovered over 3 pore volumes. For DNAcol in Tulip synthetic groundwater conditions, the relative mass recovery during transient conditions was approximately ($M_{transient}/M_{inj.}$) 70%.

The calculated values of k_{att} for synthetic Huppel and Tulip groundwater were 0.078 and 0.086, respectively, with corresponding sticking efficiencies of 0.52 and 0.58. The obtained mass recovery of DNAcol was only around 1%, suggesting a significant attachment and/or retention of DNAcol within the sand column.

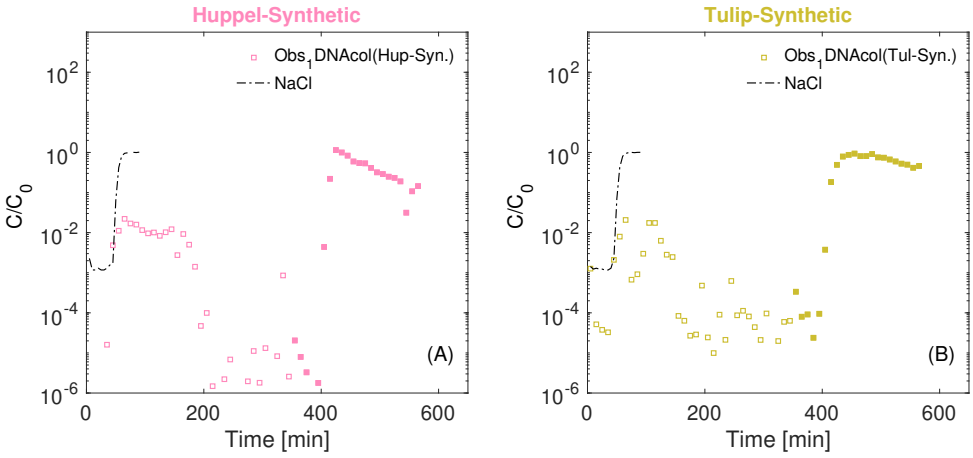

Figure 4.2.: Experimental breakthrough curves of DNAcol (symbols), and NaCl tracer breakthrough curves (black dashed lines). The background solutions for DNAcol experiments are (A) Huppel synthetic groundwater, and (B) Tulip synthetic groundwater. Open symbols represent steady porewater chemistry conditions, and filled symbols represent transient porewater chemistry conditions.

UNDISTURBED SOIL COLUMN EXPERIMENTS WITH NATURAL GROUNDWATER

Fig. 4.3 presents the breakthrough curves of DNAcol transported within undisturbed soil columns excavated from the Tulip field. In Fig. 4.3(A-1 and A-2), the breakthrough curve of the first experiment displays the injection of DNAcol(S1) at a concentration of 0.01 mg L^{-1} (corresponding to D_6 in the dilution series) with a Darcy velocity of 0.04 cm min^{-1}. The breakthrough curves are depicted in both linear (upper panels (A-1)) and semi-log (lower panels (A-2)) scales to better visualize

the shape of the obtained breakthrough curves. Under these conditions, no clear breakthrough curves were observed, indicating a high attachment and/or retention of DNAcol within the soil media.

Fig. 4.3(B-1 and B-2) shows the breakthrough curve of the second experiment using DNAcol(S2) at a higher concentration 0.1 mg L^{-1} (corresponding to D_5 in the dilution series) with a Darcy velocity 0.07 cm min^{-1}. Similarly, a negligible amount of DNAcol was collected from the sand column effluent. Overall, in both tested conditions, the mass recovery of DNAcol was low during steady porewater chemistry conditions.

At the end elution phase of the second experiment, the column was flushed with Milli-Q water, resulting in an observed increase in the concentration of DNAcol in the collected samples. This observation was attributed to the remobilization of retained DNAcol. It is important to note that the sampling collection during remobilization was terminated early, missing the capture of the entire rising and declining limb associated with the remobilization peak. Consequently, calculating the mass of remobilized DNAcol under transient porewater chemistry was not possible. Additionally, the results showed that during the remobilization phase, the rising limb of DNAcol was longer compared to results obtained from acid-washed sands. Although the duration of the injection and elution phase for undisturbed and acid-washed were not identical, the longer duration of the rising limb suggested a slower release rate of retained DNAcol.

In this series of experiments, after the injection of Milli-Q water to reduce the EC of the soil column, the NaCl tracer test was conducted as the final tracer experiment. For this experiment, only the rising limb was sampled to determine the porosity and dispersivity of the undisturbed soil (Fig. 4.3(B-1 and B-2), and Table 4.5).

For the experiment conducted with DNAcol(S2), the collected samples were reanalyzed to assess the stability of DNAcol over time (11 days). Additionally, to examine the effect of storage temperature on DNAcol, the sub-samples were kept at -20 °C (freezing temperature). These results are presented in the Appendix, Fig. C.5.

4.4. Discussion

In the first two series of experiments, we investigated the transport of DNAcol suspended in two types of natural groundwater and synthetic groundwater. The synthetic groundwater was prepared with a similar ion composition as natural groundwater but lacked natural organic matter. This allowed us to assess the influence of natural organic matter on the transport behavior of colloidal matter in the porous media.

The results obtained for DNAcol suspended in the two types of natural groundwater were relatively similar. The breakthrough curves reached a plateau phase on average around 0.22-0.44, followed by a long tailing, indicating a slow release of DNAcol. When compared to synthetic groundwater, the plateau of the breakthrough curves was significantly reduced to values around 0.02-0.03, suggesting high attachment and/or retention of DNAcol. The concentration of the tailing of the breakthrough curves of Tulip synthetic groundwater approached the lower detection limit. In both

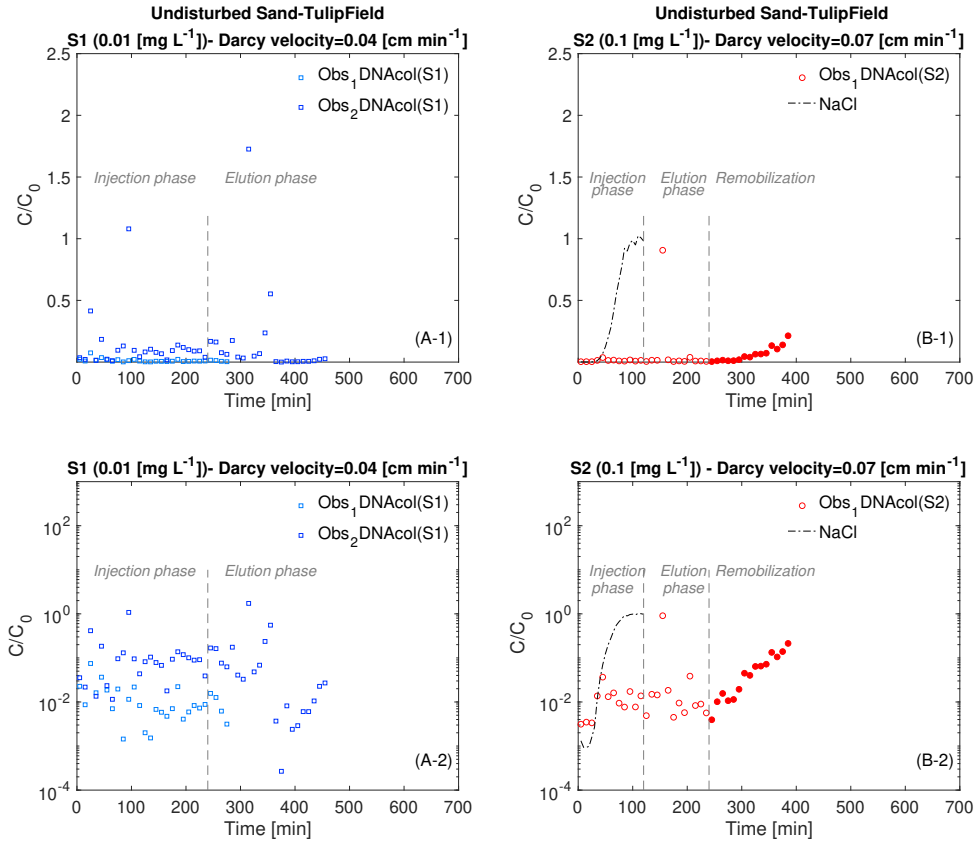

Figure 4.3.: Experimental breakthrough curves of DNAcol (symbols) obtained from undisturbed sand columns with Tulip groundwater as the background solution, and NaCl tracer breakthrough curves (black dashed lines). The top panel shows the breakthrough curves in linear scale (A-1) and (B-1), and the lower panel presents similar breakthrough curves in semi-log scale (A-2) and (B-2). In (A-1) and (A-2), the experimental breakthrough curves of DNAcol were obtained at a lower concentration with a flow velocity of 0.04 [cm min^{-1}], while in (B-1) and (B-2), experimental breakthrough curves of DNAcol obtained at a higher concentration and a flow velocity of 0.07 [cm min^{-1}].

synthetic groundwater conditions, the mass recoveries were extremely low, around 1%, indicating significant retention and/or attachment.

In both synthetic groundwater conditions, the high attachment and/or retention of DNAcol could be attributed to a decrease in the negative charge of the DNAcol. This was evident in the ζ-potential values of DNAcol in synthetic groundwater, which became less negative over the 120-minute measurement period. The reduced

negative charge diminishes the electrostatic repulsion force [62], potentially leading to increased attachment of DNAcol onto the sand grains. Although we expected the ionic strength of natural groundwater to be similar to the synthetic ones, the high concentration of organic matter in the natural groundwater resulted in a significant reduction in the retention and/or attachment of DNAcol. Additionally, it contributed to a more stable ζ-potential of DNAcol. Other researchers reported similar enhancements in the transport of nano- and micro-particles in the presence of natural organic molecules in the porous media [45, 131, 133, 144, 146, 183, 184], likely due to electrostatic and steric repulsion forces [124, 131, 146].

The attachment appears to be one of the mechanisms explaining the low mass recoveries of DNAcol (~1%) in synthetic groundwater conditions as found in our experiments. These findings compare well with the results of Chapter 3, where DNAcol was suspended in $CaCl_2$ solution with ionic strength of 1 and 10 mM, also showing mass recoveries around 1-2%. The corresponding attachment rate coefficient (k_{att}) for synthetic groundwater ranged from 78×10^{-3} to 86×10^{-3}, and for $CaCl_2$ with ionic strength of 1 and 10 mM (Chapter 3), k_{att} values ranged from 96×10^{-3} to 98×10^{-3}, indicating a similarity between the two sets of results. However, when comparing the calculated sticking efficiencies, the results were quite different. The estimated sticking efficiency values in the current experiments were around 0.52-0.58. In contrast, the estimated sticking efficiency values for $CaCl_2$ solution with ionic strengths of 1 and 10 mM approached 1, indicating high attachment rates of DNAcol. Assuming attachment as the sole mechanism contributing to the high removal rate of DNAcol, we could hypothesize that Eq.4.1 underestimated the sticking efficiency value for smaller grain sizes.

Straining is another possible mechanism that can contribute to the removal of colloidal particles within the sand column (e.g., [180, 208–210]). As previously mentioned, evidence showed an increase in the d_h of DNAcol in both Huppel and Tulip synthetic groundwater over a 120-minute period. This increase in DNAcol size is likely due to particle-particle attachment, resulting in the homo-aggregation of DNAcol. Consequently, the ratio of DNAcol diameter to sand grain diameter (d_p/d_g) became very close to or exceeded stringing values as reported by Bradford, Torkzaban, and Walker [114]. Therefore, we infer that the trapping of the particles in small pores increased, leading to an increase in the rate of DNAcol removal driven by the homo-aggregation of particles and the resulting straining mechanism. Overall, it is challenging to determine whether Eq. 4.1 underestimated the sticking efficiency for small sand grains, or if other mechanisms, such as straining, play a role besides attachment of DNAcol to sand grains. Bradford *et al.* [209] highlighted the limitations of sticking efficiency in predicting experimental data when straining is involved. They cautioned that when the ratio of particle diameter to median grain size ($d_p/d_{g(50)}$) exceeds approximately 0.0017, the application of colloid attachment theory should be approached with caution [209].

In our experiment, considering the measured hydrodynamic diameters of DNAcol in synthetic groundwater at 120 minutes, the d_p/d_g ratio became equal to or exceeded 0.0017. As evident from Eq. 4.1, the attachment efficiency is assumed to be independent of colloid size (DNAcol). However, the single-collector contact efficiency

varies depending on the colloid size (DNAcol), which can influence the attachment efficiency value. In Chapter 3, the single collector efficiency was ~3.8×10^{-2}, with a column length of 8 cm and an average sand grain of 715 μm. In the current experiments, the single collector efficiency was ~4.62×10^{-2}, with a column length of 10 cm and an average sand grain of 527.5 μm. In both cases, we assigned the DNAcol size to be 280 nm. The calculated single-collector contact efficiencies were similar to each other, with a slightly lower value for larger sand grains.

To test the effect of DNAcol size, we performed a sensitivity analysis of single-collector contact efficiency and sticking efficiency. First, we fixed the colloid size (DNAcol) to be 280 nm and used the values of the hydrodynamic diameters measured at 5- and 120-minute timeframes. Based on the calculated values of single-collector contact efficiencies, the sticking efficiencies were again calculated using Eq. 4.1 (Appendix, Table C.3). The calculated single-collector contact efficiency was found to be lower for hydrodynamic diameters of DNAcol at 5-minute timeframe, ranging between 367-468 nm, compared to DNAcol size of 280 nm. However, the calculated sticking efficiencies for this scenario were slightly higher than those for DNAcol size of 280 nm. Lastly, assuming a larger DNAcol (as proven by measured hydrodynamic diameter after 120 minutes) resulted in higher values of single-collector contact efficiency. Consequently, this led to lower values for sticking efficiencies compared to DNAcol size of 280 nm. Thus, even if we account for the increase in the size of DNAcol, it may lead to lower values of sticking efficiency.

In the final series of the experiment, we used undisturbed soil columns from the Tulip field to add complexity to our experiments. We aimed to evaluate the relevance of our findings from experiments conducted with acid-washed sand and groundwater conditions to real-world DNAcol tracer applications in field studies. Initially, we expected that the presence of organic matter would limit the removal rate of DNAcol within the column, leading to a high rate of DNAcol being collected from the column effluent. Contrary to this expectation, the experimental results of DNAcol transport within the undisturbed soil columns indicated a high removal rate of DNAcol within the column, with no clear breakthrough curves observed. Directly comparing the results of the acid-washed sand and undisturbed soil columns was challenging due to differences in sand grain sizes and the influent DNAcol concentration (C_0) used. However, several factors may have contributed to the significant attachment and/or retention of DNAcol within the undisturbed soil column. Firstly, the smaller size of sand grains in the undisturbed column (~300 μm compared to 527.5 μm for acid-washed columns) may have played a role. Additionally, the concentration of injected DNAcol was lower for the undisturbed column compared to the acid-washed sand columns. As observed from the calibration curve data, larger error bars are associated with samples containing low DNA concentrations. Furthermore, we anticipated surface heterogeneity, such as metal oxides on the soil grains from the field, contributing to the attachment of negatively charged DNAcol. XRF analysis results indicated that the sand grains contained approximately 85% SiO_2, and ~9% metal oxide (Al_2O_3, CaO, K_2O, Na_2O, MgO, and Fe_2O_3). The presence of surface heterogeneity on the grains may have led to the elimination or reduction of the repulsive energy barrier locally [180]. Another aspect that needs to be considered is

the potential impact of biofilm and biological activity on DNAcol removal within the soil column.

During transient porewater chemistry conditions, in all experimental conditions, we observed that when flushing the column with Milli-Q water, the retained DNAcol remobilized. Among the conducted experiments, the high mass recovery of DNAcol with respect to the inject concentration (C_0) was observed when synthetic groundwater was used as the background solution during steady porewater chemistry conditions. The remobilization occurred due to the reduction in ionic strength of the porewater [42, 45, 62, 114, 131, 144, 155, 157, 159, 160, 190, 211]. During the transient chemistry conditions, it seems that the electrostatic repulsion was enhanced due to the decrease in ionic strength. Moreover, some of the aggregated DNAcol in the synthetic groundwater solution likely broke down into single particles.

4.5. Conclusions

In this study, we tested the transport of DNAcol through three series of column experiments. In the first series, we examined the effect of groundwater quality and Milli-Q water on the transport of DNAcol. In the second series, we investigated the impact of the absence of natural organic matter on the transport of DNAcol using synthetic groundwater. In the third series, we used an undisturbed soil column as porous media and tested the transport of DNAcol at two different concentrations. Overall, the study aimed to understand the behavior of DNAcol transport under various conditions within sand column experiments.

- The experimental and modeling results obtained from the sand columns, using two different natural groundwater, showed moderate attachment and/or retention of DNAcol within the sand column.
- Repeated experiments with synthetic groundwater, which were free of organic matter, revealed significant retention and/or attachment of DNAcol within the sand column. This suggests that the natural organic matter plays a crucial role in enhancing the transport of DNAcol through porous media.
- The experiments revealed several experimental and laboratory challenges associated with DNAcol. One issue was the sensitivity of DNAcol when stored in natural groundwater for an extended period. This was evidenced by qPCR results, which indicated a decrease in DNA concentration over time- a concern that warrants further investigation for confirmation. Additionally, when DNAcol was suspended in synthetic groundwater, its hydrodynamic size (d_h) and ζ-potential changed over the measurement period, and there was instability in DNA concentration, particularly in Tulip samples as detected by qPCR results. These findings highlight the need for further research to improve DNAcol stability under specific environmental conditions. Despite these instability concerns, the transport behavior of DNAcol remains a key area of focus.
- In a third series of the experiment using undisturbed soil columns, DNAcol was injected at two different concentrations, both lower than in previous tests.

In both cases, the DNAcol concentration in the column effluent was very low. Determining whether the extremely low mass recovery of DNAcol was due to the reduced injection concentration, soil grain size, soil structure, grain surface heterogeneity, or a combination of these factors remained challenging.

- In all the experiments conducted under transient porewater chemistry conditions, a consistent remobilization peak was observed when Milli-Q water was injected after the DNAcol elution phase. This finding underscores the critical role that transient porewater chemistry plays in the remobilization of colloidal matter.

5

Application of Multi-DNAcol in Hillslope Vadose Zone

5.1. INTRODUCTION

The tracer technique plays a crucial role in studying subsurface and groundwater systems, addressing limitations in observation methods within subsurface media [1]. One highly attractive approach in the tracer application is the injection of tracers at multiple points or times, holding significant potential for obtaining extensive information while minimizing the need for extensive fieldwork [2, 13, 212]. However, most tracers are difficult to apply in multi-time or multi-point modes due to the residual effects of signals from previous experiments or the convolution of signals from different injecting points [14]. This may lead to misinterpretation of experimental results. Therefore, implementing a multi-point or multi-time approach requires the use of multiple and distinguishable tracers, often necessitating various advanced analytical and laboratory techniques [14], thus limiting its widespread application.

To address the challenges associated with the multiple-tracer technique, synthetic DNA tracers have emerged as innovative tools for hydrological studies. These tracers can be generated in a large number of easily distinguishable variants, all exhibiting very similar transport behavior. Additionally, they are cost-effective and environmentally safe [15, 16], potentially detectable in extremely low concentrations, and can be analyzed using quantitative polymerase chain reaction (qPCR).

Free synthetic single-stranded or double-stranded DNA has been applied as tracer in several hydrological studies [13–16, 24–27, 29, 31]. However, previous studies on free DNA have highlighted several drawbacks, including its short longevity [21], potential adsorption onto minerals and sediment, especially clay [15, 24, 213], and uncertainties about its resistance to exposure to light, ultraviolet (UV) light, and bacterial activity [14, 15, 17]. Additionally, substantial mass losses of the DNA tracer compared to conservative tracers have been observed [14, 15, 29].

The fabrication of synthetic DNA tracers has progressed with the incorporation of coating substances such as polylactic acid (PLA) [21] or silica [34]. By encapsulating DNA, it is expected that many issues associated with free DNA could be mitigated, except for the attachment problem, which requires further research. Several studies have explored the application of encapsulated DNA particles in various environmental systems [14, 21, 39, 43, 49].

Among those studies, limited research has explored the potential use of DNA tracers for multi-point or multi-time applications as hydrological tracers [14, 15, 39]. Therefore, to comprehend and validate the effectiveness of encapsulated DNA particles as a hydrological tracer tool in water flow and solute transport research, further studies across multiple scales, from laboratory to field experiments are required.

The primary objective of this study was to assess and validate the multi-tracing application of silica-encapsulated DNA (DNAcol) in the vadose zone of a hillslope (200 m^2 plot scale). More specifically, we aimed to identify the significance of both lateral and vertical subsurface flow and to identify possible preferential flow and parts of the hillslope contributing to the generation of that subsurface flow. The experiment was designed as an event-based tracers' experiment, utilizing an artificial sprinkling setup with distinct DNAcol tagged with different DNA sequences.

5.2. MATERIALS AND METHODS

5.2.1. STUDY SITE

The experimental site and instrumentation were designed by the Hydrology group at the University of Freiburg and were comprehensively described by Rinderer *et al.* [59]. A brief description of the experimental site is provided here. The study site is located in Tuttlingen (47°58′42″ N, 8°44′50″ E), approximately 125 km south of Stuttgart, Germany (Fig. 5.1). The site's elevation ranges between 720 to 840 m above sea level. The regional annual average precipitation is 900 mm. The site is predominantly covered by Beech trees, and characterized by forested landscape. The experimental site is located in fractured carbonate lithology with a 1 to 1.2 m thick regolith that consists of two distinct layers; the topsoil, with a thickness ranging from 20 cm to 40 cm, and the weathered subsoil, extended from 60 cm to 80 cm. The surface layer contains 50% rock fragments, whereas the rock fragments in the weathered subsoil is 67%.

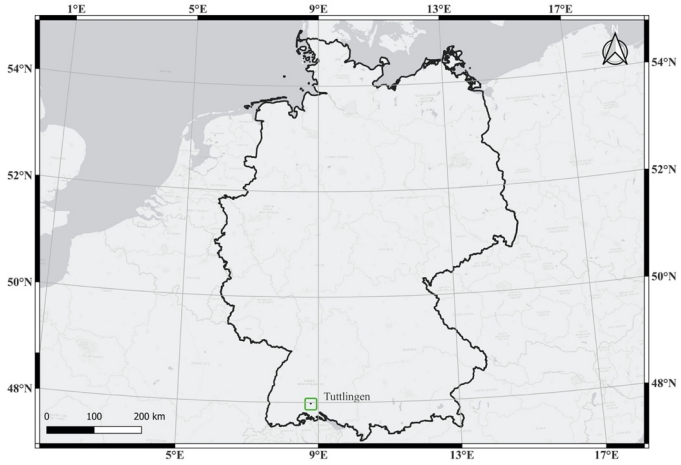

Figure 5.1.: Location of experimental site

5.2.2. EXPERIMENTAL SETUP AND INSTRUMENTATION

The experimental setup was implemented on a hillslope with a plot size of 10 m × 20 m, covering a total area of 200 m^2 (Fig. 5.2A). To control water movement from the surrounding area, a plastic foil was inserted into the soil profile on the uphill side of the plot.

On the downhill side of the plot, a 10-meter-long trench (TR) was excavated to collect lateral flow at two different depths. Drainage pipes were installed at depths of 10 cm and 60 cm (Fig. 5.2B), accompanied by a drainage mat and plastic foil.

This design facilitated the controlled collection of lateral flow at distinct outlets. The outflows from trenches (TRs) were directed through pipes to tipping buckets and automatic water samplers. Tipping buckets recorded the flow values, while the automatic water samplers collected the outflows at regular 5-minute intervals.

For collecting vertical flow, three zero-tension plate lysimeters (LYs) were installed at the side of the hillslope at depths of 10 cm, 40 cm, and 60 cm (Fig. 5.2B). Each LY was constructed with plates having dimensions of 1 m × 0.6 m. To set up the LYs, a trench was excavated at one side of the hillslope, and the three LYs were carefully inserted into the soil from the side, allowing water collection at specific depths. Once the LYs were in place, the trench was filled. Similar to the trench setups, subsurface flow from all three LYs was routed through drainage pipes to tipping buckets (at 5-minute intervals) and automatic water samplers. Volumetric soil water content and soil temperature were monitored at depths of 20 cm, 40 cm, 60 cm, and 80 cm at 5-minute intervals using SMT100 sensors (Truebner GmbH) connected to data loggers (Campbell Scientific). The experimental instrumentation was designed and described in detail by Rinderer *et al.* [59].

5.2.3. DNACOL EXPERIMENT

All four distinct DNAcol were fabricated based on the protocol developed by Paunescu *et al.* [34] and Mikutis *et al.* [39] in the Functional Materials Laboratory at ETH Zurich and kindly provided for this research. The details of the fabrication and quantification of silica-encapsulated DNA were described in Paunescu *et al.* [34] and Mikutis *et al.* [39]. The preparation of DNAcol stock solutions involved the use of four distinct DNAcol labeled S1-S4. Each DNAcol stock solution was prepared by adding 0.3 mL of the respective DNAcol to 1 L of demineralized water.

For the experiment, DNAcol S1-S4 was simultaneously used. Thereto, the experimental plot was divided into four subplots parallel to the trench, each with dimensions of 10 m in length and 5 m in width. DNAcol was manually sprayed on the soil surface along the midsection line of each sub-plots, using spray bottles. More specifically, S1 was sprayed at a distance of 2.5 m from the trench, S3 at 7.5 m, S2 at 12.5 m, and S4 at 17.5 m (Fig. 5.2B). Before spraying DNAcol, sub-samples were taken from the stock to determine initial concentrations (C_0). Table 5.1 provides the size of DNAcol S1-S4.

5.2.4. SPRINKLING EXPERIMENT

The artificial sprinkling experiment was conducted on May 21, 2019. About 15 minutes after spraying S1-S4 on the surface, the sprinkling experiment began at 8:00 AM. This experiment involved using 51350 L deionized water with electrical conductivity (EC) below 20 μm cm^{-1} to fill a water pillow (Strum Feuerschutz GmbH). To this water, 1 kg of deuterium was added. The water pillow, containing the deuterium-enriched water, was placed uphill at a location approximately 80 m above the experimental plot. This setup created a sufficient hydrostatic gradient for sprinkling the water. Constant pressure head for the sprinklers was maintained using pressure regulators.

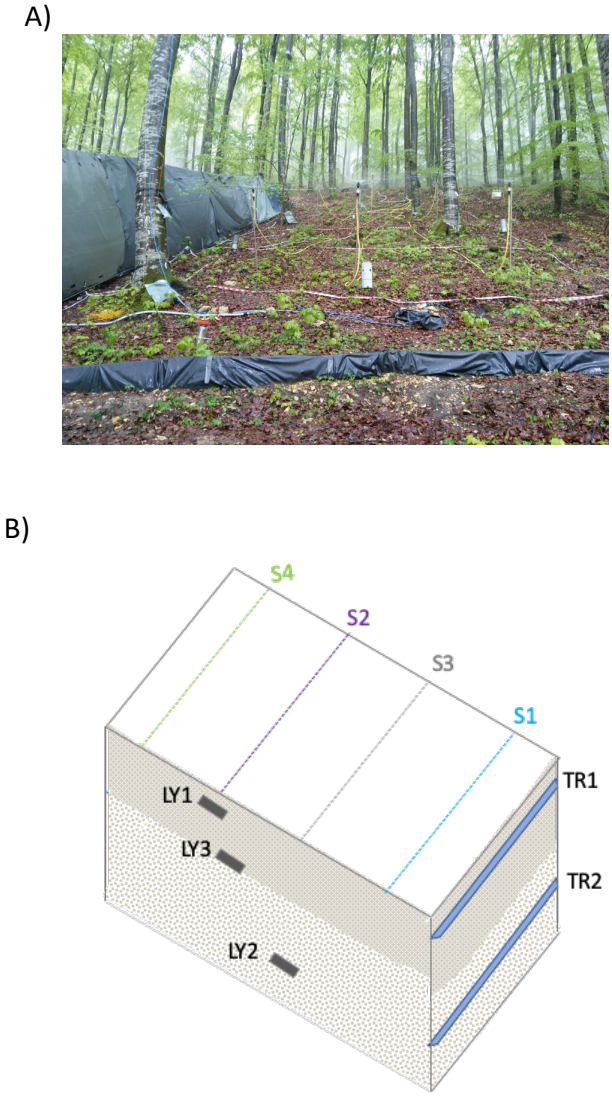

Figure 5.2.: (A) Experimental site, (B) location of two trenches (TR1 and TR2), three lysimeters (LY1, LY2, and LY3), and the area where the four DNAcol (S1, S2, S3, and S4) were applied on the surface adapted from Rinderer *et al.* [59].

Table 5.1.: Information about the primers that were used, and the hydrodynamic diameter of DNAcol were measured by the fabrication group of ETH Zurich.

DNAcol	Primer	GC	base pair
Size [nm]		[%]	[bp]
DNAcol (S1)	Forward primer (5′-ATG GGC TCT AAG GAT CTC-3′)	50	18
N.A.	Reverse primer (5′-CTC ACC CTC GAA TCG AA-3‘)	53	17
DNAcol (S2)	Forward primer (5′-CGG ACA ATC CTT TCC ATA-3′)	44	18
300± 9	Reverse primer (5′-ACG AGA CCC AGT TAA TAA G-3′)	42	19
DNAcol (S3)	Forward primer (5′-TGA GCA CCT TTG ATT CA-3′)	41	17
280± 8	Reverse primer (5′-CCG ATC TTT CAC ATA ATG G-3′)	42	19
DNAcol (S4)	Forward primer (5′- CTC TGC CCT TAC GTT TAT C-3′)	47	19
284± 9	Reverse primer (5′-AGA GGT TTG TTC GTG TTC-3′)	44	18

The sprinkling experiment was designed to mimic a rainfall intensity of 10.4 mm h^{-1} over a duration of 10.5 hours. This intensity closely represented a large rainfall event occurring every 100 years (DWD Climate Data Centre, 2010). This high-rainfall event was intended to simulate water infiltrating into the soil while preventing surface runoff [59].

Six radial sprinklers (Xcel-Wobbler and pressure regulator manufactured by Senninger) were installed on the 200 m^2 experimental plot. These sprinklers, each with a height of 2 m, covered an area of approximately 33 m^2. During the experiment, approximately 60% of the total water volume was sprinkled within the plot, while the remaining 40% was sprinkled in the surrounding area [59]. Rainfall in the experimental plot was measured using three tipping bucket rain gauges at a regular interval of 2 hours.

5.2.5. OUTFLOW-SAMPLING

During the sprinkling experiments, DANcol samples were collected at different time intervals. As mentioned earlier, both lateral and vertical flow was directed through drainage pipes connected to tipping buckets and autosamplers. However, for DNAcol, samples were collected manually at different time intervals. The sampling intervals were set at 10 minutes for the initial 2 hours, then increased to 20 minutes for the following 2-3 hours, and finally to 30 minutes for the remaining duration of the experiment. DNAcol samples were collected using 180 mL plastic bottles. In total, 198 samples were taken: 37 and 42 samples, respectively, from TR1 and TR2, and 45, 41, and 33 samples from LY1, LY2 and LY3, respectively. The collected samples were stored outdoors at ambient temperature during the 2 days of transportation to the laboratory. Upon arrival at the laboratory, the collected samples were stored at 4 °C until further analysis.

5.2.6. UP-CONCENTRATION

UP-CONCENTRATION VIA CENTRIFUGATION

Before analyzing the DNA concentration of the collected samples, an up-concentration step was performed, adapted from the protocol developed by Tang [214]. The primary objective of this up-concentration step was to increase the concentration of DNA in the collected samples. As outlined in the method section, the initial batch of injected DNAcol was prepared by spiking only 0.3 mL of DNAcol in 1 L of water, and throughout the experiment, approximately 30810 L (60% of 51350 L) of water was sprinkled within the experimental plot. Consequently, the concentration of DNAcol in the collected samples was expected to be very low. To address this issue, an up-concentration step was performed to amplify the DNAcol concentration in the collected samples.

From each sampling location (i.e., TR1, TR2, LY1, LY2, and LY3), 24 samples were selected for analysis. The chosen samples were initially vortexed for 10-20 seconds to ensure homogeneity. Subsequently, a 1 mL sub-sample was extracted from each sample and pipetted into a 1.5 mL Eppendorf tube. The tube was then centrifuged using a High-Speed Table Centrifugation (Z36HK. 221.23 V01, HERMLE Labortechnik GMbH) at 60000 g for 6 minutes. Following centrifugation, 0.9 mL of the supernatant was removed carefully from the tube. This process of adding 1 mL of the collected sample, vortexing, centrifuging, and discarding 1 mL of supernatant was repeated four more times. At the end of these up-concentration steps, the sub-samples reached a final volume of 0.1 mL.

UP-CONCENTRATION VIA LYOPHILIZATION

To enhance the DNA signal during qPCR analysis, we explored lyophilization (freeze-drying) using HETO PowerDry LL3000, in addition to the centrifugation method. For lyophilization, 10 mL subsamples were taken from selected samples and lyophilized for about 24 hours. This test was conducted for S1 within samples collected from TR1 and TR2, and S2 within samples collected from LY2 and TR2.

5.2.7. BATCH EXPERIMENT

A series of the batch experiments were conducted to understand the attachment rate of DNAcol to the soil grains collected from the experimental field. Each batch experiment contained 20 grams of soil and 40 mL of Milli-Q water, with a spike of 5 μL of S2. The batches were placed on the shaker, and sub-samples from the supernatant of each batch were taken over 36 hours for qPCR analysis.

5.2.8. QPCR ANALYSIS

For the qPCR analysis, 20 μL of the sample was pipetted into a qPCR tube. For a detailed protocol on dissolving the SiO_2 and performing qPCR, please refer to Section 2.2.4 of this dissertation. The qPCR sample preparation was automated using a QIAgility pipetting robot (Qiagen, Hilden, Germany). Table 5.1 provides information about the primers that were used for qPCR.

In each qPCR run, the concentration of the injected DNAcol was analyzed in six replicates alongside the collected samples from the field. Positive controls, corresponding to D_3 of the calibration curve, and negative controls (No Template Control (NTC) consisting of pure Milli-Q water) were included to confirm the absence of contamination (Appendix, Fig. D.1).

5.3. RESULTS

5.3.1. CALIBRATION CURVE

The regression fit over 8-fold dilution series for S1-2, and S4 suspended in Milli-Q water showed coefficients of correlation of 0.998, 0.977, and 0.994 respectively (Fig. 5.3A, B, and D). However, for S3, we observed that the data points did not follow a perfect linear regression (Fig. 5.3C). The regression fit over seven dilution series had coefficients of correlation of 0.933 and efficiency of 146%.

Examining the calibration curves for S1 and S4 at D_2 (dilution factor), which corresponds to 100 mg L^{-1}, the most concentrated sample in the dilution series, the Cq values were approximately 9.6 and 8.04, respectively. The calibration curves for S2 and S3, starting from D_1 (1000 mg L^{-1}), exhibited much higher Cq values at D_2: 20.8 and 21.6, respectively. These results indicate that S2 and S3 contained fewer number of DNA copies compared to S1 and S4.

To evaluate qPCR interference and the presence of inhibition in collected water from the field, dilution series were conducted on samples collected from LY1 and LY2. The calibration data indicated that S1 suspended in water sampled from LY1 followed a similar trend as S1 in Milli-Q water (Fig. 5.3A). Similarly, S4 suspended in water sampled from LY2 exhibited calibration data comparable to Milli-Q water conditions (Fig. 5.3D). Despite these findings, for S3 suspended in water sampled from LY1, the Cq value remained constant across the range from the most concentrated to the most diluted samples (Fig. 5.3C). This observation, where similar Cq values were obtained across an 8-fold dilution range, indicates the potential presence of inhibitory compounds or non-specific DNA. These factors could interfere with the qPCR process, possibly leading to false-negative or false-positive outcomes. Therefore, the results of experiments related to S3 were qualitatively analyzed, determining only the presence or absence of target DNA in collected samples.

5.3.2. DNACOL IN OUTFLOW FROM TRENCHES

As mentioned in the methods section, outflow from the experimental plot was collected at five measuring locations along the boundary edges of the plot (Fig. 5.2B). TR1, located downhill of the experimental plot, was designed to collect the subsurface lateral flow near the forest floor (10 cm depth). Each panel in Fig. 5.4 presents a comparison of Cq values for samples that underwent up-concentration through centrifugation against eight randomly selected original samples (without centrifugation). Note that higher Cq values correspond to a lower concentration of the target DNA, indicating that more cycles are required to pass the threshold.

Among the 24 analyzed samples for S1 (Fig. 5.4A), qPCR signals were amplified

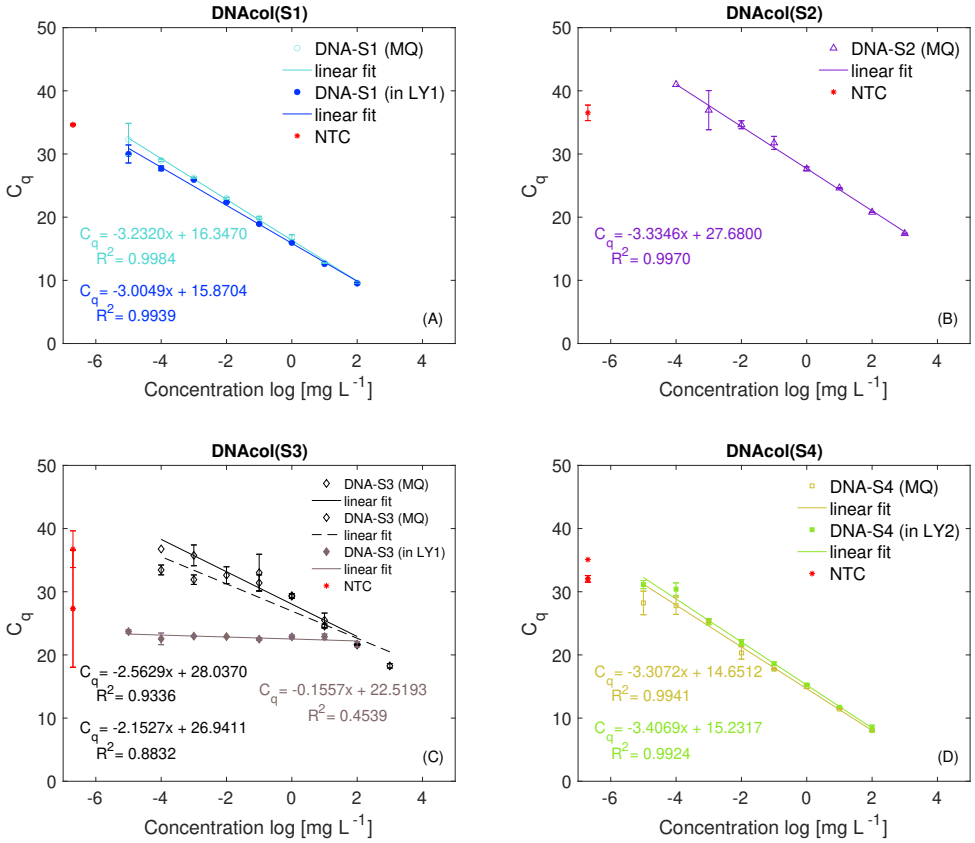

Figure 5.3.: Calibration curves for DNAcol S1-S4 and linear-regression fits (lines). Negative control values (NTC= No Template Control) of samples: red symbols. Error bars represent the standard deviation of duplicate samples. Open symbols correspond to the background solutions of Milli-Q water (MQ), while filled symbols represent background solutions of water collected from forest lysimeters (LYs).

in most samples. However, the obtained Cq values for all samples were higher than the Cq values corresponding to the NTC (Fig. 5.4A). This suggests that the concentration of DNA within these samples was either very low or, more potentially, indicative of false positives. For S2, only 11 samples exhibited an amplification of qPCR signal, with only one sample having a Cq lower than the NTC value. This implied that this particular sample had a concentration above the variation seen in the NTC (Fig. 5.4B). In the case of S3, the qPCR results showed very few sample amplifications, with all Cq values above the NTC value (Fig. 5.4C). For S4, only two samples resulted in amplification, one below and one above the quantification limit (Fig. 5.4D). The Cq values of S1 after up-concentration showed both lower and higher values compared to the corresponding samples before up-concentration (Fig.

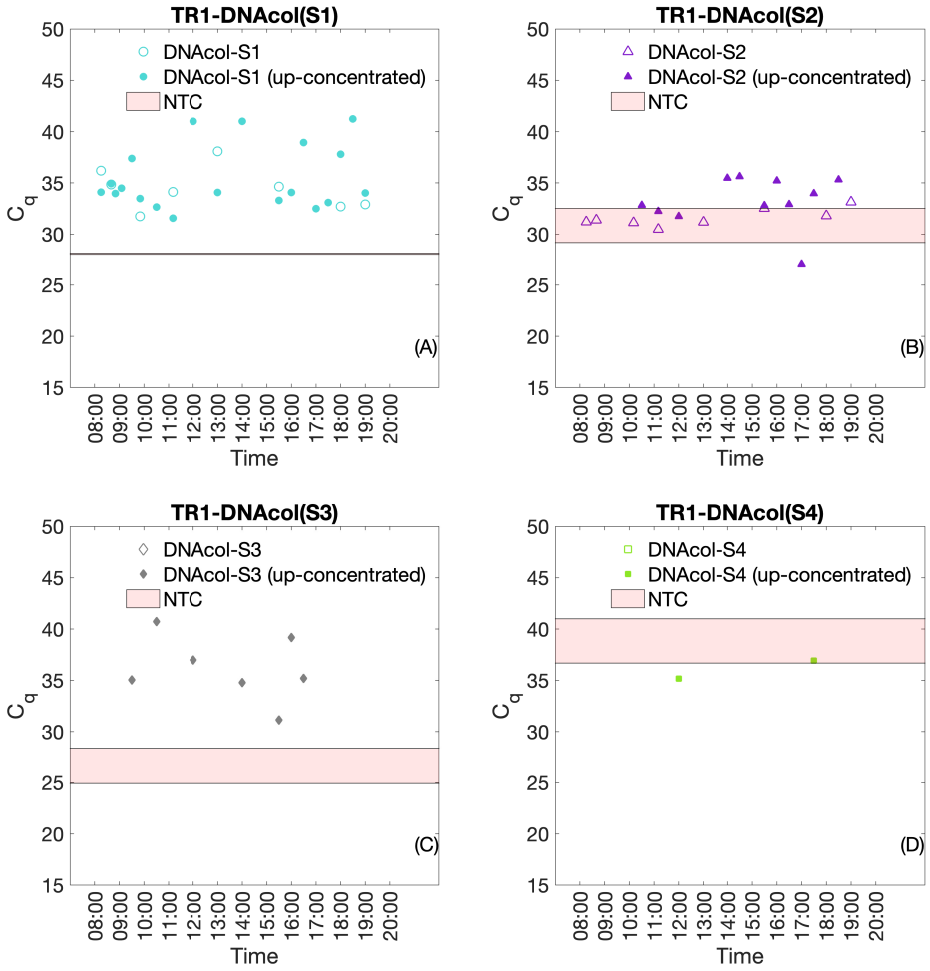

Figure 5.4.: The Cq values of samples collected from TR1 outlet. Panel (A) displays the Cq values for DNAcol (S1), panel (B) shows the Cq values for DNAcol (S2), panel (C) shows the Cq values for DNAcol (S3), and panel (D) depicts the Cq values for DNAcol (S4), In each panel, filled symbols present the up-concentrated samples via centrifugation, while the open symbols present the original samples in the absence of centrifugation. The upper and lower boundaries of the shaded area indicate No Template Control (NTC) values for each qPCR run.

5.4A). For S2, up-concentration was not effective and resulted in higher Cq values compared to the Cq values of the original samples (before centrifugation) or showed no amplification (Fig. 5.4B). The qPCR results did not show any amplifications for

the original samples analyzed for S3 and S4 (Fig. 5.4C-D).

Similar to TR1, TR2 is located downhill of the experimental plot, collecting the lateral subsurface flow at a depth of 60 cm. Once again, 24 samples were selected for up-concentration from the collected samples at the TR2 outlet, and these samples were analyzed for all four DNAcol types that were used in this experiment. The compression of Cq values before and after up-concentration indicated that the up-concentration step was effective for S1. This effect is demonstrated by the reduction in Cq values for most samples, reflecting an increase in DNA concentration (Fig. 5.5A). However, for S2, the up-concentration of samples did not lead to lower Cq values in most of the analyzed samples (Fig. 5.5B). The Cq values of the samples for S3 after up-concentration showed both increases and decreases compared to the Cq values of samples before up-concentration (Fig. 5.5C). In the case of S4, positive effects of centrifugation were observed in only one sample. However, the Cq values of all analyzed samples of S4 fell between the NTC values, indicating that the concentration of these samples was below the quantification limit (Fig. 5.5D).

5.3.3. DNACOL IN OUTFLOW FROM LYSIMETERS

The three lysimeters (LY1, LY2, and LY3) were located on one side of the experimental plot to collect vertical outflow (Fig. 5.2). LY1, situated as the most uphill measurement point, collected vertical flow from a very shallow depth (10 cm). Samples from LY1 were analyzed for S2 and S4 (Fig. 5.6). Despite the application of S2 almost on top of LY1, the obtained Cq values of the analyzed samples were above and close to the NTC (Fig. 5.6A). However, for S4, which was applied 5 m away from S2, for a few samples collected at the beginning of the experimental timeframe, the Cq values were below NTC values. Nevertheless, this raised concerns about potential false positives (Fig. 5.6B).

The second uphill measurement point was LY3, which collected vertical flow at a depth of 40 cm. Similar to LY1, we expected the presence of S2 and S4 at this outlet. In the case of S2, the analyzed samples did not show improvement after up-concentration, and most of the obtained Cq values falling within or close to the range of the NTC (Fig. 5.6C). For S4, only six samples exhibited amplification (Fig. 5.6D).

LY2 was positioned uphill from TRs, collecting vertical flow from a depth of 60 cm. The collected samples from this location were analyzed for S2, S3, and S4 (Fig. 5.7). For S2 samples, from the first sample, an amplification of the qPCR signal was observed. In most of the analyzed samples for S2, the concentration of DNA was above the NTC ranges (Fig. 5.7A). The Cq values of samples for S3 were scattered slightly below and above NTC values (Fig. 5.7B). For S4, all Cq values were above the NTC, suggesting either a very low concentration of target DNA or the presence of non-specific product amplification (Fig. 5.7C). In the case of S2, both positive and negative changes in Cq values were observed after up-concentration (Fig. 5.7A).

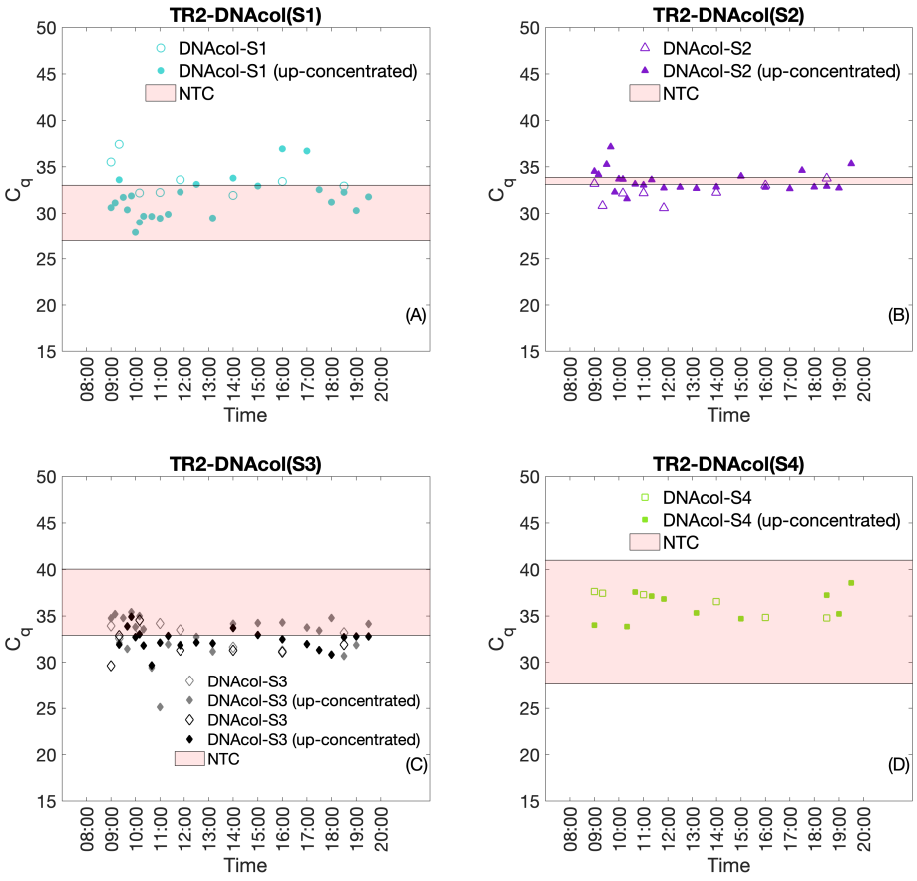

Figure 5.5.: The Cq values of samples collected from the TR2 outlet. Panel (A) displays the Cq values for DNAcol(S1), panel (B) shows the Cq values for DNAcol(S2), panel (C) presents the Cq values for DNAcol(S3), and panel (D) depicts the Cq values for DNAcol(S4), In each panel, filled symbols represent up-concentrated samples via centrifugation, while the open symbols represent the original samples in the absence of centrifugation. The upper and lower boundaries of the shaded area indicate No Template Control (NTC) values for each qPCR run.

5.3.4. UP-CONCENTRATION VIA LYOPHILIZATION

As mentioned earlier, considering the experimental conditions, we anticipated a low DNA concentration within the collected field samples. For the analyzed samples collected for TR1 for S1, several cases showed an increase in DNA concentration after lyophilization; however, the Cq values remained above NTC levels (Fig. 5.8A).

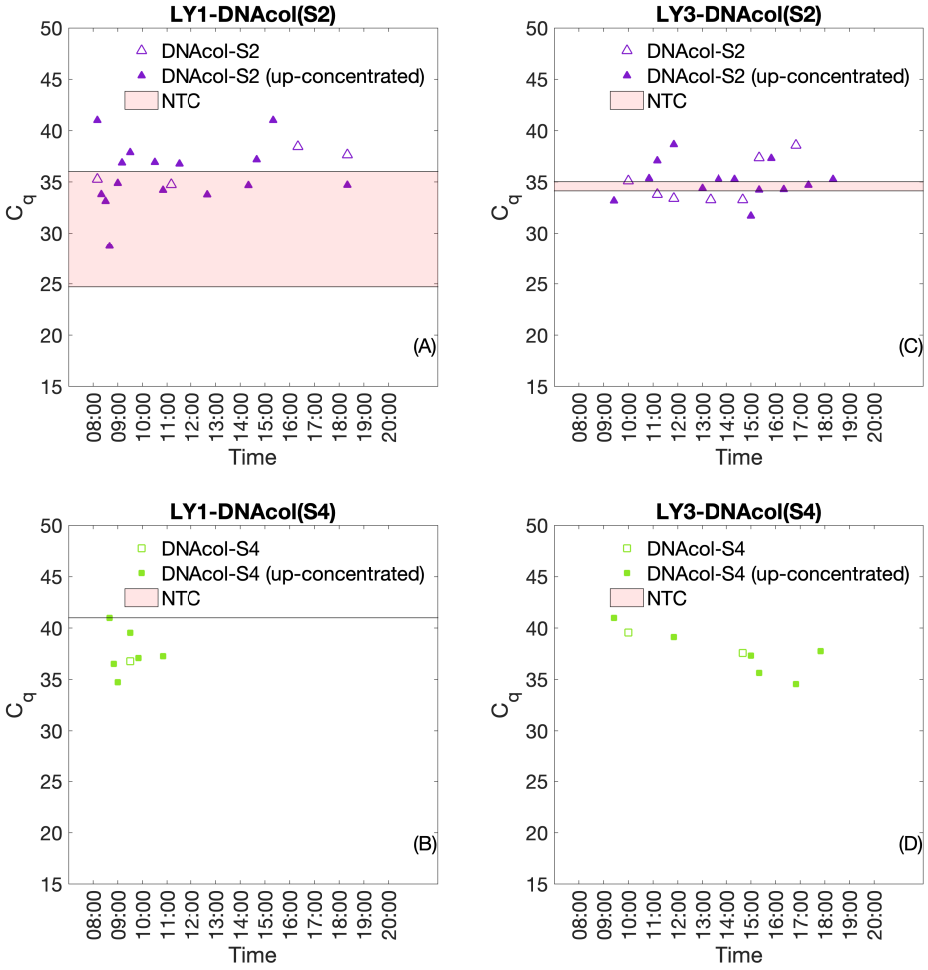

Figure 5.6.: The Cq values of samples collected from LY1 (panels A-B) and LY3 (panels C-D) outlets. Panel (A) displays the Cq values for DNAcol(S2) samples collected from LY1, panel (B) presents the Cq values for DNAcol(S4) samples collected from LY1, panel (C) presents the Cq values for DNAcol(S2) samples collected from LY3, and panel (D) shows the Cq values for DNAcol(S4) samples collected from LY3. In each panel, filled symbols represent the up-concentrated samples via centrifugation, while open symbols represent the original samples in the absence of centrifugation. The upper and lower boundaries of the shaded area indicate No Template Control (NTC) values for each qPCR run.

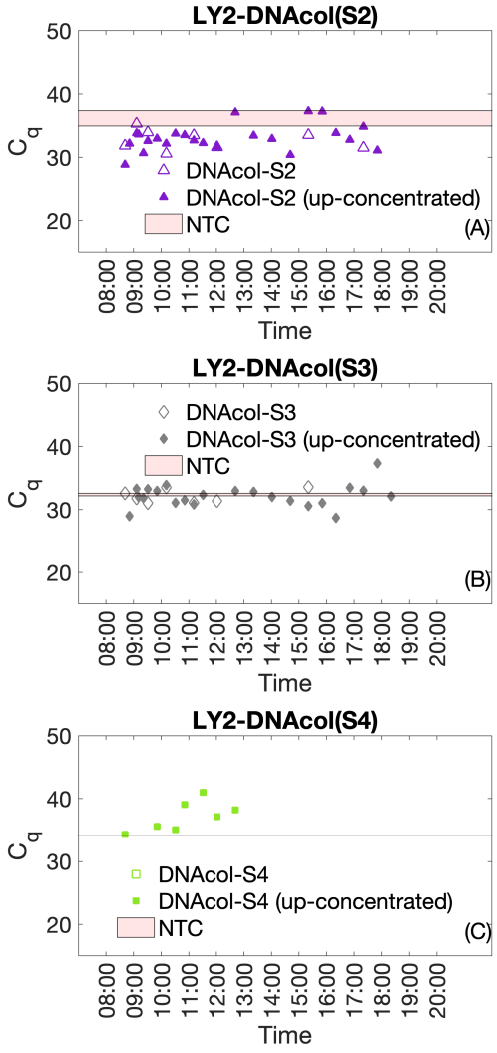

Figure 5.7.: The Cq values of samples collected from LY2 outlet. Panel (A) displays the Cq values for DNAcol(S2), panel (B) shows the Cq values for DNAcol(S3), and panel (C) shows the Cq values for DNAcol(S4). In each panel, filled symbols represent up-concentrated samples via centrifugation, while open symbols present the original samples in the absence of centrifugation. The upper and lower boundaries of the shaded area indicate No Template Control (NTC) values for each qPCR run.

The comparison of Cq values for S1 for collected samples from TR2 revealed both increases and decreases in Cq values after lyophilization (Fig. 5.8B). However, For S2 samples collected from LY2, the Cq values of lyophilized samples in most cases decreased compared to the original samples, indicating an increase in DNA concentration (Fig. 5.8C). For S2 samples collected from TR2, there was evidence of improvement in DNA concentration (Fig. 5.8D). It should be noted that, for the samples that became completely dry after lyophilization, 1 mL of Milli-Q water was added to them prior to qPCR analysis.

5.3.5. Batch Experiment

For the batch experiments, none of the samples showed an amplified curve in the qPCR results, suggesting complete inhibition of the analyzed samples, potentially due to the presence of organic matter or any other inhibitory substance. Because there was no amplification signal, the results of the batch experiments were not included.

5.3.6. Assessing of Inhibition and False-Positive Signal in qPCR Analysis

Inhibitory substances, such as humic acid, particulate matter, salt, and ethanol, can interact with DNA or interfere with qPCR amplification. However, based on the result of the dilution series curve in forest water, we did not observe an inhibition effect. While the batch experimental results indicated full inhibition. Therefore, we conducted a preliminary test for check the possibility of inhibition in some of the samples, the results of this test are presented in Appendix section D.2 and Fig. D.2. The results suggested no inhibitory effect or a very weak effect for the analyzed sample, except for one sample.

Additionally, the qPCR results for the samples collected at the five sampling locations in the field sometimes exhibited positive fluorescence signal amplification from the early phase of the sampling period. However, in most cases, the obtained Cq values were close to the NTC, raising concerns about potential false-positive results from a qPCR perspective. This suggests that the amplification signal may be a consequence of non-specific target DNA presence in the absence of DNAcol. To address this concern, selected samples collected from TR1 and TR2 underwent qPCR with and without the addition of buffered oxide etch (BOE), indicating the assessment of the samples with and without releasing the DNA from its silica shell (Appendix D.3; Fig. D.2). The obtained Cq values for both datasets were close to NTC values, suggesting that in the case of the presence of non-specific DNA within the samples, the obtained Cq values were close to NTC values (Fig. D.2).

5.4. Discussions, Limitation, and Future Work

As outlined in the method section, the experimental setup was designed by Rinderer *et al.* [59]. Their primary research focus was to understand the mechanisms behind subsurface runoff generation and phosphorus response in a forested area using

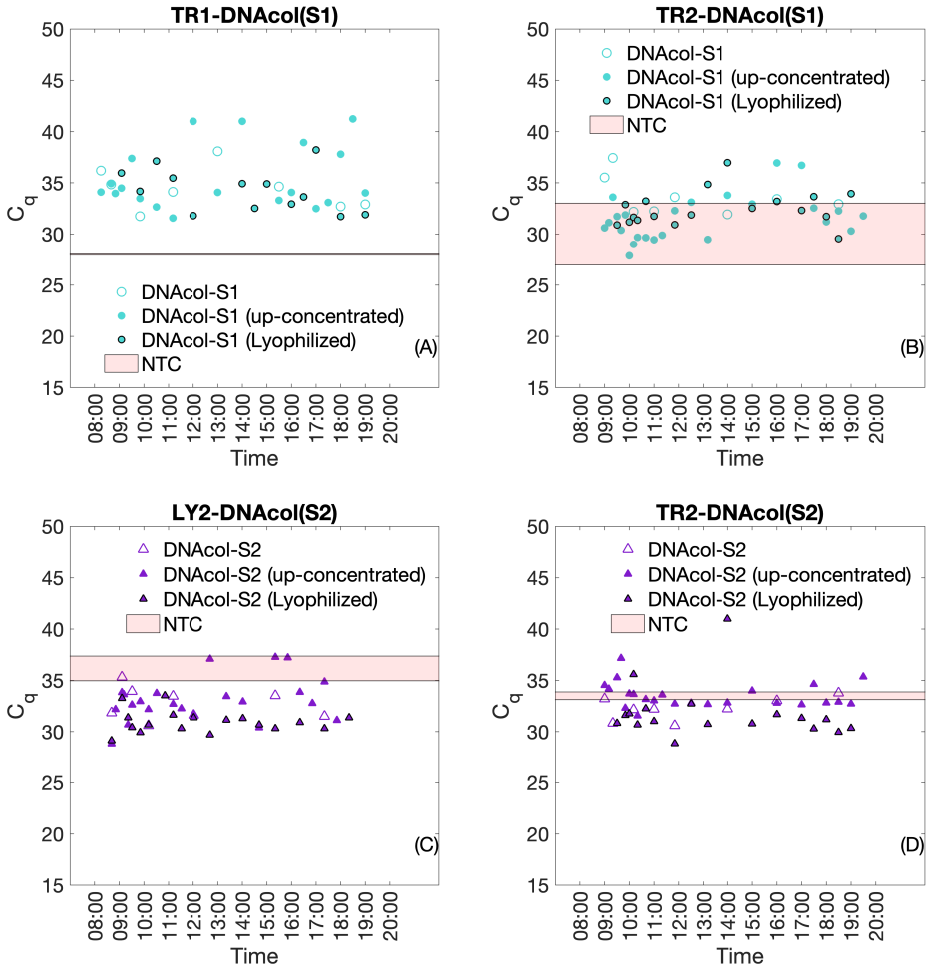

Figure 5.8.: The comparison of Cq values for samples using different up-concentration methods. In each panel, the open symbols represent the original samples without up-concentration, filled symbols present the up-concentrated samples via centrifugation, and filled symbols with a black border represent up-concentrated samples via lyophilized. The upper and lower boundaries of the shaded area indicate the No Template Control (NTC) values for each qPCR run. Panel (A) displays the Cq values for DNAcol(S1) samples collected from TR1, panel (B) shows the Cq values for DNAcol(S1) samples collected from TR2, panel (C) shows the Cq values for DNAcol(S2) samples collected from LY2, and panel (D) shows the Cq values for DNAcol(S2) samples collected from TR2.

sprinkled deuterium (^{2}H) enriched water as a tracer [59]. Concurrently, DNAcol experiment was conducted as a complementary tracer.

The results of the deuterium (^{2}H) tracer experiment, as reported by Rinderer *et al.* [59], highlighted the significance of vertical subsurface flow over lateral flow. Furthermore, the isotope hydrograph separation results indicated that at LY1 (located at a depth of 10 cm), subsurface flow predominantly consisted of event water, indicating a rapid displacement of pre-event water by event water. Conversely, for LY2 and LY3, pre-event water was predominant, suggesting a higher proportion of pre-event water at greater soil depths [59]. A similar pattern was observed for TR1 and TR2 [59]. Specifically, at TR1, located at the same depth as LY1, the dominant flow was event water, whereas for TR2 (located at a depth of 60 cm), pre-event water was dominant. The authors suggested that piston flow was the dominant flow mechanism [59]. Additionally, they also observed occurrences of preferential flow paths at shallow depths in the experimental plot, potentially attributed to the high clay content of the topsoil and soil properties at the experimental site [59].

The primary objective of our study was to assess and validate the multi-tracing application of (DNAcol) in the vadose zone of a hillslope (200 m^2 plot scale). Additionally, by conducting the multi-DNAcol tracer experiment, we aimed to gain insight into pinpointing the hillslope area contributing to subsurface flow generation and explore the potential role of preferential flow in subsurface flow. From DNAcol experiment, we concluded that, in the majority of the collected samples, the concentration of DNAcol was close to NTC values. Essentially, we had insufficient real positives to warrant a comprehensive analysis of DNAcol sample data. In that sense, the experiment did not achieve its aim and failed. However, we did learn a number of important lessons from this experience:

- Lesson 1: Concentration of injected DNAcol

The initial concentration of injected DNAcol ranged between D_3 and D_4 on the calibration curves (0.3 mL of DNAcol suspended in 1000 mL water). However, due to the substantial volume of sprinkled water, the concentration of DNAcol could have become significantly diluted during its transport in the subsurface.

- Lesson 2: Laboratory up-concentration challenges

In the laboratory, we used a centrifugation-based up-concentration method to enhance the DNAcol concentration within collected samples (technique adapted from Tang [214]). However, the results of the centrifugation were not satisfactory, as higher particle recovery (lower Cq values) was not achieved in most cases. It is crucial to note that the centrifugation protocol was initially developed for DNAcol suspended in pure Milli-Q water in the absence of inhibitory substances (see Tang [214]). Thus, before applying the protocol to samples containing organic matter and other inhibitory substances, its effectiveness requires evaluation. This is especially crucial for environmental samples, such as groundwater and surface water, as they often contain inhibitory compounds that can pose significant challenges during qPCR analysis. These compounds, including humic substances (humic and fluvic acid), bacterial cells, polysaccharides, metal ions, salts, ethanol, and nucleases

[215–218], can potentially interfere with the qPCR reaction, particularly in sample with large volumes [216]. The presence of inhibitory compounds may increase the quantification cycle (Cq) number, potentially leading to false-negative outcomes even when the target DNA is present within the sample. To ensure the reliability of qPCR data, it is crucial to thoroughly validate the accuracy of the qPCR assay. Depending on the nature of inhibitory substances, various approaches can be applied, such as purification and cleanup techniques, inhibitory removal kits (e.g., filtration resins) [219, 220], enhancing sample concentration, implementing sample dilution [29, 216, 220–224], and the addition of bovine serum albumin (BSA) to reduce the inhibitory effect [29, 225, 226]. Therefore, a control experiment is necessary to determine if centrifugation induces increased inhibition. This involves investigating whether centrifugation causes the sedimentation of inhibitors in the samples, potentially interfering with the qPCR signal. The suggested protocol for evaluating the efficiency of the up-concentration method involves generating serial dilutions of DNAcol samples suspended in both Milli-Q water as a reference and field-collected water. This approach helps assess the efficiency of up-concentration efficiency across samples with varying particle concentrations, ranging from low to high. In cases where inhibitory substances are present in the samples, spin columns [227] and/or centrifugation with washing steps can be employed to mitigate these inhibitory effects. An additional issue linked to up-concentration through centrifugation was the significant time, and effort involved, along with the large quantity of pipetting tips required. One primary strategy for assessing the impact of inhibitory substances involves diluting the samples. However, the main downside of dilution is the potential loss of DNA, especially when the target DNA concentration in the sample is low like in drinking water [216], as anticipated in our samples as well. Exploring the impact of bovine serum albumin (BSA) and using spin column purification can be considered as an approach to minimize or eliminate the inhibitory effects, particularly in samples containing humic substances.

- Lesson 3: Considering sampling duration

Another aspect requiring further consideration is the duration of field sampling. Our study focused on collecting samples during the course of the experiment, and the concentration of DNAcol was not monitored in the post-sampling subsurface runoff. To gain a better understanding of the dynamics of the detachment and remobilization process of retained particles, it is advisable to incorporate longer sampling durations. Extending sample collection may provide insights. As indicated by Wang *et al.* [30], the response times between discharge and the transport of free DNA were significantly different from each other in a laboratory-designed lysimeter under variably saturated transient flow conditions. Their observation also revealed that the peak of free DNA occurred after the discharge peak, particularly in the absence of rainfall during the system draining. Therefore, extending the sampling duration (post-event) can provide us with a better understanding of DNAcol transport, detachment, and remobilization.

5.5. CONCLUSIONS

In this study, a multi-tracer experiment of DNAcol was applied in an event-based experiment conducted at the plot scale hillslope. The primary aim was to understand the contribution of different parts of the hillslope to subsurface runoff with a potential focus on understanding the impact of preferential flow paths. Analysis of field-collected samples revealed that the concentration of DNA for the four different DNAcol was too low, approaching values similar to No Template Control (NTC). Batch experiments also showed no amplification of the qPCR signal, suggesting the presence of inhibitory compounds in the samples.

The findings of this study underscored the necessity for a critical evaluation of the application of DNAcol as a tracer, especially in subsurface environments. Several key considerations are highlighted for further research:

- Determining the optimal concentration of the injected tracer and duration of sampling is crucial for the success of the experiment. While we expected that due to the presence of DNA within the DNAcol could potentially be detectable in very low concentrations, our results indicated that encapsulating DNA within the shell requires a much higher concentration of the tracer to be above the lower limit of quantification. However, applying a high concentration also requires tests regarding the short- and long-term ecotoxicology effects and for regulatory assessment. Conducting a series of sand column experiments filled with soil media from the experimental site before the field experimental campaign could provide insights into the possibility of the low mass recovery of the tracer and understanding the main mechanisms governing the transport, retention, and attachment of DNAcol.

- Developing an up-concentration protocol is vital and requires validation in both pure water and environmental media.

- Investigating the presence of inhibitory compounds in the environmental sample water and defining appropriate mitigation strategy.

6

Conclusion

6.1. KNOWLEDGE GENERATED AND IMPLICATIONS

This dissertation aimed to validate an innovative technique for tracking colloidal contaminant transport at both laboratory and plot scales. A core-shell silica particle encapsulating synthetic double-stranded DNA (DNAcol) was selected as the tracer for this purpose.

A key question using DNAcol as a hydrological tracer is how hydrogeochemical conditions- such as flow velocity, soil grain size, ionic strength, and organic matter- affect its transport behavior, including retention, attachment, and both homo- and hetero-aggregation, as well as its mass recovery rate. To evaluate the feasibility of using DNAcol in environmental applications and to determine the effect of physicochemical factors on its transport behavior, the following research was conducted.

The first research (Chapter 2) examined the sensitivity of DNAcol transport to three solution chemistries (Demineralized water, NaCl, and $CaCl_2$) under two flow velocities and different sand grain sizes in sand column experiments. The results showed significant DNAcol retention in the sand column when using NaCl (33mM) or $CaCl_2$ (41mM), particularly with smaller sand grains. The HYDRUS-1D model provided a reasonably good fit to most of the experimental data, suggesting that DNAcol breakthrough could be described using a first-order kinetic attachment-detachment rate model. In experiments where the column was further flushed with demineralized water to induce remobilization, the results confirmed substantial DNAcol remobilization, indicating that much of the retained DNAcol was reversible, as supported by the DLVO profile. Overall, the study concluded that DNAcol has limitations as a conservative tracer in subsurface environments, particularly in fine sand and low flow velocity conditions.

The second study (Chapter 3) evaluated the effects of varying concentrations of dissolved organic matter (DOC) and ionic strength ($CaCl_2$) on DNAcol transport under both steady and transient porewater chemistry conditions. The experimental results showed significant variations in DNAcol recovery, ranging from approximately 1% to over 90% under steady porewater chemistry conditions. These findings highlighted the considerable influence of $CaCl_2$ in enhancing DNAcol removal, while natural organic matter facilitated DNAcol transport, and potentially contributed to the formation of an “environmental-corona” or “eco-corona”. The removal rate increased significantly even at 1mM ionic strength. In the experiments with 1 and 10 mM $CaCl_2$, breakthrough curves showed approximately 2-log removal, followed by a sharp decline during the tailing phase, indicating high DNAcol attachment and/or retention. When both DOC and $CaCl_2$ were present, the $[Ca^{2+}]$/DOC ratio was crucial, with negligible DNAcol attachment observed at the lowest ratios. The estimated attachment and detachment rate coefficients using HYDRUS-1D showed that increasing DOC concentration decreased attachment rate coefficients while increasing ionic strength decreased detachment rate coefficients. Sticking efficiency was around 1 for ionic strengths of 1 and 10 mM, indicating favorable or nearly favorable conditions for DNAcol attachment to grain media. However, in the presence of 1 mM ionic strengths with 20 mg-C L^{-1} DOC, sticking efficiency reduced to 0.03, indicating unfavorable attachment conditions. Under transient

porewater chemistry conditions, a second peak in the breakthrough curve indicated DNAcol re-entrainment. The magnitude of the remobilization peak varied, being more pronounced at 10 mM initial ionic strength compared to conditions with ionic strength equal to or less than 1 mM. This finding underscores the critical role of ionic strength changes in colloidal particle remobilization under transient porewater chemistry conditions, such as those caused by heavy rainfall that lowers ionic strength. This study emphasizes the need for further research beyond column experiments to better understand the mechanisms of attachment, retention, and remobilization of colloidal matter.

Building on the findings from the second study, the third study (Chapter 4) explored the potential application of DNAcol in agricultural fields by conducting laboratory-based column experiments. In the first series of experiments, natural groundwater with high levels of natural organic matter was used in the sand column. DNAcol exhibited moderate attachment and/or retention, as shown by the breakthrough curves, with a gradual decline during the tailing phase, indicating a slow release of DNAcol. In the second series of experiments, synthetic groundwaters, compositionally similar to natural groundwater but lacking organic matter, were used. The breakthrough curves in these tests displayed very low plateau concentrations, indicating significant attachment and/or retention, with negligible release during the tailing phase. Furthermore, the hydrodynamic diameter of DNAcol increased over 2 hours, suggesting that homo-aggregation was occurring under these conditions. In these cases, only 1% of DNAcol was recovered under steady porewater chemistry conditions. To further evaluate the applicability of these findings under more realistic conditions, a third series of experiments was conducted using an undisturbed soil column with natural groundwater. Contrary to expectations, the presence of organic matter did not result in a high recovery rate of DNAcol. Two experiments were conducted on undisturbed soil. In the first experiment, DNAcol was injected at a concentration two orders of magnitude lower than the previous tests with acid-washed sand and at a reduced flow rate, no clear breakthrough curve was observed. In the second experiment, with DNAcol concentration an order of magnitude lower and a flow rate similar to that used in the acid-washed sand column experiments, recovery remained negligible. Despite the very low recovery rates of DNAcol under steady porewater chemistry conditions, some remobilization of retained DNAcol was consistently observed under transient porewater chemistry conditions.

The fourth research (Chapter 5) investigated the application of multiple DNAcol tracers in the vadose zone of a 200 m^2 plot on a hillslope. The sprinkling experiment aimed to assess the significance of lateral and vertical subsurface flow, identify the role of preferential flow pathways, and determine areas contributing to subsurface flow generation. The analysis of the up-concentration samples revealed that the process was ineffective in increasing DNA concentration, as indicated by the Cq values, compared to those of the original samples before centrifugation. Most qPCR results showed signals either below or near the detection limit, suggesting either a very low concentration of target DNA or the presence of inhibitory substances. Although dilution series in forest water and tests for false-negative results showed

negligible to no inhibition effects, batch experiments indicated complete inhibition. This inhibition in batch samples was likely due to the release of organic matter or other inhibitory compounds from the soil during batch shaking. Additionally, the low or absent DNA concentrations in the analyzed samples could be related to the varying response times of DNAcol compared to subsurface discharge, implying that the sampling duration may have been too short to effectively capture the DNAcol signal. The limited number of positive results hindered a comprehensive analysis of the DNAcol sample data, leading to an unsuccessful outcome for this field experiment. It is worth noting that this field experiment was conducted before the completion of Chapters 3 and 4, meaning the insights gained from those studies were not applied in this context. Nevertheless, several lessons were learned from this experience:

1. Ensuring accurate estimation of the injected tracer concentration and accounting for dilution factors during transport in the subsurface environment.

2. Thoroughly assessing the effectiveness of up-concentration methods across samples containing varying concentrations of the tracer (DNAcol) in both pure and environmental water.

3. Considering an extended sampling duration after the sprinkling experiment (post-event) to better understand DNAcol transport and detachment.

6.2. LIMITATIONS AND CHALLENGES

This section highlights several limitations and lessons learned from using DNAcol as a hydrological tracer:

6.2.1. REMOVAL MECHANISM AND MASS BALANCE OF DNACOL

The primary mechanism of DNAcol removal is expected to be its attachment to soil grains, which results in significant variations in transport and recovery rates within the subsurface environment. Laboratory results indicated that ionic strength and the presence of organic matter have opposing effects on DNAcol's transport and attachment rates. As a result, DNAcol transport can vary significantly under different conditions. Due to its high sensitivity to environmental factors, achieving mass balance with DNAcol as a tracer can be challenging. Characterizing the ion composition and organic matter content of the subsurface can improve the interpretation of colloidal particle transport in specific locations. Additionally, conducting undisturbed sand column experiments and analyzing soil compositions can help address uncertainties related to the low mass recovery of DNAcol.

6.2.2. DNACOL CONCENTRATION AND DEVELOPING UP-CONCENTRATION PROTOCOL

As discussed in Chapter 5, the field tracer experiment was not successful, likely due to two main factors: the low concentration of injected DNAcol and the high

attachment rate of DNAcol to the forest soil. To effectively apply DNAcol or any other tracer in subsurface environments, it is crucial to estimate accurately the optimal tracer injection level to ensure clear detection at the sampling points.

The concentration of DNAcol was expected to be highly diluted during transport within the test field. Therefore, either a much higher initial concentration of injected DNAcol is needed, or methods for up-concentrating the target DNA in the collected samples could be developed.

Increasing the concentration of injected DNAcol might improve the likelihood of observing breakthrough results. Previous research indicated no acute effects on concentrations below 300 ppm and no chronic effects below 30 ppm on the tested species [47]. However, it is essential to conduct short- and long-term ecotoxicology testing on the applied concentration while considering the particle size beforehand.

In the field experiment, most collected samples from the field had volumes greater than 100 mL. Initially, 20 μL was used to dissolve the silica shell, and after shell dissolution, only 5 μL was used for qPCR analysis. To up-concentrate the samples 50 times, we used centrifugation, repeatedly adding 1 mL of sample and discarding 0.9 mL of supernatant each time to achieve a final volume of 0.1 mL. However, the primary results showed that this method was ineffective in our experiment. Additionally, the up-concentration process via centrifugation was significantly time-consuming, labor-intensive, and required a large number of pipette tips.

6.2.3. qPCR QUALITY CONTROL

The qPCR technique is known for its sensitivity in detecting and quantifying target DNA, even at very low concentrations. When working with DNA molecules in qPCR assay, robust quality control is crucial. This involves designing optimal reactions with carefully selected primers and incorporating positive and negative controls.

The concentration of target DNA measured by qPCR follows a logarithmic scale, where small variations in Cq values can lead to considerable variability between replicate analyses, a recognized limitation in the field [223, 228]. This limitation can potentially be minimized by increasing the number of replicate samples, increasing sample volume, and ensuring thorough mixing of samples prior to qPCR analysis [39]. In most experiments, except those in Chapter 2, we mitigated variation by collecting five to six subsamples from each injected DNAcol batch.

When dealing with environmental samples, it is essential to include control samples using both pure and environmental water from the sample's environment. This ensures the reliability and accuracy of qPCR results by detecting any potential contamination or inhibition that could impact the analysis outcome. Environmental samples such as groundwater can contain inhibitory compounds- including humic substances, salts, polysaccharides, and metal ions [215–218]- that can interfere with the qPCR reaction. These compounds can result in lower estimated concentrations of target DNA or even false-negative results. In this research, all the samples were analyzed without purification steps, as the tested samples exhibited low to no inhibitory effect before centrifugation. However, during the up-concentration process via centrifugation, in case of presence of inhibitory substances might increase due to

the sedimentation of these particles. Therefore, developing and validating tailor-made up-concentration methods, such as centrifugation or lyophilization, along with strategies to mitigate or eliminate inhibitory effects, is crucial. These methods and strategies should be thoroughly evaluated in both pure and environmental water across various DNA concentrations. Implementing various strategies is essential for minimizing inhibition in qPCR analysis. Washing with Milli-Q water before qPCR is recommended to reduce or eliminate inhibition effects.

6.2.4. SAMPLING STORAGE TEMPERATURE

Another factor that might contribute to a reduction in DNAcol within the collected samples could be related to the environment temperature during the transportation of the samples from the field to the laboratory. After the field experiment, the samples were stored at ambient temperature during the two-day transport to the laboratory. This could potentially lead to a loss of the qPCR signal due to ongoing biological and chemical activity within the samples. This issue warrants further investigation. Mikutis *et al.* [39] reported a substantial loss of the qPCR signal in collected samples stored at room temperature or exposed to high ambient temperatures. They recommended either freezing the sample until qPCR analysis or using chemicals to suppress the microbial activity to mitigate such losses [39].

6.3. FUTURE PERSPECTIVE

6.3.1. MECHANISM OF DNACOL RETENTION AND TRANSIENT POREWATER CHEMISTRY CONDITIONS

Initially, this research did not aim to assess the transport of DNAcol under transient porewater chemistry conditions caused by decreasing ionic strength. However, our initial study revealed significant remobilization of retained DNAcol following water injection. Across all tested transient porewater chemistry conditions, a consistent second peak was observed, although its magnitude varied among different experimental conditions. These findings highlight the importance of improving models to better understand retention mechanisms under steady porewater chemistry and release mechanisms under transient porewater chemistry conditions. A deeper understanding of these mechanisms is crucial for more accurately predicting the mobility of colloidal matter. Moreover, this research emphasizes the need to focus on the significant remobilization of colloids, such as pathogens and engineered particles, to develop robust risk mitigation plans.

Further research is also essential to refine the equation of sticking efficiency under unfavorable attachment conditions and in organic-rich environments. This will help enhance our understanding and predictive capabilities regarding colloidal transport and retention in complex environmental systems.

6.3.2. FIELD-DEPLOYABLE QPCR

Access to timely and accurate data is crucial across many scientific fields, as it forms the foundation for understating systems and developing models.

Field-deployable autoanalyzers are emerging as powerful tools for environmental and water quality monitoring, offering high-frequency data collection of nutrients and environmental solutes at sub-hourly intervals. Particularly in catchment-scale monitoring, continuously measuring chemical parameters in the environment at high frequencies over the long term can offer valuable insights into water quality and ecosystem dynamics [229]. However, this approach can be costly and requires regular maintenance, and to ensure accuracy, it remains essential to perform laboratory duplicate analyses to cross-check the results of in-situ autoanalyzers [229].

In this context, field-deployable qPCR instruments are emerging as powerful tools for early warning and risk management related to biological contamination, environmental DNA (eDNA), and pathogen detection and quantification. A study by Billington *et al.* [230] compared results from a portable qPCR instrument with those from a laboratory bench qPCR. The portable instrument, which operates in a fully enclosed system for both nucleic acid extraction and qPCR amplification, demonstrated performance comparable to laboratory qPCR settings in terms of repeatability and sensitivity. Despite these advantages, using field-deployable qPCR to detect encapsulated DNA particles, such as DNAcol, which could potentially serve as surrogates for colloidal matter, may face certain challenges. Specifically, one constraint is the need to dissolve the silica shell of DNAcol, which requires a buffered oxide etch, a process that may be impractical to perform in field conditions. To overcome this limitation, exploring alternative materials for encapsulating DNA tracers could facilitate easier dissolution, making the technology more applicable in field settings.

6.3.3. ADVANCING DNACOL SURFACE MODIFICATIONS AND ENCAPSULATING

Further research could focus on how adsorbed layers of coating materials or natural organic matter affect the transport of DNAcol, aiming to overcome attachment issues and enhance the mobility of encapsulated DNA particles in porous media. For example, Manley [231] proposed surface modifications to silica-encapsulated-DNA, using hydrophilic polymer hairs, and coating materials. Dahlke *et al.* [14] recommended examining how varying zeta potentials affect the sorption and transport of encapsulated DNA particles by creating tracers with different surface zeta potentials. Mora *et al.* [49] suggested improving the stability and recovery rate of silica-encapsulated-DNA particles by modifying their physicochemical properties, such as through surface functionalization or adding a magnetic core. Additionally, grafting silica particles with hydrophobically modified materials, as demonstrated by Yegane *et al.* [232] for enhanced oil recovery in brine conditions, could be a promising approach for hydrological applications. Therefore, surface modifications to DNAcol have the potential to expand its use across various fields, such as geothermal reservoir characterization, enhanced oil recovery, and as a more conservative tracer for both surface and subsurface hydrological studies.

6.3.4. EXPLORING EFFECT OF SOIL STRUCTURE AND PREFERENTIAL FLOW PATHS

Investigating the influence of soil structure on DNAcol transport, particularly in clay-rich soils, is essential for understanding the role of preferential flow paths in facilitating rapid movement. This area remains largely unexplored and could yield valuable insights into the behavior of colloidal contamination in diverse soil environments.

6.4. CONCLUDING REMARKS

In colloidal studies and risk management of engineered microparticles and biological contaminants, understanding travel distances, pathways, and the ultimate fate of these substances in the subsurface environment is crucial. This dissertation represents a systematic investigation into various factors that influence the transport of DNAcol within porous media. Systematic studies provide insights into the factors influencing transport, removal, and release mechanisms which in turn enhance our ability to predict the behavior of such substances. This knowledge is aiding in groundwater and soil remediation efforts and in mitigating the risk associated with colloidal contamination.

In conclusion, while DNAcol as a conservative hydrological tracer has certain limitations- such as challenges in addressing mass balance-related questions- it offers value as a complementary tracer. Moreover, it shows potential as a surrogate for other nano- and micro-particles such as nanoplastics, bacteria, viruses, and even bacteriophages. However, the successful implementation of these potential applications will require systematic testing and validation. When selecting an appropriate colloidal tracer, it is crucial to consider factors such as particle morphology, including size, charge, and surface characteristics (e.g., soft or rigid surfaces).

A

APPENDIX-A: SUPPLEMENTARY MATERIAL FOR CHAPTER 2

This chapter is based on:
Kianfar, B., Tian, J., Rozemeijer, J., van der Zaan, B., Bogaard, T. A., Foppen, J. W. (2022). Transport characteristics of DNA-tagged silica colloids as a colloidal tracer in saturated sand columns; role of solution chemistry, flow velocity, and sand grain size. Journal of Contaminant Hydrology, 246, 103954. [44]

A

A.1. DNA NUCLEOTIDE SEQUENCE

The nucleotide sequence of the dsDNA we used was (Forward) 5′-GAT TAG CTT GAC CCG CTC TGT AGG GTC GCG ACT ACG TGA GCT AGG GCT CCG GAC TGG GCT GTA TAG TCG AGT CTG ATC TCG CCC CGA CAA CTG CAA ACC CCA ACT-3′.

A.2. CALIBRATION CURVE AND STATISTICS OF QPCR EFFICIENCY

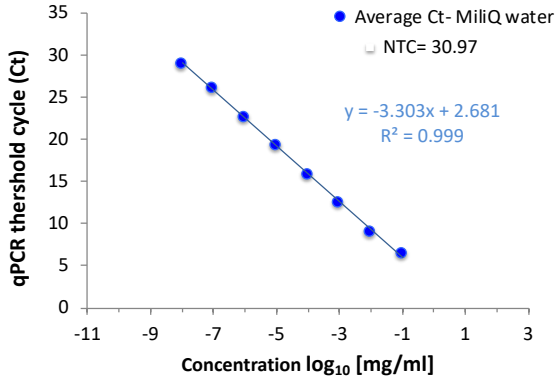

Figure A.1.: Standard curve of 8-fold dilution series of known DNA particle concentration in Milli-Q water. NTC: No Template Control.

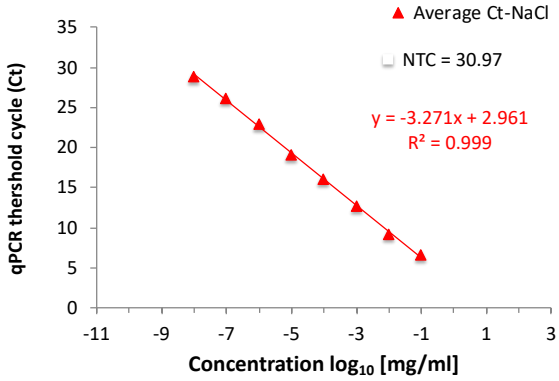

Figure A.2.: Standard curve of 8-fold dilution series of known DNA particle concentration in NaCl.

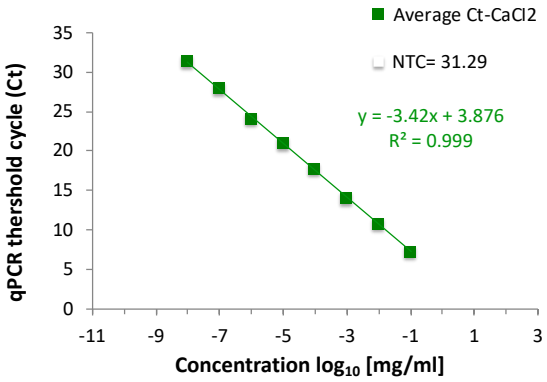

Figure A.3.: Standard curve of 8-fold dilution series of known DNA particle concentration in $CaCl_2$.

A

A.3. STICKING EFFICIENCY

Table A.1.: Overview of parameter values required to determine the sticking efficiency. Formulas are explained in the text (Methods section). Single collector contact efficiency was determined using the correlation equation developed by Tufenkji and Elimelech [70]. Case shown here is coarse sand high flow in DM water.

GENERAL FLUID PARAMETERS	**Values**	**Unit**
Temperature (T)	296	K
Fluid density (ρ_f)	1002	kg m^{-3}
Dynamic fluid viscosity	1.000 $\times 10^{-3}$	kg $m^{-1} s^{-1}$
TRANSPORT PARAMETERS		
Column inner diameter	2.5	cm
Column surface area	4.91	cm^2
Pump speed	0.8	ml min^{-1}
Darcy velocity	1.63×10^{-1}	cm min^{-1}
	2.72×10^{-5}	m s^{-1}
	(857)	m y^{-1}
SEDIMENT PARAMETERS		
Grain diameter (d_g)	1.200	mm
Porosity (ϵ)	0.45	-
DNAcol		
Particle density (ρ_p)	2200	kg m^{-3}
Particle Size (d_p)	0.27	μm
SINGLE COLLECTOR CONTACT EFFICIENCY		
Hamaker constant (H)	0.7×10^{-20}	J
Happel model parameter (A_s)	28.25	-
(η_D)	1.23×10^{-2}	-
(η_I)	1.07×10^{-5}	-
(η_G)	1.48×10^{-3}	-
(η_0) = (η_D) + (η_I)+ (η_G)	1.38×10^{-2}	-
STICKING EFFICIENCY		
Attachment rate coefficient	9.37×10^{-3}	min^{-1}
	1.56×10^{-4}	s^{-1}
Sticking efficiency	2.72×10^{-1}	-

A.4. DLVO PROFILE

DLVO theory is used to describe the interaction energy between particle-plate via adhesive (van der Waals) and repulsive electrostatic interaction energy [233, 234]. The electrostatic interaction energy (ϕ_{EDL}) between sphere (DNA-silica particle), and plate (sand grain) can be approximated by [122, 235]:

$$\phi_{EDL} = 64\pi\varepsilon_0\varepsilon_r a_p \left(\frac{k_B T}{ze}\right)^2 \Gamma_1\Gamma_2 \exp(-\kappa h) \tag{A.1}$$

where, a_p is the radius of the silica DNA-tagged particle [m], ε_0 is the dielectric permittivity in vacuum (8.854×10^{-12} F m^{-1}), ε_r is the relative permittivity of the medium (78.5 for water at 25 °C), k_B is the Boltzmann constant (1.3805×10^{-23} J K^{-1}), T is the absolute temperature [K], z is counter-ion valance, e is electron charge (1.602×10^{-19} C), Γ_1 and Γ_2 are dimensionless surface potential values of the particle and plate (sand grain), respectively. The surface potential was calculated by Γ_i=tanh(zeζ)/(4k_BT) for particle and/or plate, where ζ is the measured zeta potential [V], κ is the inverse Debye length [m^{-1}], and h is the separation distance [m]. The van der Waals interaction energy (ϕ_{vdW}) between sphere (DNA-silica particle) and plate (sand grain) can be computed from [122, 236]:

$$\phi_{vdW} = -\frac{H_{123} a_p}{6h\left(1+\frac{14h}{\lambda}\right)} \tag{A.2}$$

where H_{123} is the Hamaker constant for silica-water-silica (0.7×10^{-20} J [112]), λ is the characteristic wavelength, which was assumed to have a value of 100 nm [62]. The total interaction energy is then determined by the sum of ϕ_{EDL} and ϕ_{vdW}. Resulting energy profiles have been depicted in Figure A.4-A.5.

A

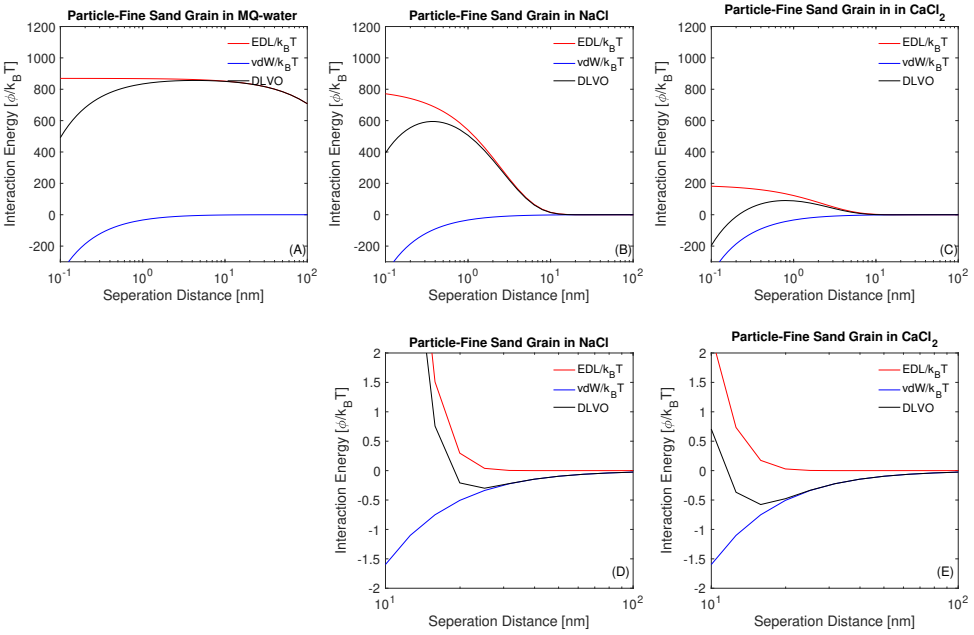

Figure A.4.: Calculated DLVO interaction energy profiles for the DNA-silica particle and fine sand grain system in Milli-Q water (A), NaCl solution (B), and in $CaCl_2$ solution (C). Bottom panels (D), and (E) show parts of panels (B), and (C), respectively, zoomed-in on the secondary minimum.

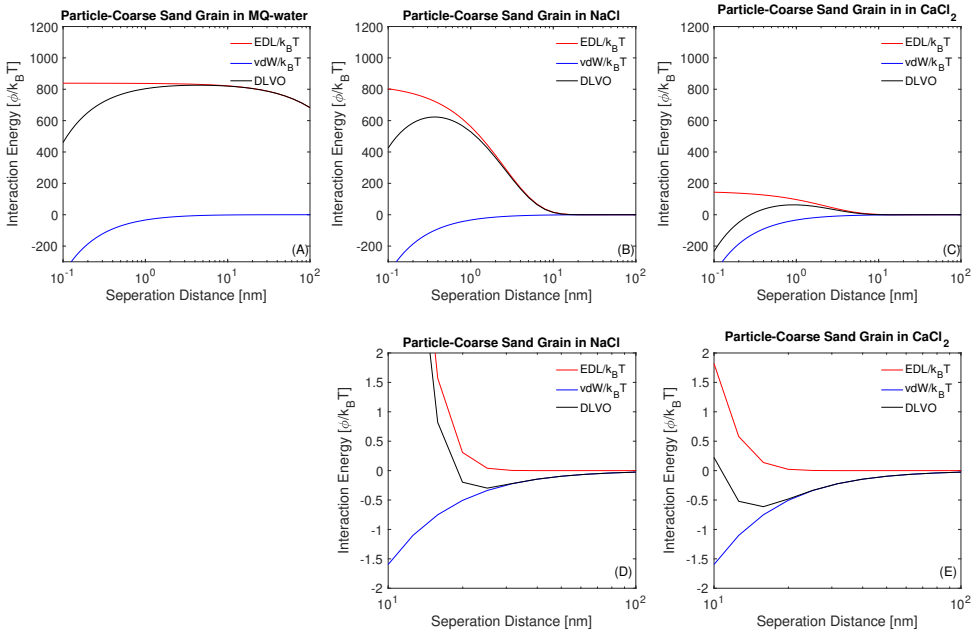

Figure A.5.: Calculated DLVO interaction energy profiles for the DNA-silica particle and coarse sand grain system in Milli-Q water (A), NaCl solution (B), and in $CaCl_2$ solution (C). Bottom panels (D), and (E) show parts of panels (B), and (C), respectively, zoomed-in on the secondary minimum.

B

APPENDIX-B: SUPPLEMENTARY MATERIAL FOR CHAPTER 3

This chapter is based on:
Kianfar, B., Hassanizadeh, S. M., Abdelrady, A., Bogaard, T., Foppen, J. W. (2023). Natural organic matter and ionic strength (CaCl2) affect transport, retention and remobilization of silica encapsulated DNA colloids (DNAcol) in saturated sand columns. Colloids and Surfaces A: Physicochemical and Engineering Aspects, 678, 132476. [45]

B.1. WORKFLOW OF DNA RELEASE AND QPCR ANALYSIS

For qPCR analysis, 20 μL of the collected column effluent samples were pipetting into the qPCR tube (8-tube strip) (BIOplastics, the Netherlands). Prior to qPCR analysis, the collected column effluent samples were vortexed to ensure the samples are homogenous. The tubes were closed with an optical 8-cap strip (BIOplastics, the Netherlands), and were centrifuged for a few seconds using (Microcentrifuge, Galaxy miniStar, VWR). To dissolve the silica, 1 μL of buffer oxide etch (BOE; containing ammonium hydrogen difluoride (2.3 g NH_4FHF, Merck, Germany) and ammonium fluoride (1.9 g NH_4F, Sigma-Aldrich) in 10 mL Milli-Q water) was added to each qPCR tube that contained 20 μL of samples, (protocol adapted from Paunescu *et al.* [34]). Following that, the pH of each sample was adjusted to a near-neutral value by adding 100 μL Tris-HCl buffer (pH 8.3, Merck, Germany). After completing the releasing step of DNA, in another set of qPCR tubes (8-tube strip) (BIOplastics, the Netherlands) the qPCR-mix was prepared, by pipetting of 10 μL Kapa SYBR Green Fast qPCR Mastermix (Kapa biosystems, Sigma-Aldrich), 3 μL DEPC-treated water (Sigma-Aldrich), 1 μL of each forward and reverse primer (DNA oligomers, Biolegio, Nijmegen, the Netherlands), and adding of 5 μL of sample from releasing step. Followed that the qPCR sample tubes were closed with an optical 8-cap strip (BIOplastics, the Netherlands). The sequence of forward primer in this work was: 5′- GCG AGA TAC ACT GCC AAA AAT -3′, and the reverse primer was 5′- AGA CCA CAG CCA GAC CAA AT -3′, with product length of 21-20 (base pair), GC content of 42.8-50%. DNA oligomers was provided by Biolegio for this research (Biolegio, Nijmegen, the Netherlands). The pipetting steps during the dissolving of silica and qPCR samples preparation was done using Qiagen QIAgility instrument automated PCR preparation (Qiagen, Hilden, Germany). DNA amplification was done under four-thermal cycling steps using a 96-well plate qPCR (Bio-Rad, Hercules, CA, USA). The thermal cycling qPCR reactions consisted of: initial pre-incubation (at 95 °C for 400 s), then 42 cycles of, denaturation (20 s at 95 °C), annealing (40 s at 58 °C), amplification (35 s at 72 °C). The results of qPCR were based on fluorescence signal measurement, in terms of quantification cycles (Cq) when the fluorescence signal passes a threshold. The Cq was determined using Bio-Rad CFX Manager maestro 3.1 software based on the regression mode.

In order to prevent cross contamination, the qPCR sample preparation and qPCR thermal cycling were carried out in two separate rooms.

B.2. CALIBRATION CURVES

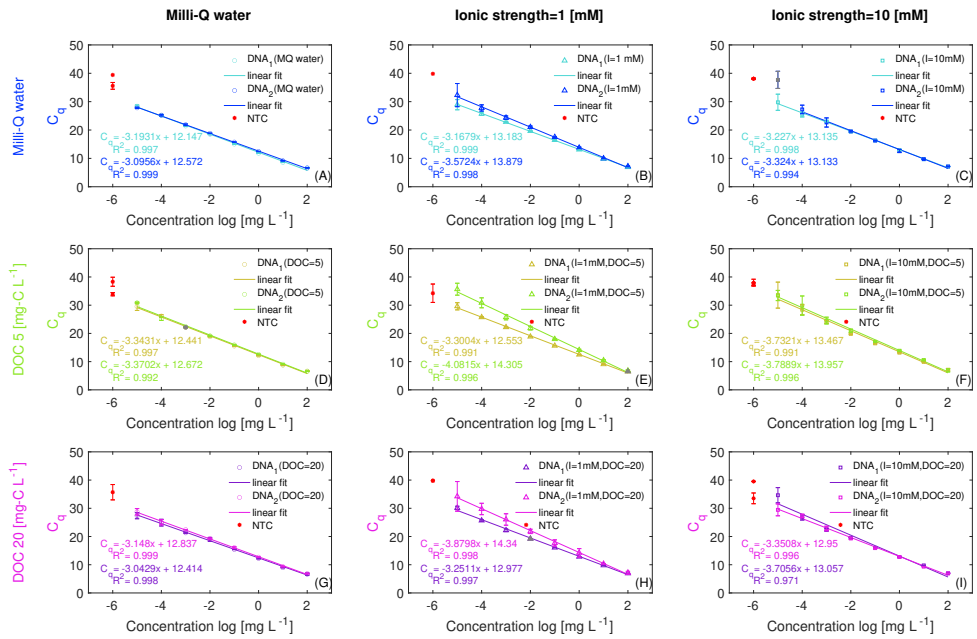

Figure B.1.: Calibration curves DNAcol (symbols in blue, green and magenta) in various solutions, and lines are linear-regression fits (lines). The negative control values (NTC) of samples presented by symbols in red. The error bars show the standard deviation of triplicate qPCR samples. The background solutions of DNAcol experiments are: (A) Milli-Q water, (B) 1 mM $CaCl_2$, (C) 10 mM $CaCl_2$, (D) DOC 5 mg-C L^{-1}, (E) DOC 5 mg-C L^{-1} with 1 mM $CaCl_2$, (F) DOC 5 mg-C L^{-1} with 10 mM $CaCl_2$, (G) DOC 20 mg-C L^{-1}, (H) DOC 20 mg-C L^{-1} with 1 mM $CaCl_2$, (I) DOC 20 mg-C L^{-1} with 10 mM $CaCl_2$.

Fig. B.1 shows the calibration curves of DNAcol for various solution chemistries based on the quantification cycle (Cq) values determined by qPCR versus log concentration of DNA copies. The lines show linear regression fit to data points. The slope of the fitted curve indicates the efficiency. The two series of data points in each panel show duplicated series of the dilution series for two different batches of primer sets. Note, each point presents the average of triplicate samples, except in three cases (i.e., symbols in grey). That means in those three cases the plotted data point presented as the average of the duplicate samples, and the third one was considered as an outlier (in Fig. B.1D, E, and H). In addition, in Fig. B.1C, the regression was applied to a 7-fold dilution series which means the presented data point at D_9 (symbol in grey) was ruled out. We observed that in some cases the variation (error bar) between triplicated samples increased at the lowest concentration D_9 dilution.

B

B.3. QUALITY CONTROL OF QPCR

Figure B.2.: Variation of Cq values of sub-samples to test reproducibility of qPCR (fill-symbols and hollow-symbols), and reproducibility of experiments (replicate experiments).

The top-first panel of Fig. B.2 shows the variation of Cq values belonging to 5-6 samples from injection tracer (C_0). For each solution chemistry, the results of replicate experiments were presented side-by-side to each other. The variation of sub-samples that was analyzed with two qPCR runs presented as filled vs. hollow symbols. The second-top panel presents the variation of Cq values belonging to two positive control samples, that each sample contains 1 mg L^{-1} of DNAcol (D_3 in dilution series) in Milli-Q water (dark blue), and in various solution chemistries as labeled. Again, each set of data points shows the variation between triplicated sub-samples. The filled vs. hollow symbols present the reproducibility of qPCR. The reproducibility of the samples was tested at D_3 concentration. The two blank-labeled panels show the variation of sub-samples and replicated experiments from column influent and effluent prior to DNAcol experiment. The lower panel presents the variation of NTC, the data points again indicate the variation between two subsamples and replicated experiments.

B.4. SINGLE-COLLECTOR CONTACT EFFICIENCY (η_0)

The single-collector contact efficiency (η_0) was defined based on equation developed by Tufenkji and Elimelech [70]:

$$\eta_0 = 2.4A_s^{1/3}N_R^{-0.081}N_{Pe}^{-0.715}N_{vdW}^{0.052} + 0.55A_sN_R^{1.675}N_A^{0.125} + 0.22N_R^{-0.24}N_G^{1.11}N_{vdW}^{0.053} \quad \text{(B.1)}$$

Where, A_s is a porosity dependent parameter, N_R is aspect ratio, N_{pe} is Peclet number, N_{vdW} is van der Waals number, N_A is attraction number, N_G is gravity number.

B.5. DLVO INTERACTION ENERGY PROFILE

The total DLVO interaction energy (ϕ_{tot}) [172, 237] between two bare spherical particles or between spherical particles and plat is the sum of van der Waals (ϕ_{vdW}), and electrostatic (ϕ_{EDL}) (Eq. B.2-B.3).

$$\phi_{tot}(h) = \phi_{vdW}(h) + \phi_{EDL}(h) \quad \text{(B.2)}$$

The van der Waals interaction energy (ϕ_{vdW}) between DNAcol (spherical particle) and sand grain (plate) can be calculated based on the following equation (proposed by Gregory [236], in Petosa *et al.* [129]:

$$\phi_{vdW} = -\frac{H_{123}r_p}{6h\left(1+\frac{14h}{\lambda}\right)} \quad \text{(B.3)}$$

Where H_{123} [J] is Hamaker constant for the combination of silica$_{(1)}$-water$_{(2)}$-silica$_{(3)}$ was assumed to be equal 0.7 $\times 10^{-20}$ J [112], r_p [m] is the radius of the spherical particle (i.e., DNAcol), λ [nm] is the characteristic wavelength, which was assumed 100 nm of decay length of vdW [62]. Note that the Hamaker constant was assumed to be the same for all tested conditions, that means for both pristine silica particles and sand grains, and particles suspended in natural organic matter. The electrostatic interaction energy (ϕ_{EDL}) for DNAcol (spherical particle) when approaching the sand grains (plate) was determined based on an equation proposed by Gregory [235](in Petosa *et al.* [122]):

$$\phi_{EDL} = 64\pi\varepsilon_0\varepsilon_r r_p\left(\frac{k_BT}{ze}\right)^2\psi_p\psi_g\exp(-\kappa h) \quad \text{(B.4)}$$

Where, ε_0 is the dielectric permittivity of vacuum (equal to 8.854 $\times 10^{-12}$ F m^{-1}), ε_r is the relative permittivity of the medium solution for water at 25 °C is equal to 78.5, k_B [J K^{-1}] is Boltzmann constant (equal to 1.3805 $\times 10^{-23}$ J K^{-1}), T [K] is the absolute temperature, z is the counterion valance, e [C] is elementary electron charge (equal to 1.602$\times 10^{-19}$ C), ψ_p and ψ_g [-] are dimensionless surface potential of the particle (DNAcol) and plate (sand grain), respectively, h [m] is the separation distance, and κ^{-1} [m] is the Debye length given by:

$$\kappa^{-1} = \left(\frac{\varepsilon_0\varepsilon_r k_BT}{2IN_Ae^2}\right)^{0.5} \quad \text{(B.5)}$$

Where, I [mmol L^{-1}] is ionic strength.

Surface potential is approximated from ζ-potential using equation B.6 [238](van Oss 1994):

$$\psi_0 = \zeta\left(1 + \frac{z}{r_p}\right)exp(kz) \tag{B.6}$$

Note, that the ζ-potential of sand grain was assumed to be equal to DNAcol. To draw the total DLVO interaction energy (ϕ_{tot}), the values were divided by k_BT, resulting in a unit of [J]/[J].

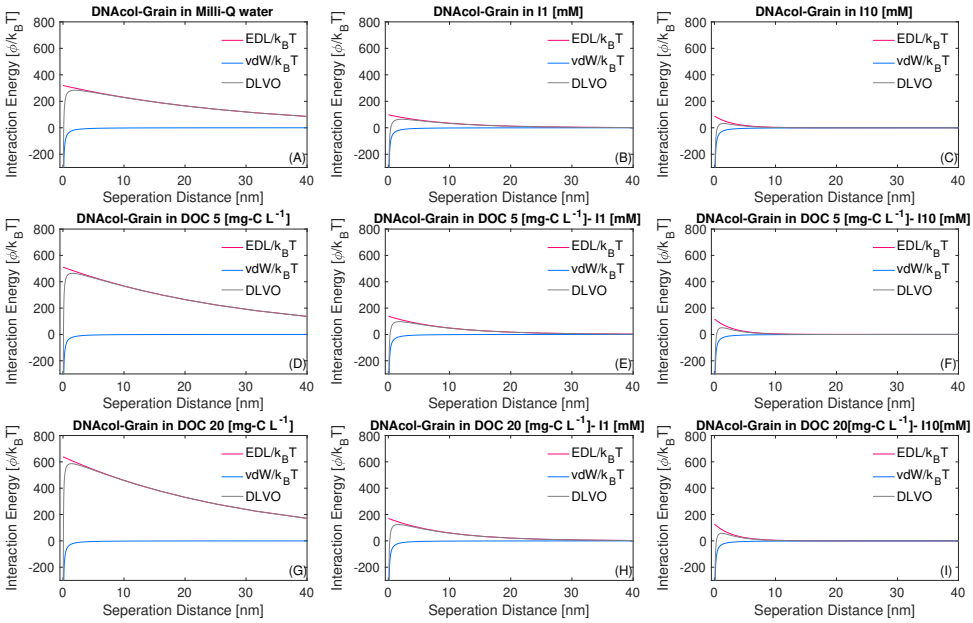

Figure B.3.: DLVO energy profile of DNAcol in various solutions (grey line), the electrostatic repulsion (red line) and van der Waals (blue line). The background solutions for tested conditions are: (A) Milli-Q water, (B) 1 mM $CaCl_2$, (C) 10 mM $CaCl_2$, (D) DOC 5 mg-C L^{-1}, (E) DOC 5 mg-C L^{-1} with 1 mM $CaCl_2$, (F) DOC 5 mg-C L^{-1} with 10 mM $CaCl_2$, (G) DOC 20 mg-C L^{-1}, (H) DOC 20 mg-C L^{-1} with 1 mM $CaCl_2$, (I) DOC 20 mg-C L^{-1} with 10 mM $CaCl_2$. The specific Conditions: d_p= 280 [nm], d_g= 0.715 [mm], H= 0.7×10^{-20} [J].

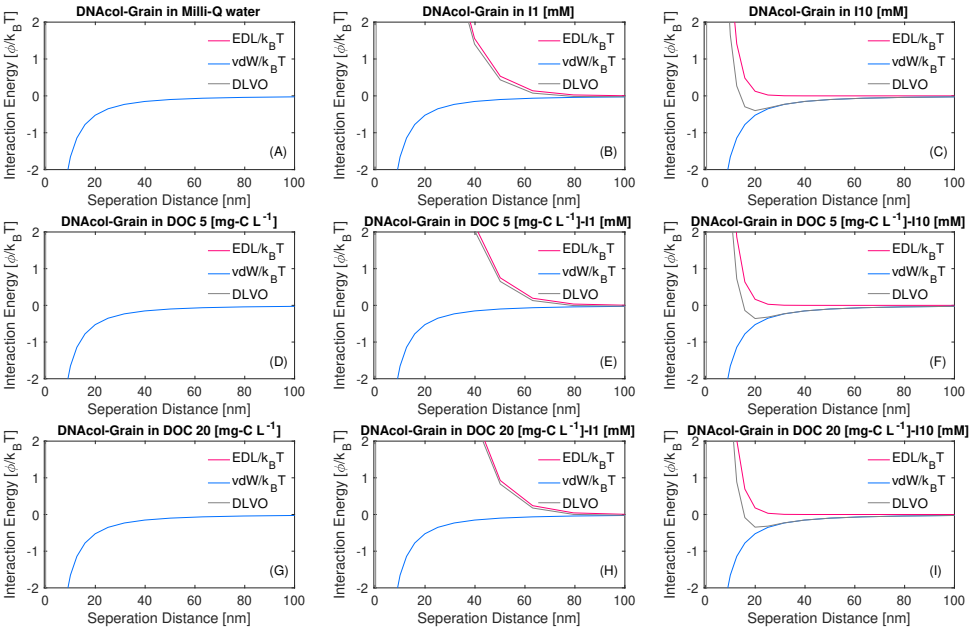

Figure B.4.: Zoom-in of the secondary minimum energy for DLVO energy profile of DNAcol in various solutions (grey line), the electrostatic repulsion (red line) and van der Waals (blue line). The background solutions for tested conditions are: (A) Milli-Q water, (B) 1 mM $CaCl_2$, (C) 10 mM $CaCl_2$, (D) DOC 5 mg-C L^{-1}, (E) DOC 5 mg-C L^{-1} with 1 mM $CaCl_2$, (F) DOC 5 mg-C L^{-1} with 10 mM $CaCl_2$, (G) DOC 20 mg-C L^{-1}, (H) DOC 20 mg-C L^{-1} with 1 mM $CaCl_2$, (I) DOC 20 mg-C L^{-1} with 10 mM $CaCl_2$. The specific Conditions: d_p= 280 [nm], d_g= 0.715 [mm], H= 0.7×10^{-20} [J].

B.6. BREAKTHROUGH CURVES OF NACL TRACER VERSUS DNACOL

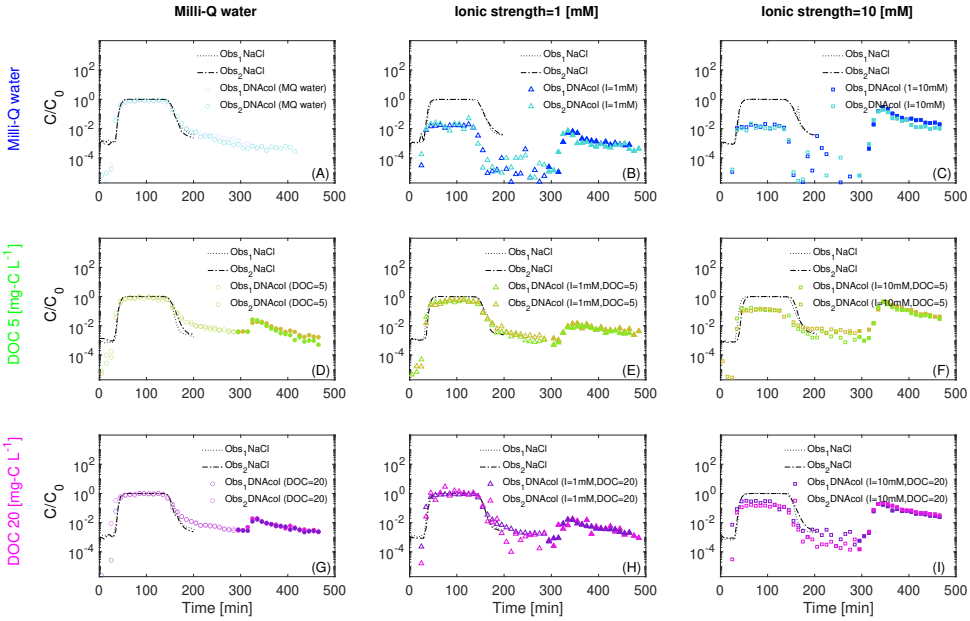

Figure B.5.: Experimental breakthrough curves of DNAcol (colored-symbols) versus breakthrough curves of NaCl tracer (black-symbols). The background solutions for DNAcol experiments are: (A) Milli-Q water, (B) 1 mM $CaCl_2$, (C) 10 mM $CaCl_2$, (D) DOC 5 mg-C L^{-1}, (E) DOC 5 mg-C L^{-1} with 1 mM $CaCl_2$, (F) DOC 5 mg-C L^{-1} with 10 mM $CaCl_2$, (G) DOC 20 mg-C L^{-1}, (H) DOC 20 mg-C L^{-1} with 1 mM $CaCl_2$, (I) DOC 20 mg-C L^{-1} with 10 mM $CaCl_2$. Hollow-symbols represent steady porewater chemistry conditions, and filled-symbols represent transient porewater chemistry conditions.

B.7. VARIATION BETWEEN THE SUB-SAMPLES OF DNACOL, AND THE VARIATION OF REPLICATED COLUMN EXPERIMENTS

To determine the variation between subsamples, for 13 experiments out of 18 column experiments, each collected sample was analyzed twice. That means two subsamples (each contains 20 μL) were taken from 2 mL collected samples. The two sub-samples were analyzed using the same batch of primer set, but were processed under two different qPCR runs (presented as dashed area).

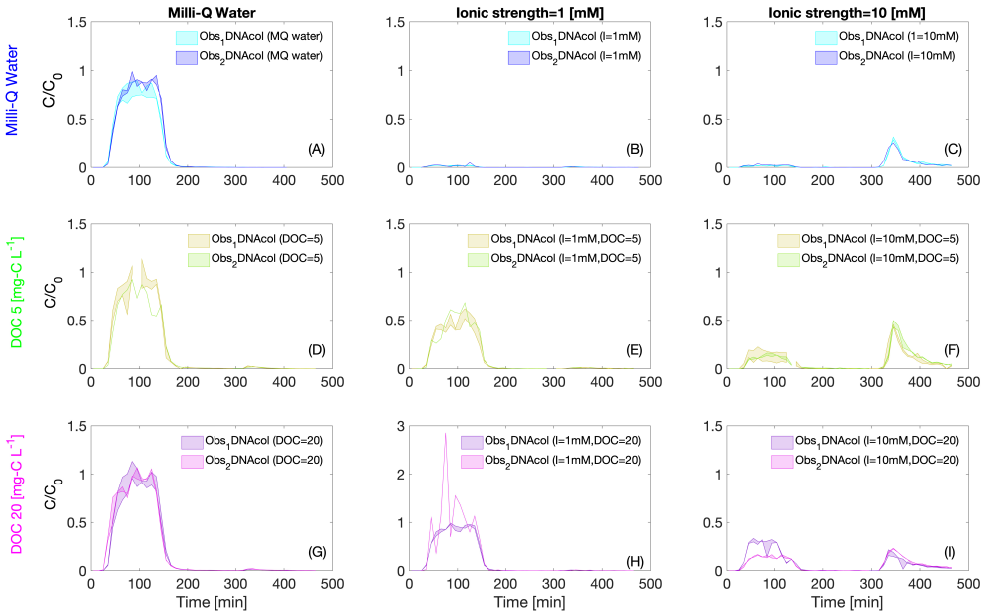

Figure B.6.: The shaded area presents the variation of two-sub samples that was analyzed with two qPCR runs. The background solutions for DNAcol experiments are: (A) Milli-Q water, (B) 1 mM $CaCl_2$, (C) 10 mM $CaCl_2$, (D) DOC 5 mg-C L^{-1}, (E) DOC 5 mg-C L^{-1} with 1 mM $CaCl_2$, (F) DOC 5 mg-C L^{-1} with 10 mM $CaCl_2$, (G) DOC 20 mg-C L^{-1}, (H) DOC 20 mg-C L^{-1} with 1 mM $CaCl_2$, (I) DOC 20 mg-C L^{-1} with 10 mM $CaCl_2$. Note, the y-axis is in linear scale in all panels, and in panel (H) has different limits.

C

APPENDIX-C: SUPPLEMENTARY MATERIAL FOR CHAPTER 4

C.1. MAJOR CATION AND ANION OF NATURAL AND SYNTHETIC GROUNDWATER

Table C.1.: Comparison of the major cation and anion composition of natural groundwater (GW) and synthetic (Syn.) groundwater based on ion chromatography.

Major	Huppel GW	Huppel Syn.	Tulip GW	Tulip Syn.
	[mg L^{-1}]	[mg L^{-1}]	[mg L^{-1}]	[mg L^{-1}]
Na^+	14.9	16.7	19.9	24.1
Ca^{2+}	121.1	122	127.4	103.2
Mg^{2+}	16.3	11.3	10.5	19.6
K^+	15.6	22.3	41.8	45.2
Cl^-	28.92	32.9	29.7	33.2
NO_3^-	151	147.1	4.2	
SO_4^{2-}	60.1	44.18	94.7	76.14
PO_4^-		13	4.7	27.23

C.2. QPCR ANALYSIS

Fig. C.1(A-E) depicts the dilution series for DNAcol(S4) in various solution chemistries. The x-axis represents the quantification cycle (Cq) values determined by qPCR, and the y-axis represents the logarithmic concentration of DNA copies. The plotted values are the average of triplicate samples, with error bars indicating the standard deviation. In each panel, the lines correspond to the linear regression fit to the data points. The dilution curves in Fig. C.1(A-D) confirmed a linear relationship between Cq values and the logarithm of DNA concentration over the 8-fold dilution points. During the 8-fold dilution series of DNAcol in Tulip synthetic groundwater, in the most diluted sample corresponding to D_9 (0.00001 mg L^{-1}), no amplification signal was observed, as shown in Fig. C.1(E). Consequently, the dilution curve consisted of 7-fold in this case. Furthermore, at D_6 (corresponding to 0.01 mg L^{-1}), the obtained Cq value was lower than the expected value. For this dilution series, we could either consider all 7-fold dilutions or opt for only 5-fold. In either case, the fitted linear regression lines were displayed in Fig. C.1(E). Subsequently, to convert the Cq values to DNAcol concentration, we used the regression lines that were fitted to the 7-fold dilution data.

Fig. C.2 displays the qPCR calibration curves of DNAcol(S1) and DNAcol(S2) in various solution chemistries. The plotted values are the average of replicated samples, with error bars indicating the standard deviation, and the lines correspond to the linear regression fit to data points. In Fig. C.2 panels (C) and (F) depict the dilution series of DNAcol in column effluent. The dilution in column effluent was conducted primarily to assess the possibility of the presence of qPCR inhibitors.

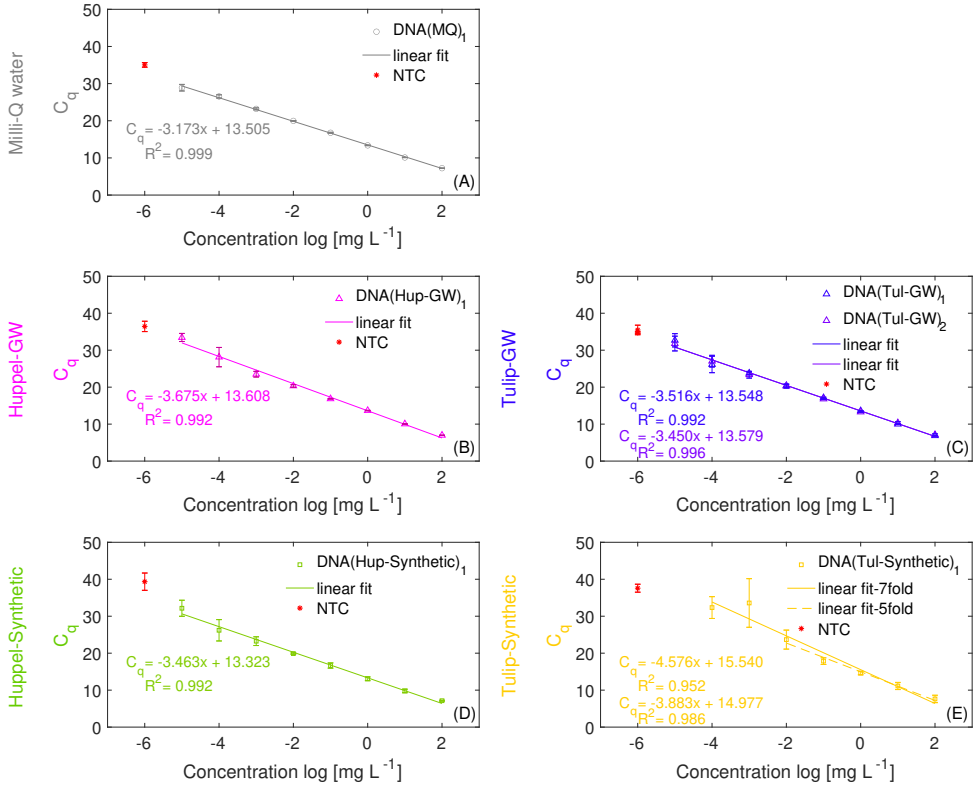

Figure C.1.: Calibration curves of DNAcol(S4) in various solutions, along with linear-regression fits (lines). The negative control values (NTC= No Template Control) of samples are presented by red symbols. Error bars indicate the standard deviation of triplicate qPCR samples. The background solutions of DNAcol experiments are: (A) Milli-Q water, (B) Huppel groundwater, (C) Tulip groundwater, (D) Huppel synthetic groundwater, and (E) Tulip synthetic groundwater.

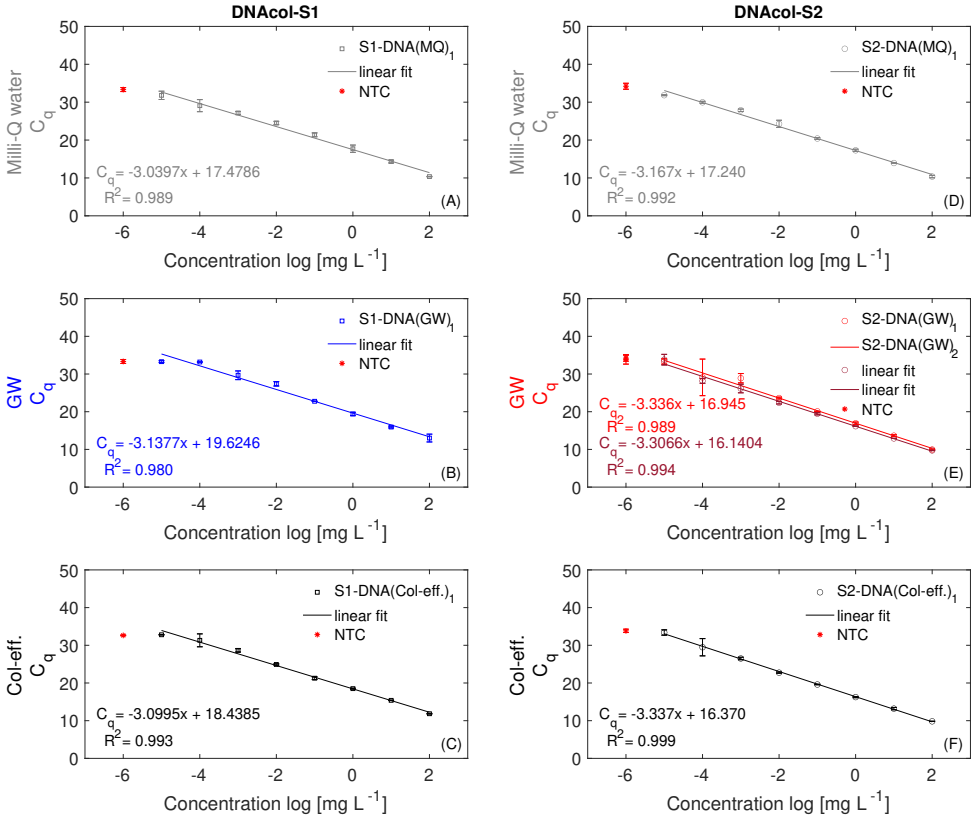

Figure C.2.: Calibration curves (DNAcol) in various solutions, along with linear-regression fits (lines). The negative control values (NTC= No Template Control) of samples are presented by red symbols. Error bars indicate the standard deviation of triplicate qPCR samples. The background solutions of DNAcol (S1) experiments are: (A) Milli-Q water, (B) Tulip groundwater, (C) Column effluent. The background solutions of DNAcol (S2) experiments are: (D) Milli-Q water, (E) Tulip groundwater, (F) Column effluent.

Table C.2.: Details of the qPCR primers used to amplify the DNA in three tested DNAcol.

DNAcol	Primer	GC [%]	base pair [bp]
DNAcol (S1)	Forward primer (5′-ATG GGC TCT AAG GAT CTC-3′)	50	18
	Reverse primer (5′-CTC ACC CTC GAA TCG AA-3′)	53	17
DNAcol (S2)	Forward primer (5′-CGG ACA ATC CTT TCC ATA-3′)	44	18
	Reverse primer (5′-ACG AGA CCC AGT TAA TAA G-3′)	42	19
DNAcol (S4)	Forward primer (5′- CTC TGC CCT TAC GTT TAT C-3′)	47	19
	Reverse primer (5′-AGA GGT TTG TTC GTG TTC-3′)	44	18

C.3. QUALITY CONTROL OF QPCR

Top panel Fig. C.3 presents the Cq values of the injected DNAcol(S4) to assess the variation between the sub-samples of DNAcol(S4) and the variation of replicated experiments. Additionally, black symbols indicate the variation of Cq of the samples that were analyzed with the mentioned lag time to assess the stability of DNAcol over time. In the second top panel, the Cq values of positive control samples containing 10 mg L^{-1} of DNAcol(S4) were examined in various background solutions in triplicates. Furthermore, the Cq values of positive control samples that contained the same concentration of positive control (10 mg L^{-1}) in Milli-Q water were carried out alongside as a reference value. The analysis aims to understand whether the background solution contains qPCR inhibitors or not.

The third and fourth panels of Fig. C.3 depict the blank samples from the column influent and effluent. The NTC values of each run are displayed in the lower panel of Fig. C.3.

For DNAcol suspended in Huppel and Tulip groundwater, the qPCR results from the first run of the experiment showed that the Cq values of C_0 were 13.31±0.26 and 13.07±0.20, respectively. Meanwhile, for the replicate experiment, the Cq values of C_0 were 20.73±0.06 and 24.70±1.95 for DNAcol suspended in Huppel and Tulip groundwater, respectively, as shown top panels in Fig. C.3. Higher Cq values indicate a lower concentration of DNA in the samples, implying that a higher number of cycles are required to detect DNA above the threshold. Despite the sample being preserved at 4 °C, the observed change in Cq values after 21 days of analysis could likely be associated with biological activity and/or chemical processes.

The positive control samples also confirmed an increase in Cq values over time (Fig. C.3). To further investigate this issue, the transport of DNAcol suspended in Tulip groundwater was tested for a third time within a freshly packed sand column with clean sand. The samples were analyzed after 4 days (Fig. 4.1D). In this experiment, to assess the stability of DNAcol suspended Tulip groundwater, the C_0 samples were reanalyzed after 45 days. The average Cq value of C_0 was initially (after 4 days) 16.51±0.84, although the expected Cq value was around 13. After 45 days, it changed to 16.85±0.69, as shown in Fig. C.3. In contrast to previous

Figure C.3.: Variation of Cq values of sub-samples to test the reproducibility of qPCR (fill-symbols and hollow-symbols), and reproducibility of experiments (replicate experiments), the stability of DNAcol over time shown with black symbols.

results, this outcome did not confirm a significant change in Cq values over 45 days. Additionally, it is noteworthy that positive control samples for this condition confirmed an increase in Cq values from 11.33 to 15.39 after 41 days (Fig. C.3). Further investigation is required to address the inconsistencies observed in the replicated experiments.

For DNAcol suspended in Tulip synthetic groundwater, we encountered several challenges. As mentioned in the method section, 5 to 6 sub-samples were taken from the influent suspension during the experiment to determine the C_0 value of DNAcol. In the cases of Tulip synthetic groundwater, the analyzed C_0 values revealed that the Cq values of these samples were not constant throughout the experimental period. The average Cq value of injected DNAcol (C_0) for the first three sub-samples was 15.12±0.42, while the Cq value for the last three samples increased to 22.71±2.04, indicating a change in DNAcol concentration. This variation is most likely associated with the instability of DNAcol. It should be noted that the obtained Cq values of injected DNAcol in Huppel synthetic groundwater were 14.66±2.19, while a value around 13 was expected. In this case, the increase in Cq value of C_0 was noticeable

in the last sub-samples, which increased to 18.69. The increase in the Cq values in these conditions could also be associated with instability of the DNAcol or partial inhibition. To assess the stability of DNAcol in synthetic groundwater, the DNA concentration of 6 sub-samples of the injected batches was determined again after 45 days. For Tulip synthetic groundwater, a comparison of the initial Cq values confirmed that the values increased over this time frame; the change in Cq was around 2 cycles (initial Cq=18.92±4.21, and after 45 days Cq=20.25±4.07). The same analysis was conducted for Huppel synthetic groundwater, and the data showed no change in the Cq values (initial Cq=14.66±2.19, and after 45 days Cq=14.09±1.44).

In Fig. C.4, two breakthrough curves of DNAcol suspended in Tulip synthetic groundwater are presented: one by normalizing the concentration of collected column samples over the first 3 sub-samples of column influent (C_0), and the other one by considering all 6 sub-samples. When considering all C_0 values, the breakthrough curve reached the maximum normalized concentration (C_{max}/C_0) of ~0.06 at the plateau, and the relative mass recovery of DNAcol was approximately 1%. However, during transient porewater chemistry conditions when considering all C_0 values, it led to a significant overestimation of the recovered mass to approximately 136%.

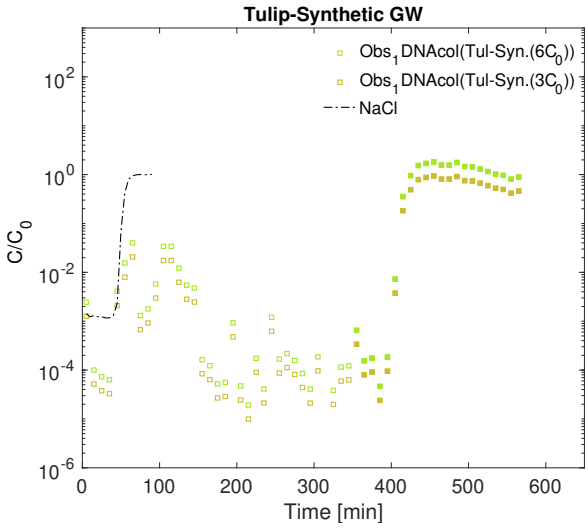

Figure C.4.: Experimental breakthrough curves of DNAcol (symbols)Tulip synthetic groundwater; normalized over 3 and 6 sub-samples of C_0 and NaCl tracer breakthrough curves (black dashed lines). Open symbols represent steady porewater chemistry conditions, and filled symbols represent transient porewater chemistry conditions.

Fig. C.5 shows the breakthrough curves of the samples DNAcol(S2) that was reanalyzed to assess the stability of DNAcol after 11 days. The data indicated a decline in the concentration of DNAcol. Furthermore, to examine the effect of storage temperature on DNAcol, the sub-samples were kept at -20 °C (freezing temperature). These samples were analyzed after 7 days, and in this case, the change in concentration of DNAcol was negligible (Fig. C.5).

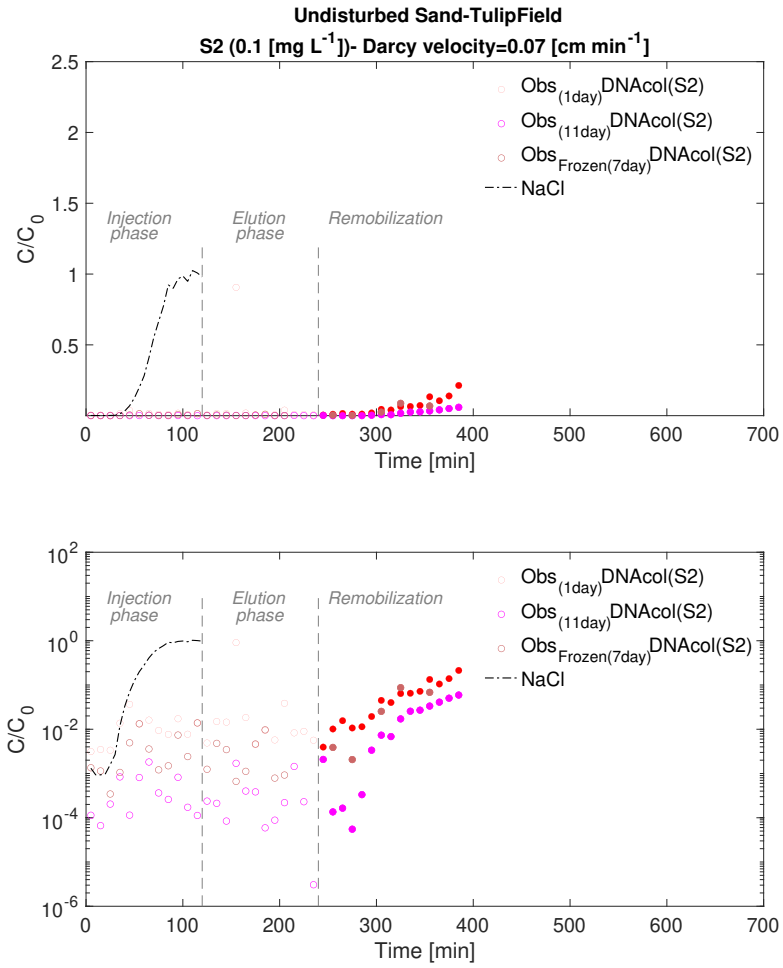

Figure C.5.: Experimental breakthrough curves of DNAcol (symbols) obtained from undisturbed sand column with background solution of Tulip groundwater, and breakthrough curves of NaCl tracer (black dashed lines). The top panel shows the breakthrough curves in a linear scale, and the lower panel presents similar breakthrough curves in a semi-log scale. The symbol colors represent the obtained values from column experiments that underwent qPCR after 1 day of the experiment (red symbols), after 11 days (pink symbols), and the samples that were kept frozen and analyzed after 7 days (brownish symbols).

C.4. SENSITIVITY OF STICKING EFFICIENCY (α) AND SINGLE-COLLECTOR CONTACT EFFICIENCY (η_0) TO DNACOL SIZE

Table C.3.: Calculated Sticking efficiencies (α) and single-collector contact efficiency (η_0) DNAcol using three different scenarios considering d_p= 280 [nm], and the measured hydrodynamic diameters (d_h) at 5- and 120-minutes time frame, d_g= 0.527 [mm], H= 0.7×10^{-20} [J], ρ_p=2200 [kg m^{-3}].

Column Experiment	Solution	d_p=280 [nm]		d_h at 5 [min]		d_h at 120 [min]	
		η_0 [-]	α [-]	η_0 [-]	α [-]	η_0 [-]	α [-]
Exp. 1	Milli-Q water (1)	0.045	0.11				
	Huppel GW(1)	0.044	0.14	0.038	0.16	0.040	0.15
	Huppel GW(2)	0.047	0.10	0.041	0.11	0.043	0.11
Exp. 2	Milli-Q water (1)	0.051	0.22				
	Tulip GW(1)	0.051	0.18	0.044	0.20	0.044	0.20
	Tulip GW(2)	0.048	0.20	0.042	0.23	0.042	0.23
	Tulip GW(3)	0.045	0.12	0.039	0.14	0.039	0.14
Exp. 3	Huppel Syn.	0.046	0.52	0.038	0.64	0.052	0.46
Exp. 4	Tulip Syn.	0.046	0.57	0.039	0.69	0.073	0.36

D

APPENDIX-D: SUPPLEMENTARY MATERIAL FOR CHAPTER 5

D.1. QUALITY CONTROL OF QPCR

In each qPCR run, the concentration of the injected DNAcol was analyzed in six replicates alongside the collected samples from the field. Positive control samples, corresponding to the D_3 sample in the dilution series curve, and NTC samples, both in duplicate, were also included in the analysis (Fig. D.1). The top panel of Fig. D.1 presents the variation in Cq values of injected DNAcol (S1-S4) (C_0) within a single qPCR run and the variation between different qPCR runs (Fig. D.1(A)). The comparison of Cq values of the four different DNAcol types used in this experiment showed that the obtained Cq values for S2 and S3 were much higher than those for S1 and S4. This result confirmed the lower concentration of DNA in both S2 and S3, as evidenced by the calibration curves as well. The middle panel illustrates the variation in the positive control (1000 times diluted DNAcol, corresponding to D_3 in the calibration curve) (Fig. D.1(B)). The primary purpose of the positive control is to ensure the accuracy and reproducibility of qPCR assay to detect target DNA. It is important to note that Milli-Q water was used as the background of all positive control samples, and the label only indicates the location of the collected samples. The lower panel displays duplicate values of NTC samples in each qPCR run. The objective of the NTC was to ensure there was no contamination (Fig. D.1(C)). One issue highlighted by NTC values was that Cq values below 30 cycles in some of the qPCR runs, potentially indicating the presence of non-specific products or primer-dimer.

D.2. FALSE NEGATIVE SIGNAL AND PRESENCE OF QPCR INHIBITION

A preliminary test was conducted by spiking S2 into certain water samples from the experimental field. Initially, S2 was diluted threefold in Milli-Q water (D_3). Subsequently, this diluted solution was further diluted into selected samples collected from TR1 and TR2 to achieve a concentration equivalent to D_4 on the calibration curve. The results of this test are displayed in Fig. D.2. More specifically, for this experiment, 16 samples from TR2 were selected. In the first series of the experiments, 2 μL of S2 with concentration D_3 was spiked into 18 μL of sub-samples of these 16 selected samples. The obtained average Cq values for the analyzed samples were 28.47±0.80 (Fig. D.2(A)). In the second series of the experiment, 1 μL of S2 with a D_3 concentration was spiked into 19 μL of sub-samples of the 16 selected samples. This adjustment resulted in a final concentration slightly lower than that of the D_4 sample, with an average Cq of 28.67±0.82 (Fig. D.2(A)). Based on the results of the dilution series, the Cq values corresponding to D_4 for S2 in the Milli-Q water was 27.65± 0.31. Comparing the inhibitory test results with the calibration curve data indicated a very weak or no inhibitory effect.

To further test the presence of the inhibitory compounds at another sampling location, eight samples from TR1 were selected. In this case, 5 μL of S2 with a concentration of D_3 was spiked into 45 μL of sub-samples of the chosen samples. The resulting average Cq value was 27.25±0.32, indicating no inhibition effect (Fig. D.2(B)).

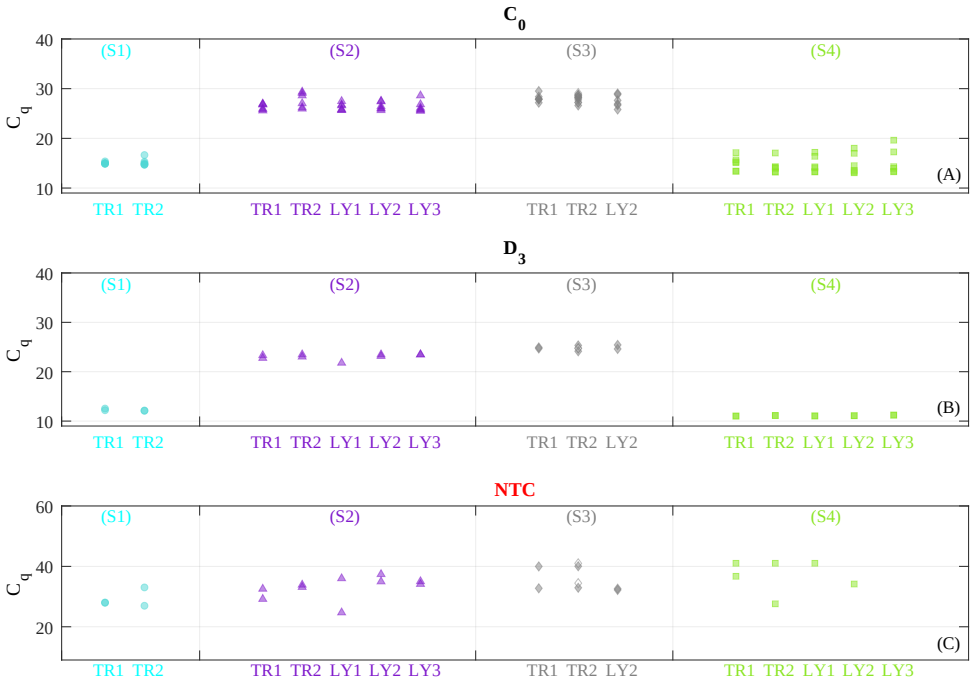

Figure D.1.: Variation in Cq values of sub-samples for injected S1-S4 and among different qPCR runs (A), variation in Cq values of sub-samples for positive control samples (B), and variation in Cq values of sub-samples for negative control samples (NTC) (C).

In addition, as shown in Fig. D.2(C), two collected samples (samples 1 and 42) from TR2 were selected, and S2 was spiked into them to achieve concentrations of D_4 and D_5. Furthermore, a control test was conducted by spiking the S2 into Milli-Q water with corresponding concentrations. For the concentration of D_4, the results indicated that the difference in Cq values between forest water and Milli-Q water was less than 2, suggesting negligible inhibition. The analysis of the samples with a lower S2 concentration (D_5) showed a deviation of Cq around 5 in one forest water sample compared to Milli-Q water condition, which, indicates potential inhibition in that specific sample. However, conducting a duplicate analysis is needed to confirm the presence of inhibitory substances in that sample.

D.3. FALSE POSITIVE SIGNAL OF QPCR

Figures D.2(A) and D.2(B) present the qPCR results in terms of Cq for forest samples with the addition of buffered oxide etch (BOE) compared to forest samples without BOE. The results of TR1 samples show negligible variation between the Cq values of analyzed samples with and without BOE. In both conditions, the obtained Cq values

were approximately 33 (Fig. D.2(B)), close to the values observed for NTC samples (~34).

For TR2 samples, the averaged Cq was found to be around 33 for samples without dissolving the silica shell (without the addition of BOE), while for analyzed samples with the addition of BOE, the Cq was around 32 (Fig. D.2(A)). Once again, the obtained Cq values for both datasets were found to be close to NTC values.

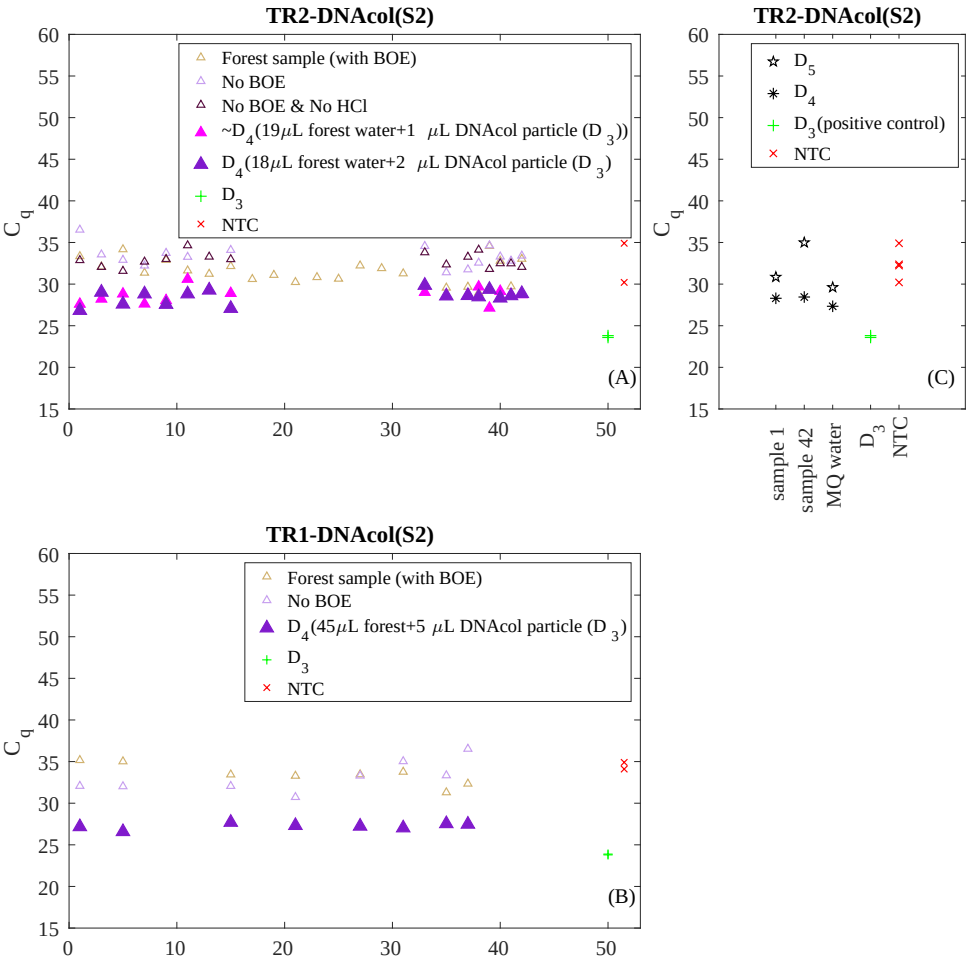

Figure D.2.: A comparison of the Cq values for samples with and without the addition of buffered oxide etch (BOE), and a comparison of the Cq values of the originally collected samples with the corresponding samples after spiking a specific concentration of DNAcol(S2) into them. (A) displays the Cq value comparison for samples collected from TR2, (B) displays the comparison for samples collected from TR1, and (C) represents the Cq values of samples with concentrations corresponding to D_4 and D_5 in different background solutions collected from TR2, compared to Milli-Q water background. The olive-colored symbols show the Cq of samples collected from the field, open symbols represent samples without the addition of BOE and filled symbols represent samples after spiking DNAcol(S2) to investigate the potential presence of inhibitory compounds. Green symbols represent positive control in Milli-Q water (D_3), and red symbols represent the NTC values.

BIBLIOGRAPHY

[1] C. Leibundgut, P. Maloszewski, and C. Külls. *Tracers in hydrology*. John Wiley & Sons, 2011.

[2] D. Boesel, M. Herfort, T. Ptak, and G. Teutsch. "Design, performance, evaluation and modelling of a natural gradient multitracer transport experiment in a contaminated heterogeneous porous aquifer." In: (2000).

[3] S. N. Davis, G. M. Thompson, H. W. Bentley, and G. Stiles. "Ground-water tracers—A short review". In: *Groundwater* 18.1 (1980), pp. 14–23.

[4] M. Flury and N. N. Wai. "Dyes as tracers for vadose zone hydrology". In: *Reviews of Geophysics* 41.1 (2003).

[5] R. Haggerty, C. F. Harvey, C. Freiherr von Schwerin, and L. C. Meigs. "What controls the apparent timescale of solute mass transfer in aquifers and soils? A comparison of experimental results". In: *Water Resources Research* 40.1 (2004).

[6] W. Kass. *Tracing technique in geohydrology*. Routledge, 2018.

[7] H. Hötzl, W. Käss, and B. Reichert. "Application of Microbial Tracers in Ground Water Studies". In: *Water Science and Technology* 24.2 (1991), pp. 295–300.

[8] B. Mahler, J.-C. Personné, G. Lods, and C. Drogue. "Transport of free and particulate-associated bacteria in karst". In: *Journal of Hydrology* 238.3-4 (2000), pp. 179–193.

[9] J. F. Schijven, S. M. Hassanizadeh, and R. H. De Bruin. "Two-site kinetic modeling of bacteriophages transport through columns of saturated dune sand". In: *Journal of Contaminant Hydrology* 57.3-4 (2002), pp. 259–279.

[10] O. Zvikelsky and N. Weisbrod. "Impact of particle size on colloid transport in discrete fractures". In: *Water Resources Research* 42.12 (2006).

[11] T. Atkinson. "Diffuse flow and conduit flow in limestone terrain in the Mendip Hills, Somerset (Great Britain)". In: *Journal of hydrology* 35.1-2 (1977), pp. 93–110.

[12] A. Auckenthaler, G. Raso, and P. Huggenberger. "Particle transport in a karst aquifer: natural and artificial tracer experiments with bacteria, bacteriophages and microspheres". In: *Water Science and Technology* 46.3 (2002), pp. 131–138.

[13] T. Ptak, M. Piepenbrink, and E. Martac. "Tracer tests for the investigation of heterogeneous porous media and stochastic modelling of flow and transport—a review of some recent developments". In: *Journal of hydrology* 294.1-3 (2004), pp. 122–163.

[14] H. E. Dahlke, A. G. Williamson, C. Georgakakos, S. Leung, A. N. Sharma, S. W. Lyon, and M. T. Walter. “Using concurrent DNA tracer injections to infer glacial flow pathways”. In: *Hydrological Processes* 29.25 (2015), pp. 5257–5274.

[15] J. W. Foppen, C. Orup, R. Adell, V. Poulalion, and S. Uhlenbrook. “Using multiple artificial DNA tracers in hydrology”. In: *Hydrological Processes* 25.19 (2011), pp. 3101–3106.

[16] I. H. Sabir, J. Torgersen, S. Haldorsen, and P. Aleström. “DNA tracers with information capacity and high detection sensitivity tested in groundwater studies”. In: *Hydrogeology Journal* 7 (1999), pp. 264–272.

[17] R. Liao, P. Yang, W. Wu, D. Luo, and D. Yang. “A DNA tracer system for hydrological environment investigations”. In: *Environmental science & technology* 52.4 (2018), pp. 1695–1703.

[18] J. W. Foppen. “Artificial DNA in hydrology”. In: *Wiley Interdisciplinary Reviews: Water* 10.6 (2023), e1681.

[19] Y. Zhang and T. Huang. “DNA-based tracers for the characterization of hydrogeological systems—Recent advances and new Frontiers”. In: *Water* 14.21 (2022), p. 3545.

[20] J. D. Watson and F. H. Crick. “The structure of DNA”. In: *Cold Spring Harbor symposia on quantitative biology*. Vol. 18. Cold Spring Harbor Laboratory Press. 1953, pp. 123–131.

[21] A. N. Sharma, D. Luo, and M. T. Walter. “Hydrological tracers using nanobiotechnology: proof of concept”. In: *Environmental science & technology* 46.16 (2012), pp. 8928–8936.

[22] S. Deepak, K. Kottapalli, R. Rakwal, G. Oros, K. Rangappa, H. Iwahashi, Y. Masuo, and G. Agrawal. “Real-time PCR: revolutionizing detection and expression analysis of genes”. In: *Current genomics* 8.4 (2007), pp. 234–251.

[23] P. Aleström. *Novel method for chemical labelling of objects, International Patent Application No.* Tech. rep. PCT/IB95/01144 and Publication No. WO 96/17954, 1995.

[24] B. J. Mahler, M. Winkler, P. Bennett, and D. M. Hillis. “DNA-labeled clay: a sensitive new method for tracing particle transport”. In: *Geology* 26.9 (1998), pp. 831–834.

[25] I. H. Sabir, S. Haldorsen, J. Torgersen, P. Alestrom, S. Gaut, H. Colleuille, T. S. Pedersen, N.-O. Kitterod, and P. Alestrom. “Synthetic DNA tracers: examples of their application in water related studies”. In: *IAHS Publication(International Association of Hydrological Sciences)* 262 (2000), pp. 159–165.

[26] V. Bovolin, A. Cuomo, D. Guida, and J. Foppen. “Using artificial DNA as tracer in a bedrock river of the Middle Bussento Karst System (Cilento, Vallo Diano and Alburni European & Global Geopark, southern Italy)”. In: *Proceedings of the the 7th International Conference on Engineering Mechanics, Structures, Engineering Geology (EMESEG14), Salerno, Italy*. 2014, pp. 3–5.

[27] L. Aquilanti, F. Clementi, S. Landolfo, T. Nanni, S. Palpacelli, and A. Tazioli. "A DNA tracer used in column tests for hydrogeology applications". In: *Environmental earth sciences* 70 (2013), pp. 3143–3154.

[28] L. Aquilanti, F. Clementi, T. Nanni, S. Palpacelli, A. Tazioli, and P. M. Vivalda. "DNA and fluorescein tracer tests to study the recharge, groundwater flowpath and hydraulic contact of aquifers in the Umbria-Marche limestone ridge (central Apennines, Italy)". In: *Environmental Earth Sciences* 75 (2016), pp. 1–17.

[29] L. Pang, B. Robson, E. McGill, A. Varsani, L. Gillot, J. Li, and P. Abraham. "Tracking effluent discharges in undisturbed stony soil and alluvial gravel aquifer using synthetic DNA tracers". In: *Science of the Total Environment* 592 (2017), pp. 144–152.

[30] C. Wang, G. Liu, C. P. McNew, T. H. M. Volkmann, L. Pangle, P. A. Troch, S. W. Lyon, M. Kim, Z. Huo, and H. E. Dahlke. "Simulation of experimental synthetic DNA tracer transport through the vadose zone". In: *Water Research* 223 (2022), p. 119009.

[31] J. W. Foppen, J. Seopa, N. Bakobie, and T. Bogaard. "Development of a methodology for the application of synthetic DNA in stream tracer injection experiments". In: *Water resources research* 49.9 (2013), pp. 5369–5380.

[32] J. McCluskey, M. E. Flores, J. Hinojosa, A. Jafarzadeh, S. V. Moghadam, D. C. Phan, R. T. Green, and V. Kapoor. "Tracking water with synthetic DNA tracers using droplet digital PCR". In: *ACS ES&T Water* 1.5 (2021), pp. 1177–1183.

[33] L. Pang, G. Abeysekera, K. Hanning, A. Premaratne, B. Robson, P. Abraham, R. Sutton, C. Hanson, J. Hadfield, L. Heiligenthal, *et al.* "Water tracking in surface water, groundwater and soils using free and alginate-chitosan encapsulated synthetic DNA tracers". In: *Water Research* 184 (2020), p. 116192.

[34] D. Paunescu, M. Puddu, J. O. Soellner, P. R. Stoessel, and R. N. Grass. "Reversible DNA encapsulation in silica to produce ROS-resistant and heat-resistant synthetic DNA'fossils'". In: *Nature protocols* 8.12 (2013), pp. 2440–2448.

[35] M. C. Garnett, P. Ferruti, E. Ranucci, M. A. Suardi, M. Heyde, and R. Sleat. *Sterically stabilized self-assembling reversibly cross-linked polyelectrolyte complexes with nucleic acids for environmental and medical applications*. 2009.

[36] X. Liu, M. D. Kaminski, Y. Guan, H. Chen, H. Liu, and A. J. Rosengart. "Preparation and characterization of hydrophobic superparamagnetic magnetite gel". In: *Journal of magnetism and magnetic materials* 306.2 (2006), pp. 248–253.

[37] C. P. McNew, C. Wang, M. T. Walter, and H. E. Dahlke. "Fabrication, detection, and analysis of DNA-labeled PLGA particles for environmental transport studies". In: *Journal of colloid and interface science* 526 (2018), pp. 207–219.

[38] C. B. Georgakakos, P. L. Richards, and M. T. Walter. “Tracing septic pollution sources using synthetic DNA tracers: proof of concept”. In: *Air, Soil and Water Research* 12 (2019), p. 1178622119863794.

[39] G. Mikutis, C. A. Deuber, L. Schmid, A. Kittilä, N. Lobsiger, M. Puddu, D. O. Asgeirsson, R. N. Grass, M. O. Saar, and W. J. Stark. “Silica-encapsulated DNA-based tracers for aquifer characterization”. In: *Environmental science & technology* 52.21 (2018), pp. 12142–12152.

[40] Y. Zhang. “DNA-Encapsulated Silica Nanoparticle Tracers for Fractured Reservoir Characterization”. PhD thesis. Stanford University, 2015.

[41] Y. Zhang, T. S. Manley, K. Li, and R. N. Horne. “Uniquely identifiable DNA-embedded silica nanotracer for fractured reservoir characterization”. In: *Proceedings of the 41st Workshop on Geothermal Reservoir Engineering*. Stanford University Stanford, CA. 2016.

[42] S. Chakraborty, J. W. Foppen, and J. F. Schijven. “Effect of concentration of silica encapsulated ds-DNA colloidal microparticles on their transport through saturated porous media”. In: *Colloids and Surfaces A: Physicochemical and Engineering Aspects* 651 (2022), p. 129625.

[43] R. N. Grass, J. Schälchli, D. Paunescu, J. O. Soellner, R. Kaegi, and W. J. Stark. “Tracking trace amounts of submicrometer silica particles in wastewaters and activated sludge using silica-encapsulated DNA barcodes”. In: *Environmental Science & Technology Letters* 1.12 (2014), pp. 484–489.

[44] B. Kianfar, J. Tian, J. Rozemeijer, B. van der Zaan, T. A. Bogaard, and J. W. Foppen. “Transport characteristics of DNA-tagged silica colloids as a colloidal tracer in saturated sand columns; role of solution chemistry, flow velocity, and sand grain size”. In: *Journal of Contaminant Hydrology* 246 (2022), p. 103954.

[45] B. Kianfar, S. M. Hassanizadeh, A. Abdelrady, T. Bogaard, and J. W. Foppen. “Natural organic matter and ionic strength (CaCl2) affect transport, retention and remobilization of silica encapsulated DNA colloids (DNAcol) in saturated sand columns”. In: *Colloids and Surfaces A: Physicochemical and Engineering Aspects* 678 (2023), p. 132476.

[46] A. Kittilä, M. Jalali, K. F. Evans, M. Willmann, M. O. Saar, and X.-Z. Kong. “Field comparison of DNA-labeled nanoparticle and solute tracer transport in a fractured crystalline rock”. In: *Water Resources Research* 55.8 (2019), pp. 6577–6595.

[47] J. Koch, S. Doswald, G. Mikutis, W. J. Stark, and R. N. Grass. “Ecotoxicological assessment of DNA-tagged silica particles for environmental tracing”. In: *Environmental Science & Technology* 55.10 (2021), pp. 6867–6875.

[48] X.-Z. Kong, C. A. Deuber, A. Kittilä, M. Somogyvári, G. Mikutis, P. Bayer, W. J. Stark, and M. O. Saar. “Tomographic reservoir imaging with DNA-labeled silica nanotracers: the first field validation”. In: *Environmental science & technology* 52.23 (2018), pp. 13681–13689.

[49] C. A. Mora, H.-J. Schärer, T. Oberhänsli, M. Ludwig, R. Stettler, P. R. Stoessel, R. N. Grass, and W. J. Stark. “Ultrasensitive quantification of pesticide contamination and drift using silica particles with encapsulated DNA”. In: *Environmental Science & Technology Letters* 3.1 (2016), pp. 19–23.

[50] Y. Tang, J. W. Foppen, and T. A. Bogaard. “Transport of silica encapsulated DNA microparticles in controlled instantaneous injection open channel experiments”. In: *Journal of Contaminant Hydrology* 242 (2021), p. 103880.

[51] M. Puddu, D. Paunescu, W. J. Stark, and R. N. Grass. “Magnetically recoverable, thermostable, hydrophobic DNA/silica encapsulates and their application as invisible oil tags”. In: *ACS nano* 8.3 (2014), pp. 2677–2685.

[52] A. Sharma, J. W. Foppen, A. Banerjee, S. Sawssen, N. Bachhar, D. Peddis, and S. Bandyopadhyay. “Magnetic nanoparticles to unique DNA tracers: Effect of functionalization on physico-chemical properties”. In: *Nanoscale research letters* 16 (2021), pp. 1–16.

[53] S. Chakraborty, R. Elhaj, J. W. Foppen, and J. Schijven. “Effect of injection water ionic strength on estimating hydraulic parameters in a 3D sand tank using silica encapsulated magnetic DNA particles”. In: *Advances in Water Resources* 179 (2023), p. 104507.

[54] Y. Tang, F. van Rhijn, A. Abdelrady, J. W. Foppen, and T. Bogaard. “Effect of channel bed sediment on the transport behaviour of superparamagnetic silica encapsulated DNA microparticles in open channel injection experiments”. In: *Hydrological Processes* 37.9 (2023), e14962.

[55] R. Liao, J. Zhang, T. Li, D. Luo, and D. Yang. “Biopolymer/plasmid DNA microspheres as tracers for multiplexed hydrological investigation”. In: *Chemical Engineering Journal* 401 (2020), p. 126035.

[56] A. Abdelrady, Y. Tang, T. Bogaard, and J. W. Foppen. “The use of silica encapsulated DNA particles with a supermagnetic iron core (SiDNAMag) in sand filtration system: Effect of water chemistry”. In: *Journal of Water Process Engineering* 62 (2024), p. 105316.

[57] C. Wang, C. P. McNew, S. W. Lyon, M. T. Walter, T. H. Volkman, N. Abramson, A. Sengupta, Y. Wang, A. A. M. Neto, L. Pangle, *et al.* “Particle tracer transport in a sloping soil lysimeter under periodic, steady state conditions”. In: *Journal of Hydrology* 569 (2019), pp. 61–76.

[58] J. Smith, B. Gao, H. Funabashi, T. N. Tran, D. Luo, B. A. Ahner, T. S. Steenhuis, A. G. Hay, and M. T. Walter. “Pore-scale quantification of colloid transport in saturated porous media”. In: *Environmental science & technology* 42.2 (2008), pp. 517–523.

[59] M. Rinderer, J. Krüger, F. Lang, H. Puhlmann, and M. Weiler. “Subsurface flow and phosphorus dynamics in beech forest hillslopes during sprinkling experiments: how fast is phosphorus replenished?” In: *Biogeosciences* 18.3 (2021), pp. 1009–1027.

[60] M. Scotoni, J. Koch, T. R. Julian, L. Clack, A. K. Pitol, A. Wolfensberger, R. N. Grass, and H. Sax. “Silica nanoparticles with encapsulated DNA (SPED)–a novel surrogate tracer for microbial transmission in healthcare”. In: *Antimicrobial Resistance & Infection Control* 9 (2020), pp. 1–10.

[61] J. Koch, S. Gantenbein, K. Masania, W. J. Stark, Y. Erlich, and R. N. Grass. “A DNA-of-things storage architecture to create materials with embedded memory”. In: *Nature biotechnology* 38.1 (2020), pp. 39–43.

[62] M. Elimelech, J. Gregory, and X. Jia. *Particle deposition and aggregation: measurement, modelling and simulation*. Butterworth-Heinemann, 2013.

[63] M. Elimelech, J. Gregory, X. Jia, and R. Williams. “Particle deposition and aggregation, measurement, modeling and simulation”. In: *Colloids and Surfaces A: Physicochemical and Engineering Aspects* 1.125 (1997), pp. 93–94.

[64] I. L. Molnar, W. P. Johnson, J. I. Gerhard, C. S. Willson, and D. M. O’carroll. “Predicting colloid transport through saturated porous media: A critical review”. In: *Water Resources Research* 51.9 (2015), pp. 6804–6845.

[65] I. L. Molnar, E. Pensini, M. A. Asad, C. A. Mitchell, L. C. Nitsche, L. J. Pyrak-Nolte, G. L. Miño, and M. M. Krol. “Colloid transport in porous media: a review of classical mechanisms and emerging topics”. In: *Transport in Porous Media* 130 (2019), pp. 129–156.

[66] K.-M. Yao, M. T. Habibian, and C. R. O’Melia. “Water and waste water filtration. Concepts and applications”. In: *Environmental science & technology* 5.11 (1971), pp. 1105–1112.

[67] H. Ma, M. Hradisky, and W. P. Johnson. “Extending applicability of correlation equations to predict colloidal retention in porous media at low fluid velocity”. In: *Environmental science & technology* 47.5 (2013), pp. 2272–2278.

[68] W. Long and M. Hilpert. “A correlation for the collector efficiency of Brownian particles in clean-bed filtration in sphere packings by a Lattice-Boltzmann method”. In: *Environmental science & technology* 43.12 (2009), pp. 4419–4424.

[69] R. Rajagopalan and C. Tien. “Trajectory analysis of deep-bed filtration with the sphere-in-cell porous media model”. In: *AIChE Journal* 22.3 (1976), pp. 523–533.

[70] N. Tufenkji and M. Elimelech. “Correlation equation for predicting single-collector efficiency in physicochemical filtration in saturated porous media”. In: *Environmental science & technology* 38.2 (2004), pp. 529–536.

[71] K. E. Nelson and T. R. Ginn. “New collector efficiency equation for colloid filtration in both natural and engineered flow conditions”. In: *Water Resources Research* 47.5 (2011).

[72] C. V. Chrysikopoulos and V. E. Katzourakis. “Colloid particle size-dependent dispersivity”. In: *Water Resources Research* 51.6 (2015), pp. 4668–4683.

[73] C. V. Chrysikopoulos and V. I. Syngouna. “Effect of gravity on colloid transport through water-saturated columns packed with glass beads: modeling and experiments”. In: *Environmental science & technology* 48.12 (2014), pp. 6805–6813.

[74] P. Bedrikovetsky, F. D. Siqueira, C. A. Furtado, and A. L. S. Souza. “Modified particle detachment model for colloidal transport in porous media”. In: *Transport in porous media* 86 (2011), pp. 353–383.

[75] P. Bedrikovetsky, A. Zeinijahromi, F. D. Siqueira, C. A. Furtado, and A. L. S. de Souza. “Particle detachment under velocity alternation during suspension transport in porous media”. In: *Transport in Porous Media* 91 (2012), pp. 173–197.

[76] S. A. Bradford, H. N. Kim, B. Z. Haznedaroglu, S. Torkzaban, and S. L. Walker. “Coupled factors influencing concentration-dependent colloid transport and retention in saturated porous media”. In: *Environmental science & technology* 43.18 (2009), pp. 6996–7002.

[77] S. A. Bradford, S. Torkzaban, F. Leij, and J. Simunek. “Equilibrium and kinetic models for colloid release under transient solution chemistry conditions”. In: *Journal of contaminant hydrology* 181 (2015), pp. 141–152.

[78] C. A. Ron, K. VanNess, A. Rasmuson, and W. P. Johnson. “How nanoscale surface heterogeneity impacts transport of nano-to micro-particles on surfaces under unfavorable attachment conditions”. In: *Environmental Science: Nano* 6.6 (2019), pp. 1921–1931.

[79] C. A. Ron and W. P. Johnson. “Complementary colloid and collector nanoscale heterogeneity explains microparticle retention under unfavorable conditions”. In: *Environmental Science: Nano* 7.12 (2020), pp. 4010–4021.

[80] C. Liu, N. Xu, G. Feng, D. Zhou, X. Cheng, and Z. Li. “Hydrochars and phosphate enhancing the transport of nanoparticle silica in saturated sands”. In: *Chemosphere* 189 (2017), pp. 213–223.

[81] I. Kim, A. Taghavy, D. DiCarlo, and C. Huh. “Aggregation of silica nanoparticles and its impact on particle mobility under high-salinity conditions”. In: *Journal of Petroleum Science and Engineering* 133 (2015), pp. 376–383.

[82] C. Wang, A. D. Bobba, R. Attinti, C. Shen, V. Lazouskaya, L.-P. Wang, and Y. Jin. “Retention and transport of silica nanoparticles in saturated porous media: effect of concentration and particle size”. In: *Environmental science & technology* 46.13 (2012), pp. 7151–7158.

[83] C. Zeng, F. Shadman, and R. Sierra-Alvarez. “Transport and abatement of fluorescent silica nanoparticle (SiO 2 NP) in granular filtration: effect of porous media and ionic strength”. In: *Journal of Nanoparticle Research* 19 (2017), pp. 1–10.

[84] J. E. Saiers, G. M. Hornberger, and C. Harvey. “Colloidal silica transport through structured, heterogeneous porous media”. In: *Journal of Hydrology* 163.3-4 (1994), pp. 271–288.

[85] P. R. Johnson, N. Sun, and M. Elimelech. “Colloid transport in geochemically heterogeneous porous media: Modeling and measurements”. In: *Environmental science & technology* 30.11 (1996), pp. 3284–3293.

[86] E. Vitorge, S. Szenknect, J. M. Martins, V. Barthès, A. Auger, O. Renard, and J.-P. Gaudet. “Comparison of three labeled silica nanoparticles used as tracers in transport experiments in porous media. Part I: syntheses and characterizations”. In: *Environmental pollution* 184 (2014), pp. 605–612.

[87] E. Vitorge, S. Szenknect, J. M.-F. Martins, V. Barthès, and J.-P. Gaudet. “Comparison of three labeled silica nanoparticles used as tracers in transport experiments in porous media. Part II: transport experiments and modeling”. In: *Environmental pollution* 184 (2014), pp. 613–619.

[88] Q. Liu, Z. Sun, and J. C. Santamarina. “Transport and adsorption of silica nanoparticles in carbonate reservoirs: A sand column study”. In: *Energy & Fuels* 33.5 (2019), pp. 4009–4016.

[89] J. N. Ryan, M. Elimelech, R. A. Ard, R. W. Harvey, and P. R. Johnson. “Bacteriophage PRD1 and silica colloid transport and recovery in an iron oxide-coated sand aquifer”. In: *Environmental science & technology* 33.1 (1999), pp. 63–73.

[90] C.-H. Ko and J. Y. Chen. “Dynamics of silica colloid deposition and release in packed beds of aminosilane-modified glass beads”. In: *Langmuir* 16.17 (2000), pp. 6906–6912.

[91] Y. V. Li and L. M. Cathles. “Retention of silica nanoparticles on calcium carbonate sands immersed in electrolyte solutions”. In: *Journal of Colloid and Interface Science* 436 (2014), pp. 1–8.

[92] J. Zhou, W. Zhang, D. Liu, Z. Wang, and S. Li. “Influence of humic acid on the transport and deposition of colloidal silica under different hydrogeochemical conditions”. In: *Water* 9.1 (2016), p. 10.

[93] M. Zhang, D. Li, Z. Ye, S. Wang, N. Xu, F. Wang, S. Liu, J. Chen, and H. Gu. “Effect of humic acid on the sedimentation and transport of nanoparticles silica in water-saturated porous media”. In: *Journal of Soils and Sediments* 20 (2020), pp. 911–920.

[94] J. Higgo, G. Williams, I. Harrison, P. Warwick, M. Gardiner, and G. Longworth. “Colloid transport in a glacial sand aquifer. Laboratory and field studies”. In: *Colloids in the Aquatic Environment*. Elsevier, 1993, pp. 179–200.

[95] C. Dai, H. Zhou, X. You, Y. Duan, Y. Tu, S. Liu, F. Zhou, and L. K. Hon. “Silica colloids as non-carriers facilitate Pb 2+ transport in saturated porous media under a weak adsorption condition: Effects of Pb 2+ concentrations”. In: *Environmental Science and Pollution Research* 27 (2020), pp. 15188–15197.

[96] W. Hou, Z. Lei, E. Hu, H. Wang, Q. Wang, R. Zhang, and H. Li. “Co-transport of uranyl carbonate and silica colloids in saturated quartz sand under different hydrochemical conditions”. In: *Science of The Total Environment* 765 (2021), p. 142716.

[97] E. M. d. Oliveira, E. E. Garcia-Rojas, I. C. R. P. Valadão, A. d. S. F. Araújo, and J. A. d. Castro. “Effects of the silica nanoparticles (NPSiO 2) on the stabilization and transport of hazardous nanoparticle suspensions into landfill soil columns”. In: *REM-International Engineering Journal* 70 (2017), pp. 317–323.

[98] Y. Qin, Z. Wen, W. Zhang, J. Chai, D. Liu, and S. Wu. “Different roles of silica nanoparticles played in virus transport in saturated and unsaturated porous media”. In: *Environmental Pollution* 259 (2020), p. 113861.

[99] H. Selim, R. Schulin, and H. Flühler. “Transport and ion exchange of calcium and magnesium in an aggregated soil”. In: *Soil Science Society of America Journal* 51.4 (1987), pp. 876–884.

[100] M. T. Van Genuchten and R. Wagenet. “Two-site/two-region models for pesticide transport and degradation: Theoretical development and analytical solutions”. In: *Soil Science Society of America Journal* 53.5 (1989), pp. 1303–1310.

[101] M. T. Van Genuchten, J. Šimunek, F. Leij, N. Toride, and M. Šejna. “STANMOD: Model use, calibration, and validation”. In: *Transactions of the ASABE* 55.4 (2012), pp. 1355–1366.

[102] V. E. Katzourakis and C. V. Chrysikopoulos. “Fitting the transport and attachment of dense biocolloids in one-dimensional porous media: ColloidFit”. In: *Groundwater* 55.2 (2017), pp. 156–159.

[103] J. F. Schijven and J. Šimnek. “Kinetic modeling of virus transport at the field scale”. In: *Journal of Contaminant Hydrology* 55.1-2 (2002), pp. 113–135.

[104] V. E. Katzourakis and C. V. Chrysikopoulos. “Two-site colloid transport with reversible and irreversible attachment: analytical solutions”. In: *Advances in Water Resources* 130 (2019), pp. 29–36.

[105] J. Simunek, M. T. Van Genuchten, and M. Sejna. “The HYDRUS-1D software package for simulating the one-dimensional movement of water, heat, and multiple solutes in variably-saturated media”. In: *University of California-Riverside Research Reports* 3 (2005), pp. 1–240.

[106] J. Šimnek and M. T. van Genuchten. “Modeling nonequilibrium flow and transport processes using HYDRUS”. In: *Vadose zone journal* 7.2 (2008), pp. 782–797.

[107] J. Šimnek, M. T. van Genuchten, M. M. Gribb, and J. W. Hopmans. “Parameter estimation of unsaturated soil hydraulic properties from transient flow processes”. In: *Soil and Tillage Research* 47.1-2 (1998), pp. 27–36.

[108] D. W. Marquardt. “An algorithm for least-squares estimation of nonlinear parameters”. In: *Journal of the society for Industrial and Applied Mathematics* 11.2 (1963), pp. 431–441.

[109] G. Lutterodt, J. Foppen, and S. Uhlenbrook. “Transport of Escherichia coli strains isolated from natural spring water”. In: *Journal of contaminant hydrology* 140 (2012), pp. 12–20.

[110] R. W. Harvey and S. P. Garabedian. “Use of colloid filtration theory in modeling movement of bacteria through a contaminated sandy aquifer”. In: *Environmental science & technology* 25.1 (1991), pp. 178–185.

[111] J. N. Ryan and M. Elimelech. “Colloid mobilization and transport in groundwater”. In: *Colloids and surfaces A: Physicochemical and engineering aspects* 107 (1996), pp. 1–56.

[112] M. Rhodes. *Particle technology*. 2008.

[113] M. T. Van Genuchten. “Analytical solutions for chemical transport with simultaneous adsorption, zero-order production and first-order decay”. In: *Journal of hydrology* 49.3-4 (1981), pp. 213–233.

[114] S. A. Bradford, S. Torkzaban, and S. L. Walker. “Coupling of physical and chemical mechanisms of colloid straining in saturated porous media”. In: *Water research* 41.13 (2007), pp. 3012–3024.

[115] J. Foppen and J. Schijven. “Evaluation of data from the literature on the transport and survival of Escherichia coli and thermotolerant coliforms in aquifers under saturated conditions”. In: *Water Research* 40.3 (2006), pp. 401–426.

[116] L. Xu, M. Xu, R. Wang, Y. Yin, I. Lynch, and S. Liu. “The crucial role of environmental coronas in determining the biological effects of engineered nanomaterials”. In: *Small* 16.36 (2020), p. 2003691.

[117] T. S. Galloway, M. Cole, and C. Lewis. “Interactions of microplastic debris throughout the marine ecosystem”. In: *Nature ecology & evolution* 1.5 (2017), p. 0116.

[118] I. Lynch, K. A. Dawson, J. R. Lead, and E. Valsami-Jones. “Macromolecular coronas and their importance in nanotoxicology and nanoecotoxicology”. In: *Frontiers of nanoscience*. Vol. 7. Elsevier, 2014, pp. 127–156.

[119] J. McCarthy and J. Zachara. “ES&T Features: Subsurface transport of contaminants”. In: *Environmental science & technology* 23.5 (1989), pp. 496–502.

[120] M. R. Wiesner, G. V. Lowry, K. L. Jones, M. F. Hochella Jr, R. T. Di Giulio, E. Casman, and E. S. Bernhardt. *Decreasing uncertainties in assessing environmental exposure, risk, and ecological implications of nanomaterials*. 2009.

[121] M. R. Wiesner, G. V. Lowry, P. Alvarez, D. Dionysiou, and P. Biswas. *Assessing the risks of manufactured nanomaterials*. 2006.

[122] A. R. Petosa, D. P. Jaisi, I. R. Quevedo, M. Elimelech, and N. Tufenkji. “Aggregation and deposition of engineered nanomaterials in aquatic environments: role of physicochemical interactions”. In: *Environmental science & technology* 44.17 (2010), pp. 6532–6549.

[123] S. Torkzaban, S. Hassanizadeh, J. Schijven, H. De Bruin, and A. de Roda Husman. “Virus transport in saturated and unsaturated sand columns”. In: *Vadose Zone Journal* 5.3 (2006), pp. 877–885.

[124] G. Chen, X. Liu, and C. Su. “Distinct effects of humic acid on transport and retention of TiO2 rutile nanoparticles in saturated sand columns”. In: *Environmental science & technology* 46.13 (2012), pp. 7142–7150.

[125] P. Han, X. Wang, L. Cai, M. Tong, and H. Kim. “Transport and retention behaviors of titanium dioxide nanoparticles in iron oxide-coated quartz sand: effects of pH, ionic strength, and humic acid”. In: *Colloids and Surfaces A: Physicochemical and Engineering Aspects* 454 (2014), pp. 119–127.

[126] P. N. Mitropoulou, V. I. Syngouna, and C. V. Chrysikopoulos. “Transport of colloids in unsaturated packed columns: role of ionic strength and sand grain size”. In: *Chemical Engineering Journal* 232 (2013), pp. 237–248.

[127] G. Sadeghi, T. Behrends, J. F. Schijven, and S. M. Hassanizadeh. “Effect of dissolved calcium on the removal of bacteriophage PRD1 during soil passage: The role of double-layer interactions”. In: *Journal of contaminant hydrology* 144.1 (2013), pp. 78–87.

[128] J. W. Foppen, Y. Liem, and J. Schijven. “Effect of humic acid on the attachment of Escherichia coli in columns of goethite-coated sand”. In: *Water research* 42.1-2 (2008), pp. 211–219.

[129] A. R. Petosa, S. J. Brennan, F. Rajput, and N. Tufenkji. “Transport of two metal oxide nanoparticles in saturated granular porous media: role of water chemistry and particle coating”. In: *Water research* 46.4 (2012), pp. 1273–1285.

[130] B. Espinasse, E. M. Hotze, and M. R. Wiesner. “Transport and retention of colloidal aggregates of C60 in porous media: effects of organic macromolecules, ionic composition, and preparation method”. In: *Environmental science & technology* 41.21 (2007), pp. 7396–7402.

[131] A. Franchi and C. R. O’Melia. “Effects of natural organic matter and solution chemistry on the deposition and reentrainment of colloids in porous media”. In: *Environmental science & technology* 37.6 (2003), pp. 1122–1129.

[132] L. Goswami, K.-H. Kim, A. Deep, P. Das, S. S. Bhattacharya, S. Kumar, and A. A. Adelodun. “Engineered nano particles: nature, behavior, and effect on the environment”. In: *Journal of Environmental Management* 196 (2017), pp. 297–315.

[133] V. L. Morales, W. Zhang, B. Gao, L. W. Lion, J. J. Bisogni Jr, B. A. McDonough, and T. S. Steenhuis. “Impact of dissolved organic matter on colloid transport in the vadose zone: deterministic approximation of transport deposition coefficients from polymeric coating characteristics”. In: *water research* 45.4 (2011), pp. 1691–1701.

[134] W. Zhang, U.-s. Rattanaudompol, H. Li, and D. Bouchard. “Effects of humic and fulvic acids on aggregation of aqu/nC60 nanoparticles”. In: *Water research* 47.5 (2013), pp. 1793–1802.

[135] H. Ohshima. “Electrophoretic mobility of soft particles”. In: *Journal of colloid and interface science* 163.2 (1994), pp. 474–483.

[136] G. V. Lowry, R. J. Hill, S. Harper, A. F. Rawle, C. O. Hendren, F. Klaessig, U. Nobbmann, P. Sayre, and J. Rumble. “Guidance to improve the scientific value of zeta-potential measurements in nanoEHS”. In: *Environmental Science: Nano* 3.5 (2016), pp. 953–965.

[137] J. E. Patiño, T. L. Kuhl, and V. L. Morales. “Direct measurements of the forces between silver and mica in humic substance-rich solutions”. In: *Environmental Science & Technology* 54.23 (2020), pp. 15076–15085.

[138] K. L. Chen and M. Elimelech. “Influence of humic acid on the aggregation kinetics of fullerene (C60) nanoparticles in monovalent and divalent electrolyte solutions”. In: *Journal of colloid and interface science* 309.1 (2007), pp. 126–134.

[139] N. B. Saleh, L. D. Pfefferle, and M. Elimelech. “Aggregation kinetics of multiwalled carbon nanotubes in aquatic systems: measurements and environmental implications”. In: *Environmental science & technology* 42.21 (2008), pp. 7963–7969.

[140] Y. Zhang, Y. Chen, P. Westerhoff, and J. Crittenden. “Impact of natural organic matter and divalent cations on the stability of aqueous nanoparticles”. In: *Water research* 43.17 (2009), pp. 4249–4257.

[141] G. R. Aiken, H. Hsu-Kim, and J. N. Ryan. *Influence of dissolved organic matter on the environmental fate of metals, nanoparticles, and colloids*. 2011.

[142] A. Amirbahman and T. M. Olson. “The role of surface conformations in the deposition kinetics of humic matter-coated colloids in porous media”. In: *Colloids and Surfaces A: Physicochemical and Engineering Aspects* 95.2-3 (1995), pp. 249–259.

[143] R. Grillo, A. H. Rosa, and L. F. Fraceto. “Engineered nanoparticles and organic matter: a review of the state-of-the-art”. In: *Chemosphere* 119 (2015), pp. 608–619.

[144] D. P. Jaisi, N. B. Saleh, R. E. Blake, and M. Elimelech. “Transport of single-walled carbon nanotubes in porous media: filtration mechanisms and reversibility”. In: *Environmental science & technology* 42.22 (2008), pp. 8317–8323.

[145] S. M. Louie, E. R. Spielman-Sun, M. J. Small, R. D. Tilton, and G. V. Lowry. “Correlation of the physicochemical properties of natural organic matter samples from different sources to their effects on gold nanoparticle aggregation in monovalent electrolyte”. In: *Environmental science & technology* 49.4 (2015), pp. 2188–2198.

[146] A. J. Pelley and N. Tufenkji. “Effect of particle size and natural organic matter on the migration of nano-and microscale latex particles in saturated porous media”. In: *Journal of colloid and interface science* 321.1 (2008), pp. 74–83.

[147] T. Phenrat, J. E. Song, C. M. Cisneros, D. P. Schoenfelder, R. D. Tilton, and G. V. Lowry. “Estimating attachment of nano-and submicrometer-particles coated with organic macromolecules in porous media: development of an empirical model”. In: *Environmental science & technology* 44.12 (2010), pp. 4531–4538.

[148] F. Zhang, Z. Wang, S. Wang, H. Fang, and D. Wang. “Aquatic behavior and toxicity of polystyrene nanoplastic particles with different functional groups: complex roles of pH, dissolved organic carbon and divalent cations”. In: *Chemosphere* 228 (2019), pp. 195–203.

[149] Z. Li, K. Greden, P. J. Alvarez, K. B. Gregory, and G. V. Lowry. “Adsorbed polymer and NOM limits adhesion and toxicity of nano scale zerovalent iron to E. coli”. In: *Environmental science & technology* 44.9 (2010), pp. 3462–3467.

[150] R. A. Akbour, J. Douch, M. Hamdani, and P. Schmitz. “Transport of kaolinite colloids through quartz sand: influence of humic acid, Ca2+, and trace metals”. In: *Journal of colloid and interface science* 253.1 (2002), pp. 1–8.

[151] R. W. Harvey, D. W. Metge, L. B. Barber, and G. R. Aiken. “Effects of altered groundwater chemistry upon the pH-dependency and magnitude of bacterial attachment during transport within an organically contaminated sandy aquifer”. In: *water research* 44.4 (2010), pp. 1062–1071.

[152] S. Hong and M. Elimelech. “Chemical and physical aspects of natural organic matter (NOM) fouling of nanofiltration membranes”. In: *Journal of membrane science* 132.2 (1997), pp. 159–181.

[153] D. Grolimund, K. Barmettler, and M. Borkovec. “Release and transport of colloidal particles in natural porous media: 2. Experimental results and effects of ligands”. In: *Water Resources Research* 37.3 (2001), pp. 571–582.

[154] S. B. Roy and D. A. Dzombak. “Colloid release and transport processes in natural and model porous media”. In: *Colloids and Surfaces A: Physicochemical and Engineering Aspects* 107 (1996), pp. 245–262.

[155] C. Shen, B. Li, Y. Huang, and Y. Jin. “Kinetics of coupled primary-and secondary-minimum deposition of colloids under unfavorable chemical conditions”. In: *Environmental science & technology* 41.20 (2007), pp. 6976–6982.

[156] S. Torkzaban, S. A. Bradford, J. L. Vanderzalm, B. M. Patterson, B. Harris, and H. Prommer. “Colloid release and clogging in porous media: Effects of solution ionic strength and flow velocity”. In: *Journal of contaminant hydrology* 181 (2015), pp. 161–171.

[157] Y. S. R. Krishna, N. Seetha, and S. M. Hassanizadeh. “Experimental and numerical investigation of the effect of temporal variation in ionic strength on colloid retention and remobilization in saturated porous media”. In: *Journal of Contaminant Hydrology* 251 (2022), p. 104079.

[158] J. Zhuang, J. S. Tyner, and E. Perfect. “Colloid transport and remobilization in porous media during infiltration and drainage”. In: *Journal of Hydrology* 377.1-2 (2009), pp. 112–119.

[159] M. W. Hahn and C. R. O’Melia. “Deposition and reentrainment of Brownian particles in porous media under unfavorable chemical conditions: Some concepts and applications”. In: *Environmental science & technology* 38.1 (2004), pp. 210–220.

[160] J. J. Lenhart and J. E. Saiers. “Colloid mobilization in water-saturated porous media under transient chemical conditions”. In: *Environmental science & technology* 37.12 (2003), pp. 2780–2787.

[161] T. Cheng and J. E. Saiers. “Mobilization and transport of in situ colloids during drainage and imbibition of partially saturated sediments”. In: *Water resources research* 45.8 (2009).

[162] Y. Wang, S. A. Bradford, and J. Simunek. “Release of E. coli D21g with transients in water content”. In: *Environmental Science & Technology* 48.16 (2014), pp. 9349–9357.

[163] M. Bendersky and J. M. Davis. “DLVO interaction of colloidal particles with topographically and chemically heterogeneous surfaces”. In: *Journal of colloid and interface science* 353.1 (2011), pp. 87–97.

[164] R. Duffadar, S. Kalasin, J. M. Davis, and M. M. Santore. “The impact of nanoscale chemical features on micron-scale adhesion: Crossover from heterogeneity-dominated to mean-field behavior”. In: *Journal of colloid and interface science* 337.2 (2009), pp. 396–407.

[165] E. Pazmino, J. Trauscht, B. Dame, and W. P. Johnson. “Power law size-distributed heterogeneity explains colloid retention on soda lime glass in the presence of energy barriers”. In: *Langmuir* 30.19 (2014), pp. 5412–5421.

[166] I. Caltran, L. Rietveld, H. Shorney-Darby, and S. Heijman. “Separating NOM from salts in ion exchange brine with ceramic nanofiltration”. In: *Water Research* 179 (2020), p. 115894.

[167] C. Chassagne and M. Ibanez. “Hydrodynamic size and electrophoretic mobility of latex nanospheres in monovalent and divalent electrolytes”. In: *Colloids and Surfaces A: Physicochemical and Engineering Aspects* 440 (2014), pp. 208–216.

[168] Y. Tian, B. Gao, L. Wu, R. Muñoz-Carpena, and Q. Huang. “Effect of solution chemistry on multi-walled carbon nanotube deposition and mobilization in clean porous media”. In: *Journal of hazardous materials* 231 (2012), pp. 79–87.

[169] B. E. Logan, D. Jewett, R. Arnold, E. Bouwer, and C. O’Melia. “Clarification of clean-bed filtration models”. In: *Journal of environmental engineering* 121.12 (1995), pp. 869–873.

[170] J. E. Saiers, G. M. Hornberger, and L. Liang. “First-and second-order kinetics approaches for modeling the transport of colloidal particles in porous media”. In: *Water Resources Research* 30.9 (1994), pp. 2499–2506.

[171] J. F. Schijven and S. M. Hassanizadeh. “Removal of viruses by soil passage: Overview of modeling, processes, and parameters”. In: *Critical reviews in environmental science and technology* 30.1 (2000), pp. 49–127.

[172] B. Derjaguin and L. Landau. “Theory of the stability of strongly charged lyophobic sols and of the adhesion of strongly charged particles in solutions of electrolytes”. In: *Progress in Surface Science* 43.1-4 (1993), pp. 30–59.

[173] E. Verwey and J. T. G. Overbeek. “Theory of the stability of lyophobic colloids”. In: *Journal of Colloid Science* 10.2 (1955), pp. 224–225.

[174] S. A. Bradford, M. Bettahar, J. Simunek, and M. T. Van Genuchten. “Straining and attachment of colloids in physically heterogeneous porous media”. In: *Vadose Zone Journal* 3.2 (2004), pp. 384–394.

[175] Z. Liu, P. Hedayati, E. J. Sudhölter, R. Haaring, A. R. Shaik, and N. Kumar. “Adsorption behavior of anionic surfactants to silica surfaces in the presence of calcium ion and polystyrene sulfonate”. In: *Colloids and Surfaces A: Physicochemical and Engineering Aspects* 602 (2020), p. 125074.

[176] J. E. Patiño, W. P. Johnson, and V. L. Morales. “Relating mechanistic fate with spatial positioning for colloid transport in surface heterogeneous porous media”. In: *Journal of Colloid and Interface Science* 641 (2023), pp. 666–674.

[177] S. Torkzaban and S. A. Bradford. “Critical role of surface roughness on colloid retention and release in porous media”. In: *Water research* 88 (2016), pp. 274–284.

[178] K. VanNess, A. Rasmuson, C. A. Ron, and W. P. Johnson. “A unified force and torque balance for colloid transport: Predicting attachment and mobilization under favorable and unfavorable conditions”. In: *Langmuir* 35.27 (2019), pp. 9061–9070.

[179] E. Pazmino, J. Trauscht, and W. P. Johnson. “Release of colloids from primary minimum contact under unfavorable conditions by perturbations in ionic strength and flow rate”. In: *Environmental science & technology* 48.16 (2014), pp. 9227–9235.

[180] N. Tufenkji and M. Elimelech. “Deviation from the classical colloid filtration theory in the presence of repulsive DLVO interactions”. In: *Langmuir* 20.25 (2004), pp. 10818–10828.

[181] J. E. Tobiason. “Chemical effects on the deposition of non-Brownian particles”. In: *Colloids and Surfaces* 39.1 (1989), pp. 53–75.

[182] W. P. Johnson and M. Tong. “Observed and simulated fluid drag effects on colloid deposition in the presence of an energy barrier in an impinging jet system”. In: *Environmental science & technology* 40.16 (2006), pp. 5015–5021.

[183] A. Amirbahman and T. M. Olson. “Transport of humic matter-coated hematite in packed beds”. In: *Environmental Science & Technology* 27.13 (1993), pp. 2807–2813.

[184] D. Wang, S. A. Bradford, R. W. Harvey, B. Gao, L. Cang, and D. Zhou. “Humic acid facilitates the transport of ARS-labeled hydroxyapatite nanoparticles in iron oxyhydroxide-coated sand”. In: *Environmental science & technology* 46.5 (2012), pp. 2738–2745.

[185] T. Cheng and J. E. Saiers. “Effects of dissolved organic matter on the co-transport of mineral colloids and sorptive contaminants”. In: *Journal of contaminant hydrology* 177 (2015), pp. 148–157.

[186] W. P. Johnson and B. E. Logan. “Enhanced transport of bacteria in porous media by sediment-phase and aqueous-phase natural organic matter”. In: *Water Research* 30.4 (1996), pp. 923–931.

[187] A. Amirbahman and T. M. Olson. “Deposition kinetics of humic matter-coated hematite in porous media in the presence of Ca2+”. In: *Colloids and Surfaces A: Physicochemical and Engineering Aspects* 99.1 (1995), pp. 1–10.

[188] A. A. MacKay and B. Canterbury. “Oxytetracycline sorption to organic matter by metal-bridging”. In: *Journal of environmental quality* 34.6 (2005), pp. 1964–1971.

[189] B. Pan and B. Xing. “Adsorption mechanisms of organic chemicals on carbon nanotubes”. In: *Environmental science & technology* 42.24 (2008), pp. 9005–9013.

[190] M. Zhang, S. A. Bradford, J. Šimnek, H. Vereecken, and E. Klumpp. “Roles of cation valance and exchange on the retention and colloid-facilitated transport of functionalized multi-walled carbon nanotubes in a natural soil”. In: *Water research* 109 (2017), pp. 358–366.

[191] J. Nocito-Gobel and J. E. Tobiason. “Effects of ionic strength on colloid deposition and release”. In: *Colloids and Surfaces A: Physicochemical and Engineering Aspects* 107 (1996), pp. 223–231.

[192] S. Torkzaban, H. N. Kim, J. Simunek, and S. A. Bradford. “Hysteresis of colloid retention and release in saturated porous media during transients in solution chemistry”. In: *Environmental science & technology* 44.5 (2010), pp. 1662–1669.

[193] N. Tufenkji and M. Elimelech. “Breakdown of colloid filtration theory: Role of the secondary energy minimum and surface charge heterogeneities”. In: *Langmuir* 21.3 (2005), pp. 841–852.

[194] W. P. Johnson, E. Pazmino, and H. Ma. “Direct observations of colloid retention in granular media in the presence of energy barriers, and implications for inferred mechanisms from indirect observations”. In: *water research* 44.4 (2010), pp. 1158–1169.

[195] C. Shen, S. A. Bradford, T. Li, B. Li, and Y. Huang. “Can nanoscale surface charge heterogeneity really explain colloid detachment from primary minima upon reduction of solution ionic strength?” In: *Journal of Nanoparticle Research* 20 (2018), pp. 1–18.

[196] S. Galafassi, L. Nizzetto, and P. Volta. “Plastic sources: A survey across scientific and grey literature for their inventory and relative contribution to microplastics pollution in natural environments, with an emphasis on surface water”. In: *Science of the Total Environment* 693 (2019), p. 133499.

[197] C. Xu, B. Zhang, C. Gu, C. Shen, S. Yin, M. Aamir, and F. Li. “Are we underestimating the sources of microplastic pollution in terrestrial environment?” In: *Journal of hazardous materials* 400 (2020), p. 123228.

[198] Y. Huang, Q. Liu, W. Jia, C. Yan, and J. Wang. “Agricultural plastic mulching as a source of microplastics in the terrestrial environment”. In: *Environmental Pollution* 260 (2020), p. 114096.

[199] E.-L. Ng, E. H. Lwanga, S. M. Eldridge, P. Johnston, H.-W. Hu, V. Geissen, and D. Chen. “An overview of microplastic and nanoplastic pollution in agroecosystems”. In: *Science of the total environment* 627 (2018), pp. 1377–1388.

[200] N. Katsumi, T. Kusube, S. Nagao, and H. Okochi. “Accumulation of microcapsules derived from coated fertilizer in paddy fields”. In: *Chemosphere* 267 (2021), p. 129185.

[201] M. Bläsing and W. Amelung. “Plastics in soil: Analytical methods and possible sources”. In: *Science of the total environment* 612 (2018), pp. 422–435.

[202] J. Rozemeijer and H. Broers. “The groundwater contribution to surface water contamination in a region with intensive agricultural land use (Noord-Brabant, The Netherlands)”. In: *Environmental Pollution* 148.3 (2007), pp. 695–706.

[203] J. Rozemeijer, Y. Van Der Velde, R. McLaren, F. Van Geer, H. Broers, and M. Bierkens. “Integrated modeling of groundwater–surface water interactions in a tile-drained agricultural field: The importance of directly measured flow route contributions”. In: *Water Resources Research* 46.11 (2010).

[204] E. Smith, W. Davison, and J. Hamilton-Taylor. “Methods for preparing synthetic freshwaters”. In: *Water research* 36.5 (2002), pp. 1286–1296.

[205] D. L. Parkhurst and C. Appelo. *User’s guide to PHREEQC (Version 2): A computer program for speciation, batch-reaction, one-dimensional transport, and inverse geochemical calculations*. Tech. rep. US Geological Survey, 1999.

[206] Z.-P. Wang and T. Zhang. “Characterization of soluble microbial products (SMP) under stressful conditions”. In: *Water Research* 44.18 (2010), pp. 5499–5509.

[207] W. P. Johnson, K. A. Blue, B. E. Logan, and R. G. Arnold. “Modeling bacterial detachment during transport through porous media as a residence-time-dependent process”. In: *Water Resources Research* 31.11 (1995), pp. 2649–2658.

[208] S. A. Bradford, J. Simunek, M. Bettahar, M. T. Van Genuchten, and S. R. Yates. “Modeling colloid attachment, straining, and exclusion in saturated porous media”. In: *Environmental science & technology* 37.10 (2003), pp. 2242–2250.

[209] S. A. Bradford, S. R. Yates, M. Bettahar, and J. Simunek. “Physical factors affecting the transport and fate of colloids in saturated porous media”. In: *Water resources research* 38.12 (2002), pp. 63–1.

[210] L. M. McDowell-Boyer, J. R. Hunt, and N. Sitar. “Particle transport through porous media”. In: *Water resources research* 22.13 (1986), pp. 1901–1921.

[211] Y. Liang, S. A. Bradford, J. Simunek, M. Heggen, H. Vereecken, and E. Klumpp. “Retention and remobilization of stabilized silver nanoparticles in an undisturbed loamy sand soil”. In: *Environmental science & technology* 47.21 (2013), pp. 12229–12237.

[212] K.-J. Kung, E. Kladivko, T. Gish, T. Steenhuis, G. Bubenzer, and C. Helling. “Quantifying preferential flow by breakthrough of sequentially applied tracers silt loam soil”. In: *Soil Science Society of America Journal* 64.4 (2000), pp. 1296–1304.

[213] M. Greaves and M. Wilson. “The adsorption of nucleic acids by montmorillonite”. In: *Soil Biology and Biochemistry* 1.4 (1969), pp. 317–323.

[214] Y. Tang. “Hydrodynamic behaviour of silica-DNA microparticles in surface water: A systematic laboratory-based understanding of SiDNA (Fe) tracers”. In: (2023).

[215] C. N. Albers, A. Jensen, J. Bælum, and C. S. Jacobsen. “Inhibition of DNA polymerases used in Q-PCR by structurally different soil-derived humic substances”. In: *Geomicrobiology Journal* 30.8 (2013), pp. 675–681.

[216] K. Gibson, K. Schwab, S. Spencer, and M. Borchardt. “Measuring and mitigating inhibition during quantitative real time PCR analysis of viral nucleic acid extracts from large-volume environmental water samples”. In: *Water Research* 46.13 (2012), pp. 4281–4291.

[217] J. F. Huggett, T. Novak, J. A. Garson, C. Green, S. D. Morris-Jones, R. F. Miller, and A. Zumla. “Differential susceptibility of PCR reactions to inhibitors: an important and unrecognised phenomenon”. In: *BMC research notes* 1 (2008), pp. 1–9.

[218] I. G. Wilson. “Inhibition and facilitation of nucleic acid amplification”. In: *Applied and environmental microbiology* 63.10 (1997), pp. 3741–3751.

[219] S. McDonald, J. M. Pringle, A. G. Bishop, P. D. Prenzler, and K. Robards. “Isolation and seasonal effects on characteristics of fulvic acid isolated from an Australian floodplain river and billabong”. In: *Journal of Chromatography A* 1153.1-2 (2007), pp. 203–213.

[220] A. Schriewer, A. Wehlmann, and S. Wuertz. “Improving qPCR efficiency in environmental samples by selective removal of humic acids with DAX-8”. In: *Journal of microbiological methods* 85.1 (2011), pp. 16–21.

[221] K. L. Cook and J. S. Britt. “Optimization of methods for detecting Mycobacterium avium subsp. paratuberculosis in environmental samples using quantitative, real-time PCR”. In: *Journal of Microbiological Methods* 69.1 (2007), pp. 154–160.

[222] R. A. Haugland, S. C. Siefring, L. J. Wymer, K. P. Brenner, and A. P. Dufour. “Comparison of Enterococcus measurements in freshwater at two recreational beaches by quantitative polymerase chain reaction and membrane filter culture analysis”. In: *Water research* 39.4 (2005), pp. 559–568.

[223] Y. Karlen, A. McNair, S. Perseguers, C. Mazza, and N. Mermod. “Statistical significance of quantitative PCR”. In: *BMC bioinformatics* 8 (2007), pp. 1–16.

[224] V. B. Rajal, B. S. McSwain, D. E. Thompson, C. M. Leutenegger, B. J. Kildare, and S. Wuertz. “Validation of hollow fiber ultrafiltration and real-time PCR using bacteriophage PP7 as surrogate for the quantification of viruses from water samples”. In: *Water Research* 41.7 (2007), pp. 1411–1422.

[225] C. A. Kreader. “Relief of amplification inhibition in PCR with bovine serum albumin or T4 gene 32 protein”. In: *Applied and environmental microbiology* 62.3 (1996), pp. 1102–1106.

[226] P. Rådström, C. Löfström, M. Lövenklev, R. Knutsson, and P. Wolffs. “Strategies for overcoming PCR inhibition”. In: *Cold Spring Harbor Protocols* 2008.3 (2008), pdb–top20.

[227] D. Miller, J. Bryant, E. Madsen, and W. Ghiorse. “Evaluation and optimization of DNA extraction and purification procedures for soil and sediment samples”. In: *Applied and environmental microbiology* 65.11 (1999), pp. 4715–4724.

[228] D. Hospodsky, N. Yamamoto, and J. Peccia. “Accuracy, precision, and method detection limits of quantitative PCR for airborne bacteria and fungi”. In: *Applied and environmental microbiology* 76.21 (2010), pp. 7004–7012.

[229] J. W. Kirchner, X. Feng, C. Neal, and A. J. Robson. “The fine structure of water-quality dynamics: The (high-frequency) wave of the future”. In: *Hydrological processes* 18.7 (2004), pp. 1353–1359.

[230] C. Billington, G. Abeysekera, P. Scholes, P. Pickering, and L. Pang. “Utility of a field deployable qPCR instrument for analyzing freshwater quality”. In: *Agrosystems, Geosciences & Environment* 4.4 (2021), e20223.

[231] T. S. Manley. “Evaluation of DNA-Embedded Silica Nanoparticle Tracers”. PhD thesis. Stanford University, 2015.

[232] M. M. Yegane, F. Hashemi, F. Vercauteren, N. Meulendijks, R. Gharbi, P. E. Boukany, and P. Zitha. “Rheological response of a modified polyacrylamide–silica nanoparticles hybrid at high salinity and temperature”. In: *Soft Matter* 16.44 (2020), pp. 10198–10210.

[233] B. Derjaguin and L. Landau. “Theory of the stability of strongly charged lyophobic sols and the adhesion of strongly charged particles in solutions of electrolytes: Acta Physicochim URSS, v. 14”. In: *Laboratory of Thin Films, and Instilute of Physical Problems, Moscow (Received 1941)* (1941).

[234] E. J. W. Verwey, K. van NES, and J. T. G. OVERBEEK. *Theory of the Stability of Lyophobic Colloids. The Interaction of Sol Particles Having an Electric Double Layer. By EJW Verwey and J. Th. G. Overbeek... with the Collaboration of K. Van Nes*. New York; Leiden printed, 1948.

[235] J. Gregory. “Interaction of unequal double layers at constant charge”. In: *Journal of colloid and interface science* 51.1 (1975), pp. 44–51.

[236] J. Gregory. “Approximate expressions for retarded van der Waals interaction”. In: *Journal of colloid and interface science* 83.1 (1981), pp. 138–145.

[237] E. J. W. Verwey. “Theory of the stability of lyophobic colloids.” In: *The Journal of Physical Chemistry* 51.3 (1947), pp. 631–636.

[238] C. J. Van Oss. *Interfacial forces in aqueous media*. CRC press, 2006.

ACKNOWLEDGEMENTS

I would like to express my deepest gratitude to everyone who supported me throughout the journey of completing this thesis.

I am immensely grateful to my supervisory team— Prof. Thom Bogaard, Dr. Jan Willem Foppen, and Dr. Joachim Rozemeijer— for granting me the opportunity and placing their trust in me to pursue this research journey. Their unwavering support and guidance throughout my PhD have been invaluable. Dear Thom, thank you for your invaluable guidance and for all your support in bringing this thesis to completion. To my supervisor, Dear Jan Willem, I write these words with a heavy heart. Your invaluable guidance, insightful feedback, and critical observations were pivotal in shaping this research and fostering my growth as an independent researcher. It deeply saddens me that you are no longer here with us to share in the completion of this journey, but your wisdom and kindness remain a constant source of inspiration. This work is, in many ways, a testament to your mentorship, and I will always remain grateful for the profound impact you had on my academic development. Dear Joachim, I am sincerely grateful for your consistent support and for facilitating my research, especially through your efforts at the Deltares laboratory.

My heartfelt gratitude to Prof. Majid Hassanizadeh for agreeing to mentor me during my PhD. I was truly overjoyed by your support. Your encouragement, accessibility, and insightful guidance were invaluable throughout this journey. I deeply appreciate your contributions and your unwavering support every step of the way.

Special thanks go to Dr. Bas van der Zaan for your inspiring ideas and support. Your contributions have been invaluable and are deeply appreciated.

I extend my heartfelt thanks to Prof. Jack Schijven for your insightful advice and guidance, from modeling to experimental work. Your support has been greatly valued and sincerely appreciated.

I am especially grateful to two master's students, Jingya Tian and Felix Nyarko, whose theses contributed so much to this research. It was a pleasure working with both of you. Jingya, thank you for your dedication and hard work during the early stages of the project as we navigated challenges together. Felix, I deeply appreciate your enthusiasm, effort, and the collaboration opportunity your thesis facilitated with the University Freiburg. My gratitude extends to Dr. Michael Rinderer from the University Freiburg for initiating and making that collaboration possible.

To Watertagging team, I extend my appreciation to Jesse van der Hoeven for your thoughtful collaboration and teamwork in the early stages of the project, as well as for conducting experiments together. My appreciation goes to Coco (Yuchan) Tang, Swagatam Chakraborty, and Ahmed Abdelrady, for your invaluable support in the laboratory, insightful scientific input, and all the lunch and coffee break chats.

I would like to thank all the members of the Watertagging project team for their invaluable contributions and support. Thank you Pierrick Spekreijse, for being such an independent and creative master's student. I am also deeply grateful to Menno Tiesma for your help during fieldwork in the Netherlands and for your support in groundwater sample extraction.

I am grateful to Prof. Robert Grass, Dr. Gediminas Mekutis, and Dr. Julian Koch from the Chemistry and Applied Biosciences Department of ETH Zürich for kindly providing the DNA-based particles.

To the laboratory staff who played an essential role in bringing this research to life, I am profoundly thankful. Yvonne Hoiting, your guidance in the qPCR laboratory was invaluable, and I am especially grateful to Yvonne, Ali Ben Hadi, and Bright Namata for their support with qPCR performance. Ferdi Battes, your guidance with the zeta sizer was truly instrumental. My gratitude extends to Fred Kruis, Merlien Reddy, Zina Al Saffar, Peter Heerings, Berend Lolkema, Frank Wiegman, and Lyzette Robbemont from the IHE Delft, Armand Middeldorp from WaterLab TU Delft, Andre Cinjee, Fredericke Hannes, and Rob van Galen from Deltares for their invaluable contributions.

Special thanks to Dr. Ahemed Abdelrady and Dr. Mohsen Mirzaie Yegane for engaging in scientific discussions and inspiring new ideas. I would also like to thank Dr. Nasir Mangel for generously providing the humic acid stock.

I am sincerely grateful to the Water Management staff and Groundwater Group at TU Delft for their insightful discussions during the colloquium. My heartfelt thanks also go to the Water Management staff for all their support throughout my journey at TU Delft: thank you, Lydia de Hoog, Betty Rothfusz, Fleur van de Water, Louise Holslag, Eef Neijenhuis, Maureen Smith, and Linda Otten.

Special thanks to my colleagues in the CITG PhD council at TU Delft and to Prof. Giovanni Bertotti for your enthusiasm and uplifting support during some of the toughest times, especially pandemic isolation.

I would like to thank my officemates, colleagues, and friends at TU Delft, Camille, Andreas, Petra, Alireza Shefaei, Vincent, Gaby, Jerom, Ali Vahidi, Ali Moradvandi, Cesar Jimenez, Arash, Derya, Chelsea, Banafsheh, Bart, Fatima, Soham, Alexandra, Juan Aguilar, Mario, Xin Tian, Dengxiao, Akshit, David, Bas, Luuk, Yana, Verlee, Ibrahim, Fransje, Julia, Tessel, Nathalie, Nessia, Devanita, Monica, Indushree, Adela, and many others, for your friendliness, support, lunch breaks, and conference trips.

I am deeply thankful to the IHE support staff and many PhD and master's students of IHE with whom I shared laboratory facilities. Our small evening chats made those long hours in the lab feel much more enjoyable.

My heartfelt thanks to my dear friends Saeed, Maedeh, Azita, and Sepideh. You have been my constant support in Delft, my companions on sunny days, and my strength when challenges arose. I will cherish the laughs we shared and the countless moments we spent together, which made this journey so much more meaningful.

I am deeply grateful for the constant support of so many wonderful friends, both in Delft and abroad. In particular, to my lifelong friends, Pegah, thank you for all your constant encouragement and for designing the cover page of this work. To Leila, Shima, Manos, Mousa, Kiarash, Termeh, Zahra, Bojana, and many more, thank

you for your support and the wonderful moments we shared.

Finally, my deepest gratitude goes to my Mama and Baba, my two brothers, Kaveh and Roozbeh, and Negar for their love and unwavering support through all my ups and downs. You have always been my constant, offering boundless love and encouragement. To my little nephew and niece, Arian and Liana, thank you for bringing so much joy, laughter, and hope— a beautiful reminder of life's brighter moments.

Thank you all,

Bahareh

Delft, January 2025

CURRICULUM VITÆ

Bahareh Kianfar pursued her PhD at Delft University of Technology in Water Resources Management department. Her doctoral research focused on the systematic study of silica-encapsulated DNA particles (DNAcol) in saturated porous media to better understand their behavior as surrogates for colloidal particle contamination. Specifically, she examined the stability and transport of DNAcol particles under various physicochemical conditions relevant to subsurface and agricultural fields. Through laboratory sand column experiments, she investigated colloidal remobilization under transient porewater chemistry conditions.

Bahareh holds a Master's degree in Environmental Engineering from ETH Zürich, with specializations in Water Resources Management, and Ecological Systems Design, Air Quality Control, and Waste Management. Her master's thesis, conducted at the Analytical Chemistry Laboratory at EMPA, examined the effects of weathering on carbon nanotube-epoxy composites and the potential environment release of carbon nanotubes during mechanical abrasion. She earned a Bachelor's degree from Tehran University.

Her professional experience includes a research assistantship in the Urban Water Systems group at the Environmental Engineering department of ETH Zürich. She also worked in a short-term role in the Air Quality Control group at ETH Zürich, and gained experience at a consulting engineering company.

LIST OF PUBLICATIONS

4. **Kianfar Bahareh**, S.Majid Hassanizadeh, Ahmed Abdelrady, Thom Bogaarad, and Jan Willem Foppen, "Natural organic matter and ionic strength (CaCl2) affect transport, retention and remobilization of silica encapsulated DNA colloids (DNAcol) in saturated sand column", Colloid and Surfaces A: Physicochemical and Engineering Aspects, 678 (2023): 132476.

3. **Kianfar Bahareh**, Jingya Tian, Joachim Rozemeijer, Bas van der Zaan, Thom Bogaard, and Jan Willem Foppen, "Transport characteristics of DNA-tagged silica colloids as a colloidal tracer in saturated sand columns; role of solution chemistry, flow velocity and sand grain size" Journal of Contaminant Hydrology, 246 (2022) 103954.

2. **Kianfar Bahareh**, Simone Fatichi, Athansios Paschalis, Max Maurer, and Peter Molnar, "Climate change and uncertainty in high-resolution rainfall extremes" Hydrology and Earth System Sciences Discussions, 2016 (2016) 1-17.

1. Schlagenhauf, Lukas, **Bahareh Kianfar**, Tina Buerki-Thurnherr, Yu-Ying Kuo, Adrian. Wichser, Frank Nüesch, Peter Wick, and Jing Wang, "Weathering of a carbon nanotube/epoxy nanocomposite under UV light and in water bath: impact on abraded particles" Nanoscale, 7, no. 44 (2015): 18524-18536.